NUMERICAL INVESTIGATION OF PARTICLE SIZE SEGREGATION IN PILING, HOPPER FILLING AND DISCHARGING PROCESSES

By

Tengfang ZHANG

A THESIS SUBMITTED FOR THE DEGREE

OF

DOCTOR OF PHILOSOPHY

AT MONASH UNIVERSITY IN MARCH 2018

LABORATORY FOR SIMULATION AND MODELLING OF PARTICULATE SYSTEMS, DEPARTMENT OF CHEMICAL ENGINEERING, MONASH UNIVERSITY, CLAYTON, VIC 3800, AUSTRALIA

To my family,

Love and Thanks.

COPYRIGHT NOTICE

This page is intentionally blank

ABSTRACT

Granular materials are prone to segregate spatially with different sizes, densities and shapes. This is also a common problem in a variety of industries, including pharmaceuticals, food and agricultural processing, chemical and metallurgical industries. Segregation might render undesirable blend quality and induce flow problems. Therefore, understanding how and why segregation occurs is of great importance. This thesis presents numerical investigations of three processes: piling, hopper filling, and hopper discharging. Four components are included in the thesis to provide a comprehensive overview of the segregation induced by particle size.

To identify the effects of surface properties and water content, different sliding and rolling friction coefficients and various moisture contents are investigated in a basic but complicated sandpile formation process. The results present that the difference of the slope angle of the pile is the main cause of particles stratification. For particles in the binary with a large size and small angle of repose, segregation is most serious. Several fitting correlations between the porosity, force ratio and angle of repose are proposed, which reveal the structural and force characteristics of sandpile formation process.

Material hopper is ‘V’ shape container as one important device in the processing of granular materials. The fundamentals governing particle size segregation during the hopper filling process have been examined. The results show that particles with large velocity and small cluster size easily bounce to the container boundary while particles with small velocity and large cluster size are obstructed by their neighbours and stop moving early. Further, a contour plot regarding particle scale mixing index with different friction coefficients is drawn, illustrating that larger sliding friction and a moderate rolling friction lead to pronounced segregation. A correlation is then proposed

to quantify the degree of segregation of materials with various initial volume fraction of small particles.

Furthermore, the segregation of granular materials with a large size difference during discharging from a hopper is studied. The ratio of the small particles number N_{cs} in contacts with large particles to the small particles number N_s in each Voronoi cell showing the fraction of free drop particles is first proposed to explain the segregation extent. Results show that the mixtures with large porosity and small number ratio encounters serious percolation and a small fully discharging time of small particles.

The effects of different variables such as filling position, filling angle and flow rate on segregation in a Paul-Wurth hopper, which is widely used in the ironmaking blast furnace are examined. Results illustrate that the left side wall filling position leads to serious segregation due to the long slope when filling. Steep filling angle changes particles trajectories significantly and large particles tend to gather in the side wall region. Increasing flow rate at the fixed hopper size decreases the segregation.

ORIGINALITY STATEMENT

‘I hereby declare that this submission is my own work and to the best of my knowledge this thesis contains no material which has been accepted for the award of any other degree or diploma at any university or equivalent institution and that, to the best of my knowledge and belief, this thesis contains no material previously published or written by another person, except where due reference is made in the text of the thesis. Any contribution made to the research by others, with whom I have worked at Monash University or elsewhere, is explicitly acknowledged in the thesis. I also declare that the intellectual content of this thesis is the product of my own work, except to the extent that assistance from others in the project’s design and conception or in style, presentation and linguistic expression is acknowledged.’

Signature: 张腾方

Print Name: Tengfang ZHANG

Date: 12/03/2018

This page is intentionally blank

ACKNOWLEDGEMENTS

I would like to express my sincere gratitude to my project supervisors, Dr Zongyan Zhou and Prof. Aibing Yu, for giving me the opportunity to work on this project and all the help and guidance. I wish to thank Dr Zongyan Zhou for teaching me the basics of the project and for his encouragement, helpful guidance and strong support. This work would not be possible without their wise guidance and extraordinary inspiration.

I am very grateful to Australian Research Council and BlueScope Steel for the financial support. I wish to thank Monash University and the University of New South Wales (UNSW), for providing me with the tuition fee scholarship.

I would like to thank my colleagues and all the staffs in SIMPAS (Lab for Computer Simulation and Modelling of Particulate Systems) for providing me with a great deal of help in my studies and fantastic life in Melbourne and Sydney. I also wish to pass on my gratitude to the staffs in the Department of Chemical Engineering at Monash University and the School of Materials Science and Engineering at UNSW for their various help during the course of my study.

Many thanks must be made to my parents, my husband and my friends for their love, encouragement and strong support, which have always been a source of inspiration for my work. Thanks for the coming of my little baby, Yuyang, giving me happiness and love.

This page is intentionally blank

TABLE OF CONTENTS

LIST OF FIGURES

This page is intentionally blank

LIST OF TABLES

This page is intentionally blank

CHAPTER 1 INTRODUCTION

1.1 Background

Granular materials with different particle properties may segregate. Segregation is a common phenomenon and can occur during handling and transport process of granular materials, such as particle flow in a hopper which is widely used as a storage container to dispense or collect granular materials in engineering. However, industries are often troubled with the problem of non-uniform mixtures and hence products when particles with different sizes are discharged from a hopper. It can impact the effectiveness of medicine in pharmaceutics, and poor long-term durability for the concrete structure and uneven coke or ore distribution in an ironmaking blast furnace. Therefore, the understanding the segregation in several typical processes is important and should be paid more attention to.

Sandpile formation is one of the most typical processes for particles as the geometry is the simplest. It has been investigated in a two-dimensional (2D) box or a three-dimensional (3D) plane.. Particles fall down in the central part and pack on the bottom surface. The angle of repose is an important indicator widely used in both experiments and simulation to quantify the pile property. It is related to many parameters, including both geometry properties, such as jetting height and box thickness, and also material properties, such as size, shape and density. Due to the effect of angle of repose, for mixtures with different sizes, segregation happens when large particles roll down to the bottom. In the meantime, when particles are different in both size and shape, segregation ceases and stratification substitutes (Makse et al., 1997a). It is generally agreed that the angle of repose is the main cause of different phenomena for the various mixtures. Particle properties, such as size ratio and surface properties, have a significant impact on the formation of a sandpile.

Material hopper is one important device in the processing of granular materials. It can provide functions of both storage and transport, therefore, it is indispensable in industries, such as pharmaceuticals, food and agricultural, chemical and metallurgical industries. Segregation happens when particles are in different properties, such as size, shape or density. In the filling process of a hopper, a chute with different angles is generally used and, due to the different chute angles, the trajectory mechanism (Williams, 1976) is typical in this case, with large particles travelling a longer distance. Then after jetting, a heap is formed on the surface, which is similar to piling process. The heap in a hopper has relatively large flow rate and has bounded walls around compared with piling process. Percolation and rolling mechanisms are the main controlling factors. The two mechanisms are mainly affected by the geometry of a hopper, such as width, and also materials properties, such as size ratio and volume fraction.

The filling process of a transport-function hopper is then followed by the discharging process. The mono-sized particle flow dynamics of discharging from a hopper has been thoroughly investigated on the flow rate and arching phenomena. However, studies on the flow of mixtures with different particle sizes and other materials properties are still needed. For mixtures of different particle sizes, the percolation mechanism is the main controlling factor. This mechanism is mostly related to the size ratio and volume fraction.

Paul-Wurth (PW) hopper is a component of the burden distribution system in an ironmaking blast furnace. It is one parallel hopper type. Burden materials (coke, sinter, pellets and fluxes) are weighed from bins in the storehouse and delivered to the furnace top bins before discharged into the furnace by the burden distribution system. Therefore,

the particle distribution in and out a PW hopper has a significant influence on the smooth operation of a blast furnace. Same with a simple cone hopper, percolation and rolling are the main mechanisms in this process. The system geometry and materials properties are the governing factors for the particle distribution. In a real top blast furnace charging system, the geometry is closely related to the chute filling angles and chute positions. An even distribution is demanded after optimizing the chute filling angles and positions.

Three main research methods have been used in the past: physical experiments, theoretical models and dynamic simulations. Each method has its advantages and disadvantages. The physical experiments provide reliable results and sometimes use high-speed and high-resolution digital imaging techniques for deeper analysis. But the time required in preparing the facilities is long and the facilities are generally expensive. In terms of the theoretical models, they can predict the segregation phenomenon to some extent. However, assumptions often have to be made, and the accuracy is generally a problem. For dynamic simulation methods, discrete element method (DEM) is a typical and popular method, which takes into account not only the geometrical factors but also the forces involved. It can provide some microscopic parameters such as forces and structures, which are essential for mechanism understanding and can be readily obtained in the DEM simulation. The disadvantage of DEM is that it is limited by computational capacity and time. In addition, it has some assumptions and experienced constants, therefore, the simulation results always need to be validated.

1.2 Objectives of the research

The aim of this research is to improve the understanding of the segregation phenomenon that occurs in the piling, hopper filling and discharging processes by utilizing DEM

simulation method. Although plenty of efforts have been made in recent decades to explain segregation and predict its extent, some deficiencies still exist. Hence, the objectives of this thesis are to:

- Review the previous investigations on segregation mechanisms, the key findings of three research methods on piling, hopper filling and discharging processes, then to identify the knowledge gaps;
- Examine the effects of particle properties such as sliding and rolling friction coefficients and the moisture contents of water to understand the mechanisms of piling process by correlating the relationships of the structure and forces;
- Explain the size segregation phenomenon by particle velocity, cluster size and particle mixing index obtained from DEM, and establish a contour plot and a correlation to illustrate the effects of sliding and rolling friction coefficients and volume fraction on segregation of the hopper filling process;
- Identify the percolation mechanisms in particulate systems with large particle size ratio, examine the effects of size ratios and hopper angles on hopper discharging process; and explore the influence of the structural properties such as porosity, cluster size and the contact number ratio on particle distribution;
- Extend the segregation study to the real application in a Paul-Wurth hopper, examine the influence of different chute filling angles and positions on particle distribution, and provide meaningful information to industries to minimize the segregation extent.

1.3 Outline of this thesis

Based on the above analysis, the thesis has 7 chapters and the outline of each chapter is listed as follows:

Chapter 1 introduces the background of size segregation study on the piling, hopper filling and discharging processes, the research method and the objective of the present research.

Chapter 2 provides an in-depth literature review of physical experiments, theoretical models and mathematical simulation investigation on size segregation of the piling, hopper filling and discharging processes. Then current knowledge gaps are identified.

Chapter 3 explores the piling process for dry particles with different surface properties. The effect of volumetric moisture contents on the structures of wet particle piles is examined. The relationships between the structure and forces are established by fitting correlations.

Chapter 4 analyses the segregation details of binary mixtures during the hopper filling process. The model is validated with experimental results, and then a particle scale mixing index which is related to coordination number is used to quantify the segregation degree. The velocities and trajectories of large and small particles in binary mixtures are traced for understanding the segregation. In addition, effects of parameters used in DEM including sliding friction coefficient and rolling friction coefficients are examined and shown by a contour plot. Finally, a correlation to quantify the segregation extent for the various volume fraction of small particles is also established.

Chapter 5 investigates the hopper discharging process for different particle size ratios. This work begins with a validation of the experimental results from literature for a large size ratio. Then the microscopic parameters, including the velocity of small particles, the porosity of large particle and force structure are analysed for understanding the percolation and segregation during the discharging process. At last, the effects of the size ratio and the hopper geometry on segregation are also investigated.

Chapter 6 focuses on the application of a quasi-three-dimensional Paul-Wurth hopper. The effects of filling operation and filling angles on the size segregation during charging and discharging a Paul-Wurth hopper are investigated in detail. The degree of segregation is used to quantify the segregation extent during charging. Further, the map showing the various discharged time during discharging and wall stress distribution is drawn to further discuss the segregation mechanisms.

Chapter 7 concludes the whole work and discusses the strengths and limitation of the current research program, and provides recommendations for further study in this related area.

This page is intentionally blank

CHAPTER 2 LITERATURE REVIEW

2.1 Introduction

Segregation and mixing are two opposite phenomena during the handling of granular materials. Causes of segregation are introduced in some articles. For example, Williams (1976) classified the causes that can give rise to segregation into four sections, which are different properties in particle size, shape, density and particle resilience. Each of these properties can make segregation happen under certain circumstances. In particular, available evidence shows that the difference in particle size is by far the most important. Therefore, extensive attentions have been paid to the size-induced segregation. For a particulate system with different particle sizes, certain particles attempt to produce randomness, but some particles join together to resist this action by segregation. Then the result is an equilibrium between mixing and segregation setting a limit to the quality of mixing that can be achieved. Even though the mixers can make satisfactory mixtures, it is hard to make sure that the quality of the mixing will remain the same during subsequent procedures like handling and storage.

In recent decades, the segregation phenomenon has been investigated on the processes including piling, hopper filling and discharging processes under different geometrical, operational and materials conditions by various research methods. After a survey of a large amount of literature, three main methods, including physical experiments, theoretical models and simulation methods have been conducted on this topic. Each method has its pros and cons.

This chapter is divided into 5 parts. The first part is the fundamental and universal understanding of segregation phenomenon, including the segregation mechanisms and segregation indexes. The last four parts are according to the research processes studied. In each part, different research methods are comprehensively reviewed.

2.2 Segregation mechanisms and indexes

2.2.1 Segregation mechanisms

Segregation mechanisms have been reviewed by several authors (Williams, 1976, Bridgwater, 1976, Bridgwater, 1994, Rosato et al., 1987, Savage and Lun, 1988, Tang and Puri, 2004, Silva et al., 2000, Bridgwater, 2012, Fan et al., 2017) to explain why and how particulate solids segregated under specific circumstances, and what the results were with regard to the spatial or temporal distribution of the components of a mixture. As a review of segregation mechanisms in an early age, Williams (1976) summarised the mechanisms as trajectory, percolation of fine particles and the rise of coarse particles on vibration. Subsequently, a total thirteen segregation mechanisms have been summarised by Silva et al. (2000): trajectory, air current, rolling, sieving (or sifting), impact, embedding, and angle of repose, push-away, displacement, percolation, fluidization, agglomeration, and concentration-driven displacement. Attempts to simplify these thirteen causes into a small number of key mechanisms available for most segregation problems have been made by Tang and Puri (2004) and Ketterhagen et al. (2008) by assuming that some occur infrequently- such as embedding or push-away, and some can be classified into one subset of another mechanism, such as sieving and percolation. There are four primary segregation mechanisms or patterns, as shown in Figure 2-1. The last one is related to the solid-liquid system and not introduced here.

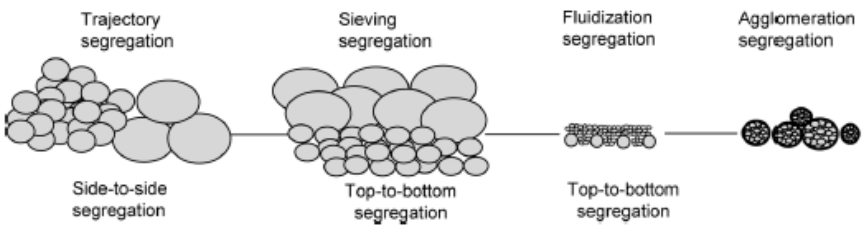

Figure 2-1 Four primary segregation mechanisms or patterns. Reprinted from Tang and Puri (2004), with permission from Taylor & Francis.

In most situations, segregation occurs combined with several mechanisms, so that no universal solution exists to solve all the problems. Therefore, the first step for the research is to restore the phenomenon, and find out what mechanisms are in this phenomenon. Next, solutions to reduce the segregation extent could be proposed by various methods. The primary mechanisms are described as following. The purpose of this content is to make these mechanisms readily to be understood by explaining their principles and provide an overall cognition on segregation.

2.2.1.1 Side-to-side segregation (Tang and Puri, 2004)

Trajectory mechanism is one mechanism which is related to particles size and density, especially for large particles. Williams (1976) demonstrated the principle of this mechanism. If a particle of diameter D and density ρ_s is projected horizontally with velocity υ, into a fluid of viscosity η, the horizontal distance that it will travel after infinite time, sometimes referred to as its "stopping distance", is equal to $\upsilon\rho D^2/18\eta$. A particle of diameter $2D$, therefore, travels four times as far. This mechanism can be called as "inertia segregation" and be understood with the help of Figure 2-2 (a). This segregation mechanism pattern mostly appears in a mixture when particles are lifted out of a mass of materials and thrown with the purpose of distributing them across the surface, for instance, large particles are free to fall or have relatively high rolling or moving velocity during heap flow or chute flow. This segregation occurs due to the fact that large particles tend to travel further, and this limits the quality of mixing that can be achieved.

Rolling segregation could be considered as a special case of trajectory segregation because large particles in these two cases move further than small particles from the filling point at heap formation, i.e., small particles in the centre are surrounded by large

particles. Enstad (2001) explained this phenomenon like this. It occurs since only large obstacles can stop large particles, whereas small particles are easily hit insurmountable obstacles and stop near the top of the heap. Therefore, the largest particles proceed down to the edge of the heap, while the smaller particles are arrested near the centre.

Embedding segregation refers to a process where larger and dense particles penetrate the upper surface of the heap layer and deposit particulate solid and become locked in this position (Figure 2-2 (b)). It is an inertia-based segregation mechanism and can be considered as one kind of side-to-side segregation pattern which is completely opposite of the materials distribution of sifting and rolling. Shinohara et al. (2001) treated this kind of segregation as “density segregation” since the difference in density is a significant inducing factor of embedding segregation.

Push-away segregation has a similar situation with embedding because this materials distribution is also determined by particle size or solid density. This means that heavier particles fall on the apex of the heap then they push away the lighter or smaller particles towards the edges of the heap. It is the so-called displacement segregation. The larger density particles displace the smaller or lighter ones and deposit among them. Embedding and push-away segregation can be illustrated in Figure 2-2 (c).

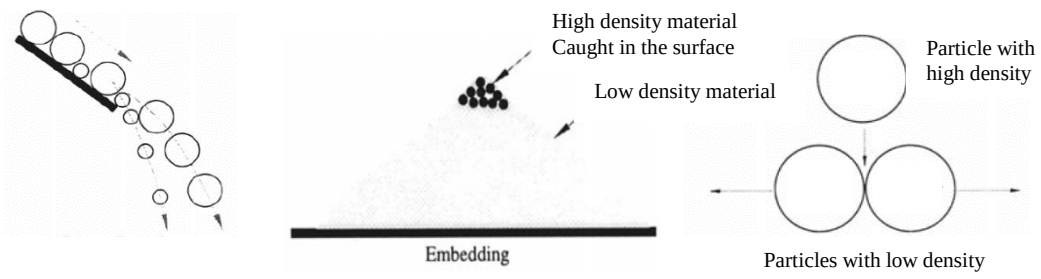

Figure 2-2 (a) Trajectory; (b) embedding and (c) push-away mechanism. Reprinted from (Silva et al., 2000), with permission from Springer Nature.

The above-mentioned mechanisms belong to “side-to-side segregation”. To some extent, these patterns may occur at packing, hopper filling and discharge process or in other flow regimes where there are significant velocity gradients within moving bulk solids.

2.2.1.2 Top-to-bottom segregation (Tang and Puri, 2004)

Percolation is assumed to be the predominant mechanism by which segregation occurs under the shear condition and attracts researchers such as Williams (1976), Savage and Lun (1988), and Scott and Bridgwater (1975) to focus considerable study on it. Small particles are the main research subject in this mechanism. This phenomenon can be explained as follows. Percolation segregation can take place whenever a mixture of particles of different characteristics is disturbed and moved then rearrangement of the particles follows. From time to time, void spaces between particles forms, allowing a particle at an upper height to fall. Then a particle in some other places moves up to fill the gaps. If the mixture contains particles with different sizes, it will be easier for a small particle to fall into the next layer than a larger one, and so there will be a tendency for the smaller particles to move downwards, leading to segregation, as shown in Figure 2-3 (a). The vast majority of the previous studies focus on causes of percolation’s emergence, mainly external energy input. Firstly, this can arise from the existence of shear motion within the mass, caused, for example, by stirring causing shear force or pouring the particles into a heap by gravity. This aspect was examined by Scott and Bridgwater (1976) and Tang et al. (2003). The former one used a simple shear cell to examine the behaviour of small particles when filled with large particles and concluded that percolation is increased with larger particle diameter ratio. The latter researcher (Tang et al., 2003) designed and fabricated a primary segregation shear cell device to

test segregation, and quantify the effect of characteristics such as size ratio, density and shape on segregation. Segregation also occurs when a mixture is in a moving bed which means that the mixture is shaken and the bed is vibrated. This was conducted by Shinohara and Golman (2002) using penetration model. Results showed that the moving bed in a wider cone angle and with a lower initial mixing ratio owned an unevenly distributed component.

Sieving and displacement segregation could be considered as a special case of percolation segregation. They are effective when particles filling fast to cause flow in layers or avalanches down a slope (Enstad, 2001). In the sliding layers, the openings between the large particles will act as a sieve or a screen, through which fine particles penetrate downwards during the process. Then the fines are collected at the bottom of the following layer and only coarse particles are left as large particles reach the edge of the heap.

Fluidization segregation patterns occur only when fine particles appear in the mixture or free-fall height exists, such as in pneumatic conveying (Engblom et al., 2012b, Silva et al., 2000). This is caused by the differences in drag forces on particles in a mixture, which entrain fine particles to segregate, then the fluidization of bulk solid mixture makes vertical segregation with accumulating fine or light components to the upper layer of the particle bed when filling of silos with free fall as shown in Figure 2-3 (b).

Air current segregation is similar with fluidization. Both of them are for materials having a wide size distribution and dust particles below 50μm. Air currents are induced by particle streams. Particles fall into the silo and turn outwards when meeting the surface of the heap already in the silo. So the finer particles are deposited near the walls and form a deposition with a certain angle (Figure 2-3 (c)).

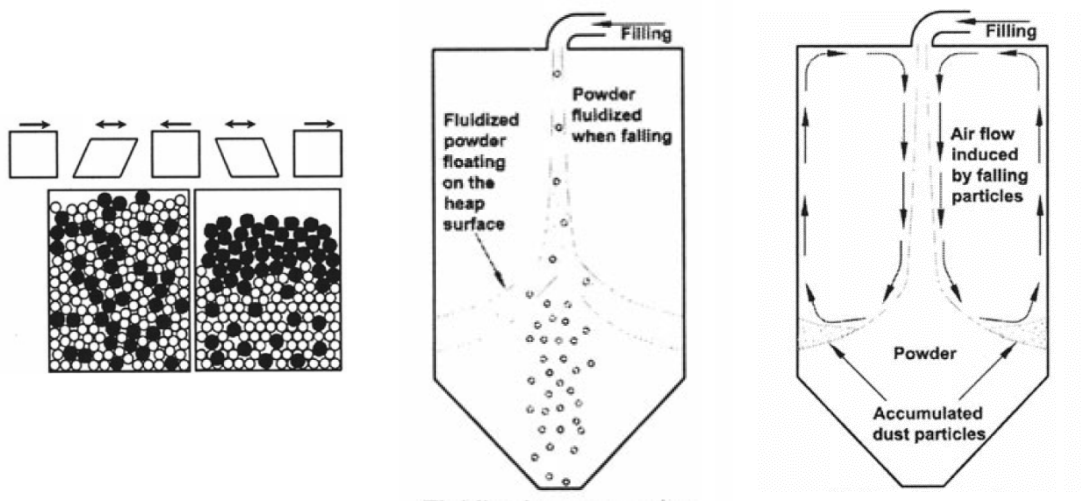

(a) (b) (c)

Figure 2-3 (a) Percolation; (b) Fluidization segregation and (c) Air-current mechanism. Reprinted from (Silva et al., 2000), with permission from Springer Nature.

Above mentioned mechanisms belong to "top-to-bottom segregation", i.e., large particles relatively move up while small particles move down.

2.2.2 Segregation indexes

2.2.2.1 Lacey index

Granular segregation or mixing can be quantified by different mixing indexes (Fan et al., 1970). Almost all the indexes are in macroscopic scale. The most popular one is Lacey index (Lacey, 1954) as the macroscopic mixing index M to quantify the degree of segregation. It can be defined by the following equation:

$$M = \frac{\sigma_0^2 - \sigma_t^2}{\sigma_0^2 - \sigma_r^2} \tag{2-1}$$

where σ_t is the standard deviation of particle fraction of the largest quantity particle in samples at time t; $\sigma_0$is to express the fully segregated state at time $t = t_0$ or the variance

before mixing; σ_r is to express the fully mixed state. And σ_t, σ_0 and σ_r are defined according to the following equations:

$$\sigma_t = \sqrt{\frac{\sum_{i=1}^{n}(x_i - p)^2}{n}} \tag{2-2}$$

$$\sigma_0 = \sqrt{p(1-p)} \tag{2-3}$$

$$\sigma_r = \sqrt{\frac{p(1-p)}{n}} \tag{2-4}$$

where x_i is the numerical proportion of small particle present in a sample square i. p is the overall particle number fraction of the target type particles considered in the binary mixture. n is the number of samples. When M is 0, particles are fully segregated. When the M is 1, it means the particles are fully mixed.

2.2.2.2 Particle scale mixing index

To investigate mixture quality at a particle scale, two approaches are generally used, one is coordination number and the other is a particle-scale mixing index (PSMI) derived from coordination number (Chandratilleke et al., 2012). Coordination number, which can be readily obtained from DEM simulation, is the number of particles in contact with a considered particle. This is a key parameter to understanding the behaviour of segregation by recording various pairs of contacts and hard to obtain from a physical experiment. PSMI is defined based on Lacey's mixing index (Eq. (2-1)), but the calculations of σ_t, σ_0 and σ_r are different and in particle scale level. For example, n in Eq. (2-2) changes to particle-scale sample size, which is equivalent to 1+ the average coordination number of mono-sized particles. n in Eq. (2-3) changes in total particle number. p in Eq. (2-3) and Eq. (2-4) is still the number ratio of a small particle in the

binary mixture when well-mixed. p in Eq. (2-2) changes into $\bar{x}_t = \frac{1}{N}\sum_{i=1}^{N} x_i$. In Eq. (2-2), the particle number fraction x_i is different and is defined by coordinate number as:

$$x_i = \frac{C_{n_{S(core)}}}{C_{n_i} + 1} \tag{2-5}$$

or

$$x_i = \frac{C_{n_{S(core)}} + 1}{C_{n_i} + 1} \tag{2-6}$$

where S means the small particle with a large amount, C_{n_i} is the total coordination number of core particle *i*, $C_{n_{S(core)}}$ is the number of small particle contacts for the core particle *i*. If the core particle is the small type, Eq. (2-6) is used. If not, Eq. (2-5) is used.

2.2.2.3 Other segregation index

Shinohara et al. (1972) proposed an equation to illustrate the segregation degree in a bounded heap flow, shown as below:

$$D_S = 1 - \frac{L_S}{L_h} \tag{2-7}$$

where L_s is the farthest distance along the heap line from the heap top to the point small particles can reach. L_h is the distance from the heap top of height to the hopper wall along the heap surface. This method can decrease the effect of the difference of heap length due to various filling positions.

Benito et al. (2013, 2014) applied two segregation indexes in their experimental results analysis. The indices I_H and $I_\perp$ were defined as:

$$I_{H,\perp} = 2\frac{V_L}{V_L+V_S} - 1 = 2\frac{n_L}{a\frac{n_S}{27}+n_L} - 1 \quad (2\text{-}8)$$

where a = 1 for size ratio of 3:1, a = 8 for size ratio of 3:2. V_L (V_s) is the total volume of the large (small) grains and n_L (n_s) is the number of large (small) grains present in the sample. Samples were taken over vertical strips all with the same volume to calculate I_H for a given pile. On the other hand, the corresponding samples to evaluate $I_\perp$ were taken over strips (all with the same volume) parallel to the free surface of the pile. These indices were defined to distinguish between the two kinds of segregation behaviours obtained in the experiments, i.e., typical segregation and stratification.

Zhang et al. (2014) used the radial segregation index (RSI) to quantify particle segregation. The RSI is the standard deviation of the normalized quantity (mass fraction or mean particle size) for all of the annul *i*, which was given as:

$$RSI = \sqrt{\frac{1}{n}\sum_{i=1}^{n}\left(\frac{x_i}{x_m} - \left(\frac{x_i}{x_m}\right)_{mean}\right)^2} \quad (2\text{-}9)$$

where n is the number of annuli, x_i is the particles mass fraction or mean particle size at the ith annulus, and x_m is the particle mass fraction or mean particle size for all annuli. The mean value of $\frac{x_i}{x_m}$ is unity. RSI can be described based on the mass fraction of each coke particle size or based on the mean particle size. This index could show the relation with the chute angles. Hence, RSI can be used to describe the effect of the chute inclination angle on the size segregation of the heap.

2.3 Sandpile

When granular materials are poured onto a surface, a sandpile forms. It is a typical system encountered in many industries dealing with particulate materials ranging from

flours, coal and sinters to concretes and medicines. Sandpile is a basic but complicated system for theoretical studies and much attention has been made to understand the different phenomena such as stress dip under the pile (Zhou et al., 2003, Zhou et al., 2014, Luding, 1997), stratification (Makse, 1997, Makse et al., 1997b), avalanching at the surface (Alexander et al., 2006) and self-organisation(Frette et al., 1990). Sandpile is similar to the heap formation process, the former one packs without a boundary and the latter one always pack with boundaries. Their packing patterns are analogous and will be discussed together here.

2.3.1 Physical experiments

Makse et al. (1997, 1997a, 1997b, 1998a, 1998b, 1998c, 1998d, 1998) explored the stratification and segregation phenomena by a large number of experiments in a quasi-2D transparent cell throwing a mixture of two species of grains and verified their proposed continuum models. In the experiment part (Makse et al., 1997b), they used grains of sand (cubic-shape with the angle of repose equal to 35^{o}) and glass beads with different angle of repose, which were smaller “less faceted” grains θ_{22} and larger “more faceted” grains θ_{11}. Through their experiment results, the control factor for stratification was the difference of the repose angles of the pure species, θ. An essential ingredient to obtain stratification was that $\theta_{22} > \theta_{11}$. On the other hand, strong segregation, but not stratification, occurred when $\theta_{22} < \theta_{11}$ (Figure 2-4). They suggested that the resulting stratification derived from the kink competition between the size and shape segregation.

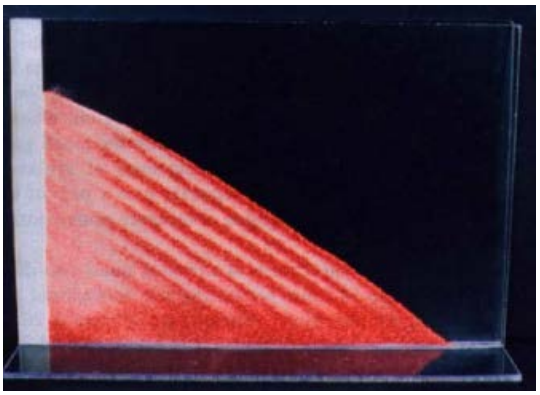

(a)

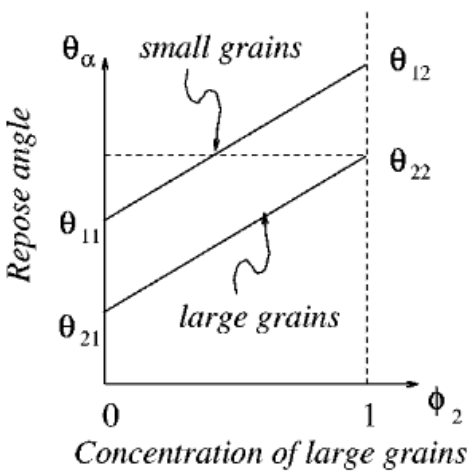

(b)

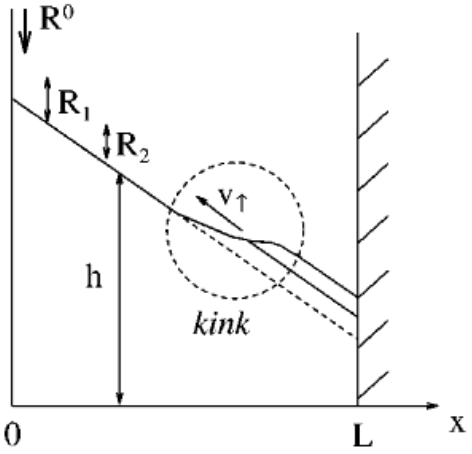

(c)

Figure 2-4 (a) A typical result of the formation of a successive layer of fine and coarse grains; (b) Dependence of the repose angle for the two types of rolling grains on the concentration of the surface of large grains; (c) The dash-circled zone is the kink zone. Reprinted from (Makse et al., 1997b), with permission from Springer Nature.

Benito et al. (2014) built up a large amount of granular piles using a versatile moving device with a discharge point to the top of the pile. The effects of the size of the injected grains, the discharged masses fraction, the free fall height and the amplitude of the horizontal motion were studied. A phase diagrams (Figure 2-5) obtained for the different flow regimes as a function of the mentioned variables, demonstrating the existence of stratification even for beads with the same round shape but different size.

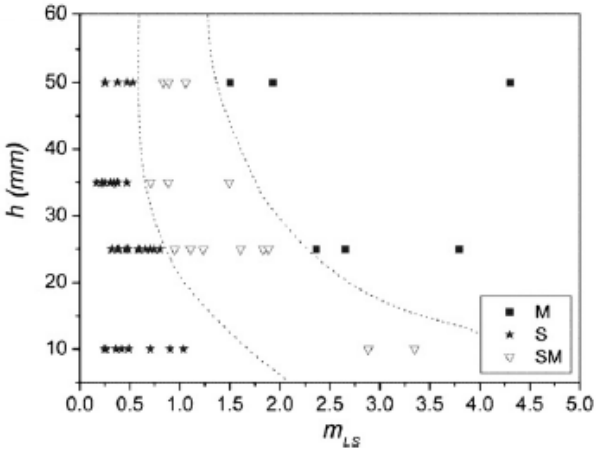

Figure 2-5 A phase diagrams obtained from the experimental results, showing the interactions between different segregation-mixture states. Reprinted from (Benito et al., 2013), with permission from Elsevier.

Grasselli and Herrmann (1997, 1998, 1999, 2001) deeply examined the angle of repose of two-dimensional heaps into a vertical Hele-Shaw cell for both mono-sized and binary mixture. Among them, segregation and stratification on a heap of binary granular mixtures with sand (rough) and glass spheres (smooth) were studied (Grasselli and Herrmann, 1998) and a phase diagram of heap morphologies considering the particle size and shape effects was drawn (see Figure 2-6). They showed that stratification occurred only when the size ratio of rough particles to small particles was greater than 1.5. They also presented that stratification depended on the separation between the walls of the cell where the pile was built and on the mass flux of the grain mixture.

Fan et al. (2012, 2014, 2017) investigated the different final particle configurations of binary granular mixtures during filling of quasi-two-dimensional silos. The control parameters, including particle size ratio, flow rate, system size, and heap rise velocity were explored. The effect of two-dimensional flow rate was found significant to the final states. The effects of particle size ratio and flowing layer length were small, as shown in the phase diagram in Figure 2-7. On the other hand, a transition from

segregated to mixed states was determined by the rise velocity of the heap which depended strongly on the particle size ratio.

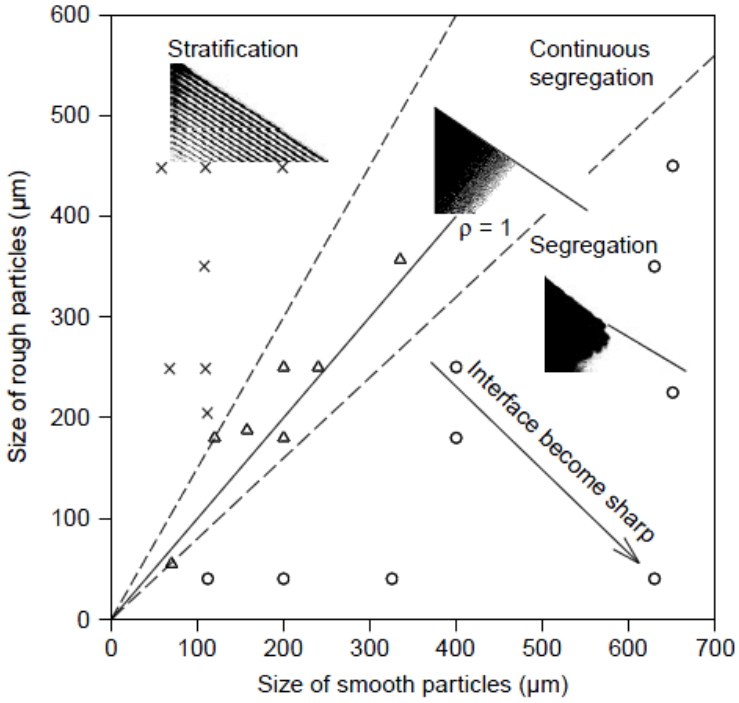

Figure 2-6 Phase diagram of heap morphologies considering the effects of size ratio and shape. Reprinted from (Grasselli and Herrmann, 1998), with permission from Springer Nature.

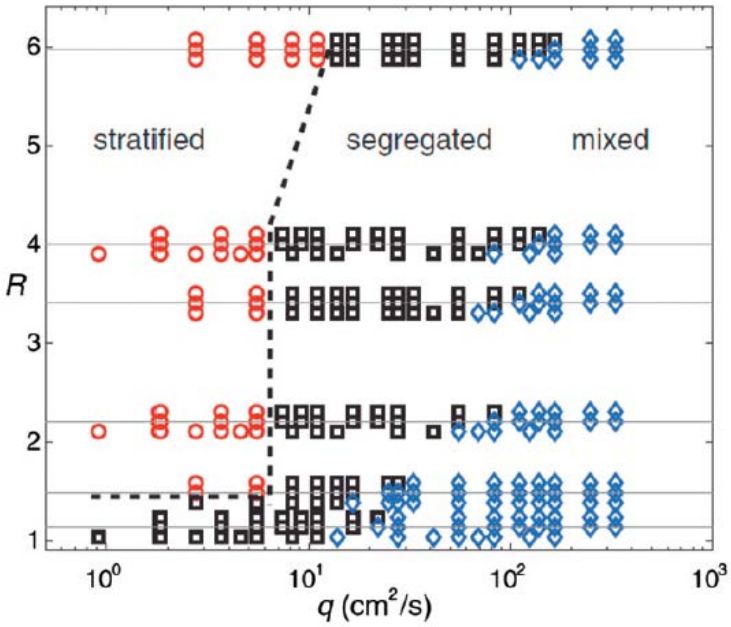

(a)

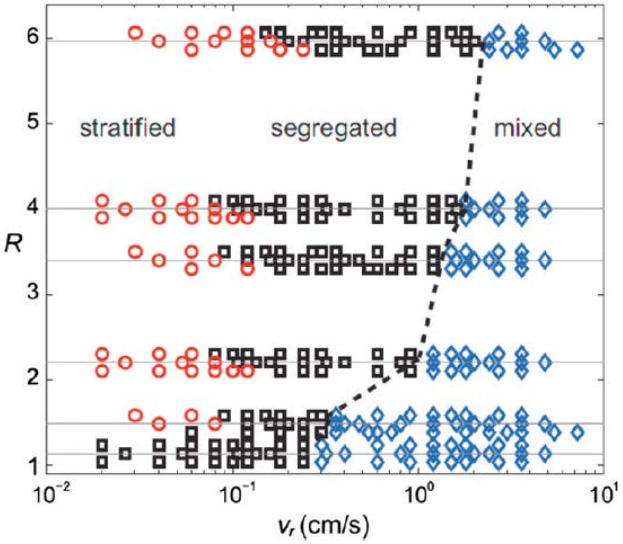

(b)

Figure 2-7 (a) Phase diagram in terms of flow rate q and size ratio R at three different silo width W; (b)Phase diagram of a final state in terms of rising velocity V_r and size ratio R at three heap widths W. Reprinted from (Fan et al., 2017), with permission from Elsevier.

2.3.2 Theoretical models

2.3.2.1 Boutreux and deGennes (BdG) model

The minimal model (Boutreux and deGennes, 1996) discussed theoretically the filling of a two-dimensional silo when a mixture of particles was poured at the centre. The basic tool was a coupled set of equations (for the local density of rolling species, and for the profile) then they were extended to a pair of species, including various processes: amplification, capture, and exchange of rolling grains. The problem was complex when considering oscillation. So they simplified the problem as a steady state one and tried to find the regulation of the downhill segregation. When collision features were simplified to the utmost it could be treated as a minimal model. By using the simplest form of the resulting equations, several predictions were obtained for the steady-state

profile and for the concentration distribution. At the bottom side of the slope, a complete purification was expected.

Boutreux et al. (1998) extended this model for mono-sized particle surface flow to flow of mixtures with different sizes. There was a sharp distinction between a static phase where grains were at rest and a thin rolling phase on top of the static phase. The different phases exchanged from the grains at rest and the rolling stream via binary collisions. It was predicted that during the filling of a two-dimensional silo, continuous segregation appeared inside the static phase: small (respectively, large) grains tended to stop uphill (respectively, downhill), although both species remained present everywhere, as shown in Figure 2-8.

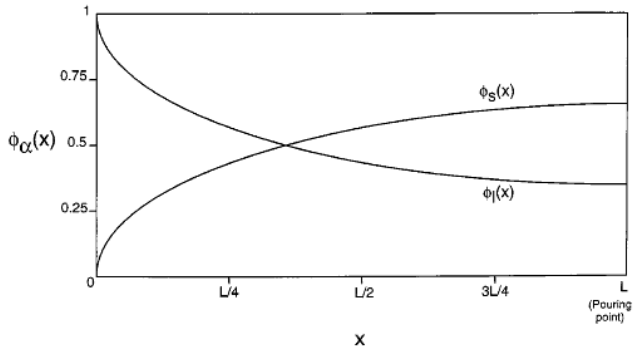

Figure 2-8 The volume fraction of small and large particles in the static phase, calculated by the numerical solution in a 2D cell. Reprinted from (Boutreux et al., 1998), with permission from Springer Nature.

2.3.2.2 Geometrical models

Shinohara et al. (1970) studied the mechanisms of segregation and blending of binary mixtures of particles flowing out of a mass-flow hopper mathematically based on the screen model, where small particles pass through the interspaces of large particles during flow out of a hopper. In the same way, mechanisms of size segregation of particles were investigated using the same models and similar equations focusing on

filling process into a hopper (Shinohara et al., 1972). At last, they validated the calculated results with experimental results and found that they showed good agreement which can elucidate the availability of screen model.

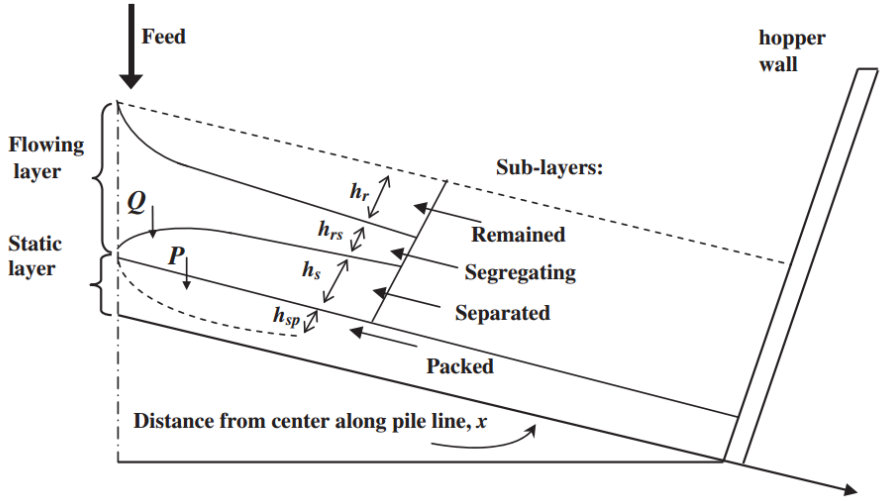

Figure 2-9 Illustration of screening layer model. Reprinted from (Shinohara et al., 1972), with permission from Copyright (1972) American Chemical Society.

This model is illustrated in Figure 2-9. The process can ideally be described as follows: particles mixtures flow along the solids heap. Small particles initiate to be separated from the mixture by passing through the interspaces of large particles from the flowing layer of the particle. Then the small particles which have passed through the flowing layer reach the stationary heap surface. Then they flow down on the surface together with the separated flowing large particles, then drop into the gaps formed by the stationary layer of large particles under the flowing layer. This segregation process continues during one cycle of the heaping process, and the stationary layer of large particles is gradually packed to be full of small particles separated from the flowing mixture. Then the same heaping is repeated while filling the hopper.

Over the next few years, mechanisms of segregation utilising this screen model in different situations were investigated, for example, differently shaped particles

(Shinohara, 1979), density segregation (Shinohara and Miyata, 1984), solids segregation over a two-dimensional dead man in an ironmaking blast furnace (Shinohara and Saitoh, 1993), multi-component mixtures (Shinohara et al., 2001), multi-size mixtures (Shinohara and Golman, 2002).

2.3.2.3 Advection-diffusion-percolation model

Fan et al. (2014) extended a model considering all of advection, diffusion and percolation and proposed the non-dimensional governing equation for the concentration of species *i* is:

$$\frac{\partial c_i}{\partial t} + \underbrace{\frac{\partial (u c_i)}{\partial x} + \frac{\partial (w c_i)}{\partial z}}_{\text{advection}} + \underbrace{\frac{\partial (w_{p,i} c_i)}{\partial z}}_{\text{percolation}} - \underbrace{\frac{\partial}{\partial z}\left(D \frac{\partial c_i}{\partial z}\right)}_{\text{diffusion}} = 0. \tag{2-10}$$

$$\frac{\partial c_i}{\partial \tilde{t}} + \tilde{u}\frac{\partial c_i}{\partial \tilde{x}} + \tilde{w}\frac{\partial c_i}{\partial \tilde{z}} + \Lambda(1-\tilde{x})\frac{\partial}{\partial \tilde{z}}\left[g(\tilde{z})c_i(1-c_i)\right] = \frac{\partial}{\partial \tilde{z}}\left(\frac{1}{Pe}\frac{\partial c_i}{\partial \tilde{z}}\right) \tag{2-11}$$

where u_i is the velocity of species *i* and *D* is the collisional diffusion coefficient. $w_{p,i}$ is a percolation velocity, for each species relative to the mean velocity w. Two dimensionless parameters Λ and *Pe* have physical meaning. Λ is the ratio of an advection timescale to a segregation timescale. *Pe*, the Péclet number, is the ratio of a diffusion timescale to the advection timescale.

This transport model could predict the final particle spatial distribution by a numerical solution with appropriate initial and boundary conditions. When the boundary condition is between the flowing layer and the static bed, particle deposition and erosion occur. The model considers two dimensionless parameters, Λ and *Pe* describe how different physical mechanisms determine the final particle distributions, as shown in Figure 2-10. It is divided into three regions, in each of which one mechanism dominates over the other two mechanisms. Among these mechanisms, advection has the role of preserving

initial conditions, collisional diffusion acted to mix the two species and percolation results in separation of the two species. At the boundaries between these regions, two or more mechanisms interact with each other and play comparable roles in determining particle spatial distributions.

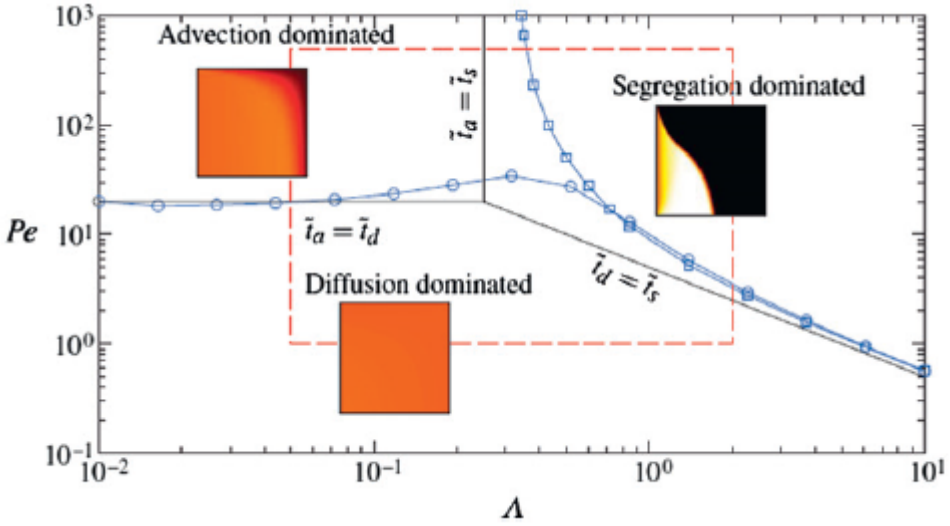

Figure 2-10 Λ–*Pe* parameter space illustrating different segregation regimes. Black lines indicate where pairs of time scales are equal and divide parameter space into regions dominated by either advection, diffusion, or segregation. Reprinted from (Fan et al., 2014), with permission from Cambridge University Press.

2.3.3 Numerical methods

Physical experiments examine the macroscopic behaviours of particulate. The particle behaviour is controlled by the interaction forces between individual particles as well as interactions with surrounding gas or liquid and wall. Therefore, understanding these microscopic mechanisms regarding the interaction forces is very significant to obtain the results that can be generally used and provide truly interdisciplinary research in the particulate matter. This aim can be achieved by particle scale research based on the detailed micro-dynamic information. In recent years, such particle scale research has been rapidly developed worldwide, mainly because of the rapid development of discrete

particle simulation technique and computer technology. Several discrete modelling techniques have been developed, including Monte Carlo method, cellular automata and discrete element method (DEM). DEM is a dynamic simulation method, which considers not only the geometrical factors but also the forces involved. It can provide some microscopic parameters, such as the trajectories of and transient forces acting on individual particles, which is extremely difficult to obtain by physical experimentation at this stage of development. These parameters are essential for mechanism understanding and are readily obtained in the DEM simulation process. Consequently, DEM has been increasingly used in the past two decades or so.

2.3.3.1 DEM

In a DEM simulation, an explicit numerical scheme is used to trace the motion of individual particles in a considered system. A particle has two types of motions, which are the translational and rotational motion (as shown in Figure 2-11). These are described by Newton's second law of motion (Cundall and Strack, 1979). During the movement, the particles may have collisions with their neighbouring particles or the hopper wall, through which the momentum is exchanged. At any time *t*, the governing equations (Zhu et al., 2007) for translational and rotational motions of particle *i* in the system are:

$$m_i \frac{d\mathbf{v}i}{dt} = \sum_{j=1}^{k}\left(\mathbf{f}_{c,ij} + \mathbf{f}_{d,ij} + \mathbf{f}_{cohe,ij}\right) + m_i\mathbf{g} \qquad (2\text{-}12)$$

$$I_i \frac{d\boldsymbol{w}i}{dt} = \sum_{j=1}^{k}(M_{t,ij} + M_{r,ij}) \qquad (2\text{-}13)$$

where $\mathbf{v}_i$ and $\boldsymbol{\omega}_i$ are the translational and angular velocities respectively of particle *i* with mass m_i and moment of inertia I_i. The forces considered are gravitational and particle-particle interaction forces including elastic contact force $\mathbf{f}_{c,ij}$ and viscous

damping force $\mathbf{f}_{d,ij}$ in both normal and tangential components at the contact point. The capillary force between particles *i* and *j* is also considered for a system with wet particles. The torque acting on particle *i* by particle *j* includes two components. One is generated by tangential force and causes particle *i* to rotate, $\mathbf{M}_{t,ij}$, and rolling friction torque $\mathbf{M}_{r,ij}$ generated by normal force that acts to oppose the relative rotation between the contacting particles. For a particle undergoing multiple interactions, the individual interaction forces and torques are vectorially summed for the k_i particles interacting with particle *i*. Equations except for capillary force, which are used to calculate difference forces and torques are referred in Zhou et al. (2005) and listed below in Table 2-1.

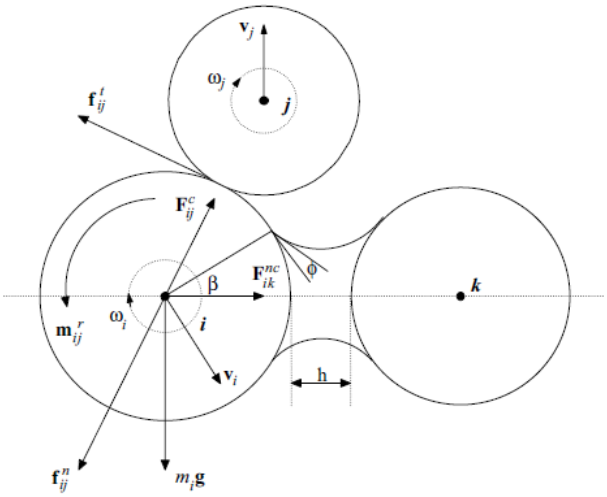

Figure 2-11 Schematic illustration of the forces acting on the particle from contacting particle *j* and non-contacting particle *k.* Reprinted from (Zhu et al., 2007), with permission from Elsevier.

On the other hand, in practice, particles are often not dry, water or moisture content might have a significant effect on other packing properties, as demonstrated in literature studies (Anand et al., 2010, Yang et al., 2007, Dong et al., 2012). The cohesive force (or so-called capillary force) between particles formed by the liquid is caused by surface

tension due to the liquid bridge between particles. Some experimental and theoretical studies have been conducted by Samadani and his colleagues (Samadani and Kudrolli, 2001, Samadani, 2002). For example, the angle of repose and segregation degree was analysed under different liquid types. Results presented that the angle of repose of the granular matter was observed to increase sharply as the volume fraction of the fluid was increased and then saturated. Meanwhile, a maximum angle of stability was proposed by Mohr-Coulomb model for a wet granular pile (Nowak et al., 2005). Some attempts have been made by some researchers on rotating drums (Liu et al., 2013) and the piling process of mono-sized particles (Dong et al., 2013).

Table 2-1 Components of forces and torque acting on particle *i*

Forces and torques	Symbols	Equations
Normal elastic force	$\mathbf{f}_{cn,ij}$	$-4/3E^*\sqrt{R^*}\delta_n^{3/2}\mathbf{n}$
Normal damping force	$\mathbf{f}_{dn,ij}$	$-c_n\left(8m_{ij}E^*\sqrt{R^*\delta_n}\right)^{1/2}\mathbf{V}_{n,ij}$
Tangential elastic force	$\mathbf{f}_{ct,ij}$	$-\mu_s\lvert\mathbf{f}_{cn,ij}\rvert(1-(1-\delta_t/\delta_{t,\max}{}^{3/2})\hat{\delta}_t$, $(\delta_t<\delta_{t,\max})$
Tangential damping force	$\mathbf{f}_{dt,ij}$	$-c_t\left(6\mu_s m_{ij}\lvert\mathbf{f}_{cn,ij}\rvert\sqrt{1-\lvert\mathbf{v}_t\rvert/\delta_{t,\max}}/\delta_{t,\max}\right)^{1/2}\mathbf{V}_{t,ij}$ $(\delta_t<\delta_{t,\max})$
Coulomb friction force	$\mathbf{f}_{t,ij}$	$-\mu_s\lvert\mathbf{f}_{cn,ij}\rvert\hat{\delta}_t$, $(\delta_t\geq\delta_{t,\max})$
Torque by tangential forces	$\mathbf{M}_{t,ij}$	$\mathbf{R}_{ij}\times(\mathbf{f}_{cn,ij}+\mathbf{f}_{dt,ij})$
Rolling friction torque	$\mathbf{M}_{r,ij}$	$\mu_{r,ij}\lvert\mathbf{f}_{n,ij}\rvert\hat{\boldsymbol{\omega}}_{t,ij}^n$

where R* is the reduced radius of the particle *i* and *j* at the contact point. $1/m_{ij}=1/m_i+1/m_j$, $E^*=E/2(1-\nu^2)$, $\hat{\boldsymbol{\omega}}_{t,ij}=\boldsymbol{\omega}_{t,ij}/\lvert\boldsymbol{\omega}_{t,ij}\rvert$, $\hat{\boldsymbol{\delta}}_t=\boldsymbol{\delta}_t/\lvert\boldsymbol{\delta}_t\rvert$, $\delta_{t,\max}=\mu_s(2-\nu)/2(1-\nu)\cdot\delta_n$, $\mathbf{V}_{ij}=\mathbf{V}_j-\mathbf{V}_i+\boldsymbol{\omega}_j\times\mathbf{R}_{c,ji}-\boldsymbol{\omega}_i\times\mathbf{R}_{c,ij}$, $\mathbf{V}_{n,ij}=(\mathbf{V}_{ij}\cdot\mathbf{n})\cdot\mathbf{n}$, $\mathbf{V}_{t,ij}=(\mathbf{V}_{ij}\times\mathbf{n})\times\mathbf{n}$. Note that tangential forces ($\mathbf{f}_{ct,ij}$+$\mathbf{f}_{dt,ij}$) should be replaced by $\mathbf{f}_{t,ij}$ when $\delta_t\geq\delta_{t,\max}$.

The calculation of the capillary force due to the formation of a liquid bridge between two adjacent particles is a numerical solution of the Laplace-Young equation (Orr et al., 1975, Lian et al., 1993, Chen et al., 2011, Lian and Seville, 2016). However, this kind of analytical solution is complex based on different approximations. Several simple expressions are proposed by using Derjaguin approximation. One equation for unequal spheres is written as (Willett et al., 2000):

$$F_{cohe,ij} = 2\pi R_{ij}\gamma \frac{R_{ij}(1-\cos\beta)\,cos\varphi}{R_{ij}(1-\cos\beta)+2S} \tag{2-14}$$

where, R_{ij} is the harmonic mean radius of particles i and j, $R_{ij} = \frac{R_i R_j}{R_i+R_j}$. $2S$ is the distance between two particles. γ is the surface tension. φ is the contact angle. β is the half-filling angle, which can be obtained by $V = 2\pi S R^2 sin^2\beta$. V is the volume of the moisture between two particles. The relationship between V and the normalized moisture content V^* is $V = V^* \times R_{ij}^3$.. The effect of particle roughness on the capillary force is complex. Once when the distance between two particles exceeds rupture distance, the liquid bridge and capillary force be removed. This rupture distance $2S_c$ is defined as (Willett et al., 2000):

$$2S_c = \left(1 + \frac{\varphi}{4}\left(\frac{R_j}{R_i}+1\right)\right)[V^{*1/3} + \left(\frac{R_j}{R_i} - \frac{2}{5}\right)V^{*2/3}]R_{ij} \tag{2-15}$$

This method is approved relatively accurate for small bridge volumes and for separation distances excluding those at close-contact and near-rupture.

To implement the capillary force in DEM simulation, liquid distribution among particles has to be determined. Yang et al. (2003) assumed liquid being distributed evenly and not transferable among particles. Once the particle gap is smaller than the

rupture distance, a liquid bridge is formed and the liquid assigned to a particle will be evenly distributed to its liquid bridges.

2.3.3.2 Piling process investigation by DEM

Angle of repose of a sandpile is one of the most important macroscopic properties in characterizing granular materials. The investigations on the angle of repose by DEM has been implemented on mono-sized spheres (Zhou et al., 2001), ellipsoid particles (Zhou et al., 2014) and cohesive mono-sized particles (Dong et al., 2013) etc..

Zhou et al. (2001) studied the effects of particle characteristics, material properties, and geometrical on the angle of repose of the piling. It was found that sliding and rolling frictions were the primary reasons for the piling formation; the detailed trend could be seen from Figure 2-12. The angle of repose was also influenced by the particle size and container thickness and was not so sensitive to density, Poisson's ratio, damping coefficient, and Young's modulus.

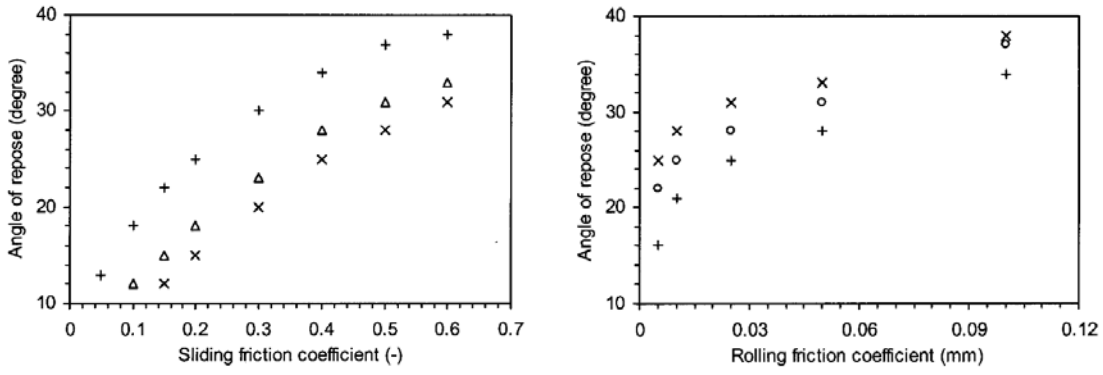

(a) (b)

Figure 2-12 Angle of repose as a function of (a) sliding friction coefficient and (b) rolling friction coefficient for sandpile formation process of mono-sided particles. Reprinted from (Zhou et al. 2001), with permission from Springer Nature.

Dong et al. (2013) examined on the piling processes of mono-sized wet particles by DEM. The effects of moisture content on the repose angle and structure of a pile were studied by a series of controlled numerical experiments. It was confirmed that the structure of a pile was similar to that of a packing for cohesive particles. Moreover, the averaged local porosity and repose angle had similar changes with the moisture content and can be linearly correlated. Therefore, the relationship between the repose angle and the cohesive force can be established.

Zhou et al. (2014) explored the angle of repose of the mono-sized ellipsoid particles' sandpile formation process. The ellipsoid particles were realized by a modified DEM study and they were characterized by different aspect ratios. The relationship between the angle of repose and aspect ratio revealed that spheres have the lowest angle of repose compared with ellipsoids. The coordination number's relationships with different aspect ratio were examined.

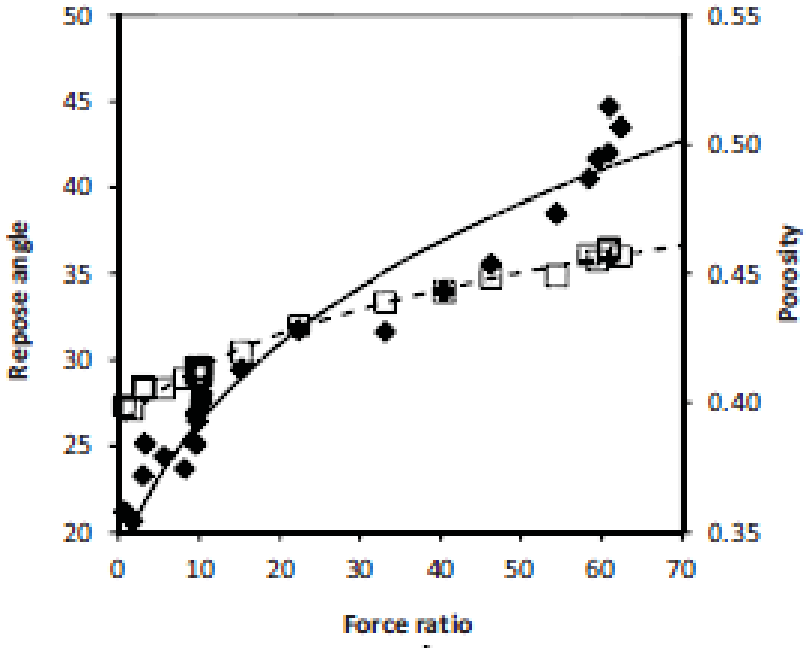

Figure 2-13 Correlations of the angle of repose and porosity with force ratio. Reprinted from (Dong et al. 2013), with permission from AIP Publishing.

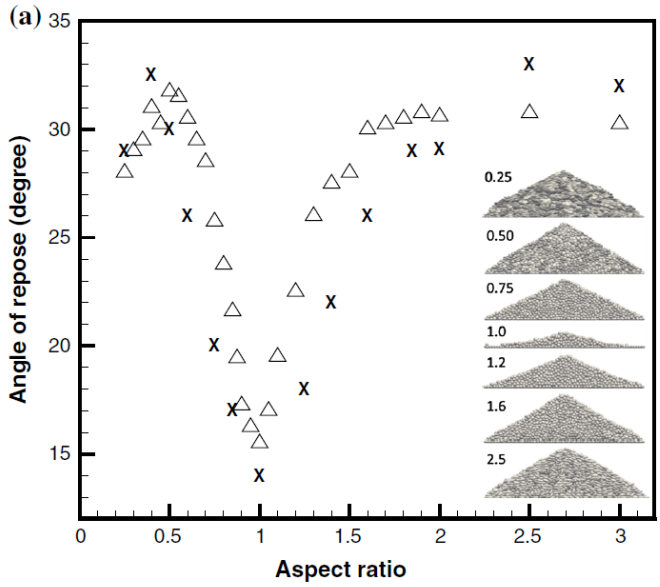

Figure 2-14 Angle of repose for different aspect ratios (the insets are sandpiles formed by the discharging method. Reprinted from (Zhou et al. 2014), with permission from Springer Nature.

2.4 Hopper filling

Particle mixtures with a wide range of sizes, shapes, and densities often experience segregation during the handling and transport operations. Material hopper is one important device in the processing of granular materials, where the fundamentals governing particle size segregation during the hopper filling process have been examined by several researchers using the three approaches.

2.4.1 Physical experiments

Aminaga et al. (1987) investigated size segregation and size variation of sinter in a bell-less type distribution system. The experimental apparatuses used were the 1/10 scale model, as shown in Figure 2-15. In their research, charging rate of burden into the bunker could have a significant influence on size segregation in the bunker during charging. Varied charging rate conditions, therefore, were examined the first time. Results they obtained were as following. First one was that with the increase of the

charging rate of sinter into the bunker, size segregation in the bunker would decelerate. As a result, the size variation during discharging from the bunker decreased. The second one was that in the aspect of restraint of the size variation from the bunker, the control of size segregation during charging into a bunker was effective and one simple method was to install a stone box.

Shinohara et al. (1972) examined size segregation of particles in filling a two-dimension transparent hopper. The experimental apparatus is shown in Figure 2-16. Results illustrated a V-shaped zone existing where smaller particles are contained as a result of segregation. This zone expanded with a smaller fraction of large particles in the feed process, longer distance of flow along the heap surface, and larger feed rate of particles. Meanwhile, the pattern of distribution of mixing ratio of large particles within the zone was derived in relation to the feed rate of particles, the initial mixing ratio of the solids feed, hopper geometry, for instance, a hopper cone angle and the height of solids heap, and material properties such as size and density.

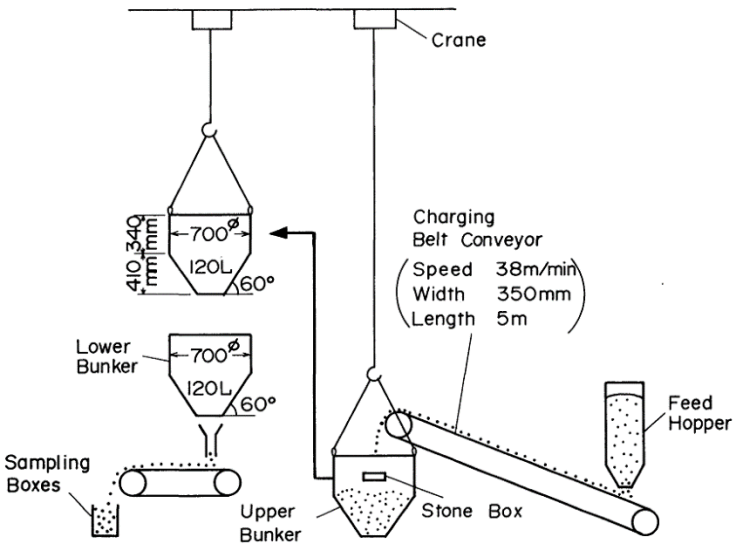

Figure 2-15 Experimental apparatus of 1/10 scale model. Reprinted from (Aminaga et al., 1987), with open access.

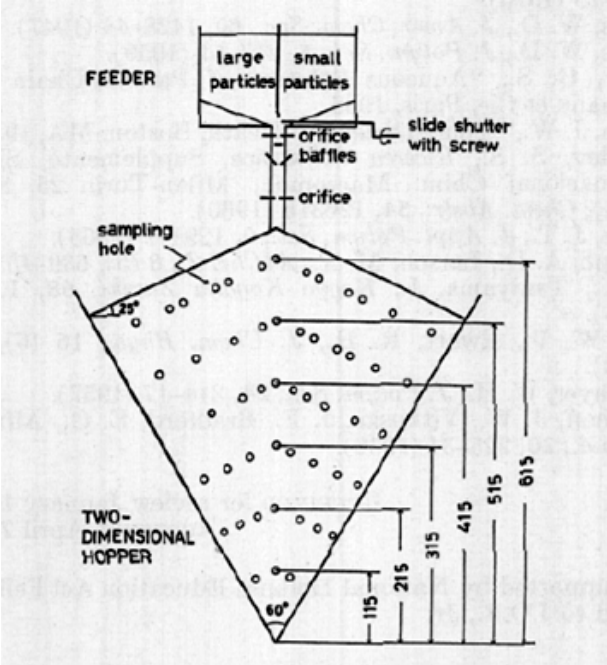

Figure 2-16 Experimental apparatus of the hopper. Reprinted from (Shinohara et al., 1972), with permission from American Chemical Society.

After filling in a bin or hopper, a cone or heap forms to cause materials to segregation. Garve (1925) noted that when grained materials were delivered from a chute into a storage bin, a heap or cone always formed on top of the fill, which would deposit as a screen and cause the material to segregate. Structure of the cone was smaller particles near the heap centre and large particles rolling down to the base of the heap. The reason for this phenomenon was that coarser and heavier particles, having the greater momentum, would roll down and collect at the bottom of the cone. The finer and lighter particles remained toward the centre or top of the cone. This theory was agreed by Boutreux and deGennes (1996) and Smith et al. (2001).

Drahun and Bridgwater (1983) conducted three mechanisms for segregation during heap formation: avalanching, percolation, and migration of large particles to the surface. They studied the effects of several factors and concluded that the primary factor affecting segregation was a size difference, then to some extent also particle shape,

density and concentration, free-fall height and slight differences of the inlet structure of the feed, e.g. slight segregation in a feed device or feed hopper. They also noted that general effects when simulating the behaviour of on a conical heap were similar but the avalanching frequency was reduced and the principal particles were turned down to the surface.

However, Standish (1985) disagreed with some results on particle movement. He thought that the conditions they used, for instance, binary mixtures of glass ballotini and ideal conditions in a rectangular bed, were impossible to analytically model the key features of free-surface segregation. For high-speed moves of heap formation had not been detected avalanching or shimmering but only a tumbling motion which suggested principal segregation mechanisms might not be same in different systems. It was concluded that concentration of heap was correlated with feed concentration. It means that the concentration of these particles in the hopper was essentially uniform and it was related to the feed concentration. It could be depicted by an equation $C=C_o^k$, where C and C_o were the concentration of small particle and feed composition respectively, k is an experimentally obtained segregation constant.

2.4.2 Simulation methods

The segregation of granular materials filling in and discharging from a hopper has been the focus of several studies in recent years. Except for the physical experimental studies, the mathematical methods, in particular, DEM by several researchers are outlined here.

Rahman et al. (2011) used DEM to validate the screening model proposed by Shinohara et al. (1972) in forming a conical pile. The distribution of mixing ratio of a segregating component of different sizes could be drawn along the pile surface and well correlated

with each other for the first time (as shown in Figure 2-17). As a result, the zone, where the segregating component of the smaller particle is contained around a central feed point, was found to expand by an increment of the initial mixing ratio, the volumetric feed rate and the flow length of the pile surface. Flowability parameters such as velocity ratio, penetration rate and packing rate of the segregating component were the key parameters.

Zhang et al. (2014) examined the behaviour of coke particles charged into the conical weighing hopper. The size segregation could be seen in the charging process. When the charging process was completed, it could be found that most of the small particles located near the top of the heap and some near the conical bottom wall, whereas many large particles are deposited at the surroundings of the heap. The reasons are because the small particles with low kinetic energy are apt to percolate through the matrix of large particles, whereas large particles can easily slide and bounce over the particle bed.

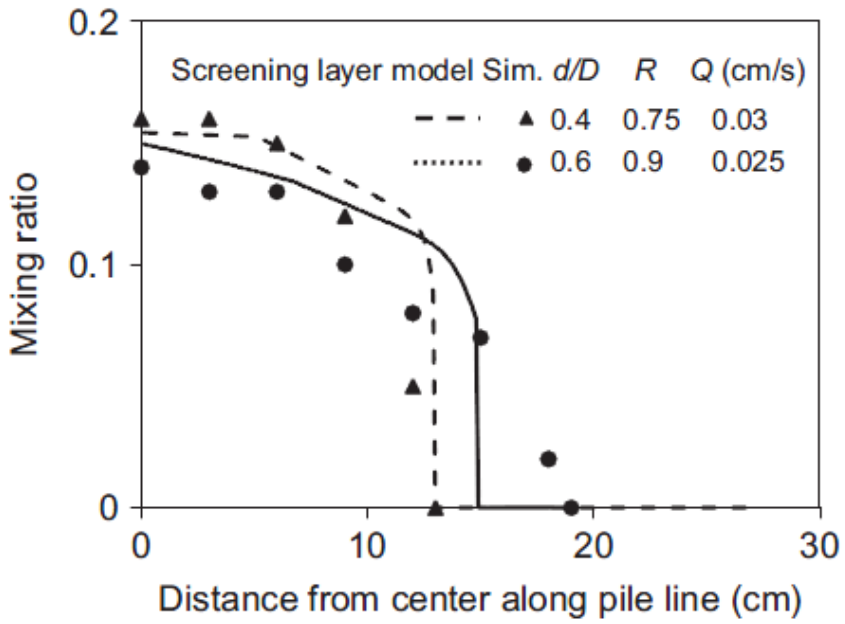

Figure 2-17 Variation of size segregation patterns with different ratios of particle diameter by DEM simulation. Reprinted from (Rahman et al., 2011), with permission from Elsevier.

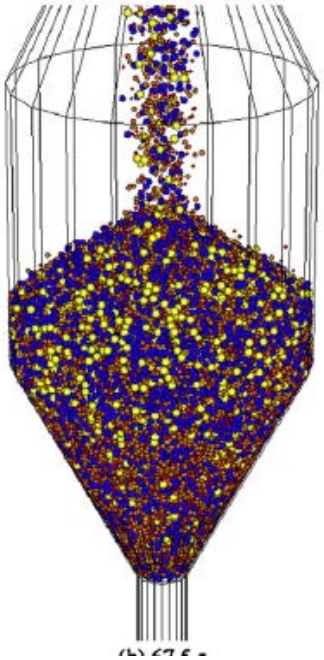

Figure 2-18 Snapshots of the particle behaviour in the weighing hopper during the charging phase. Reprinted from (Zhang et al., 2014), with permission from Elsevier.

2.4.3 Methods to minimise heap formation during filling

Three primary mechanisms may occur during the filling process, i.e. trajectory, sieving and fluidization (Mosby, 1996). The former two segregation mechanisms mainly appear due to the formation of the heap. Therefore, the best way to reduce segregation is to avoid the formation of a heap or cone during filling a silo or hopper (Clague and Wright, 1973). Recently, techniques used to prevent heap formation include the use of various types of distributors and inserts (Tang and Puri, 2004).

Two methods to prevent cone formation proposed by Garve (1925) were as follows. First one is to design a flexible spout, such as a conical distributor, star-like cone, branch pipe and conical sieve distributor. Their discharge end would always have to be on top of the material and moved around continually, to keep the top of the bin into several small heaps. Some of these tools are shown in Figure 2-19. Another way of preventing cone formation would be to use a continually rotating levelling device with

prongs or scrapers to level down the beginning of a cone before segregation sets in. However, such a device would be complicated because of the complex design, expensive fabrication, and costly operation.

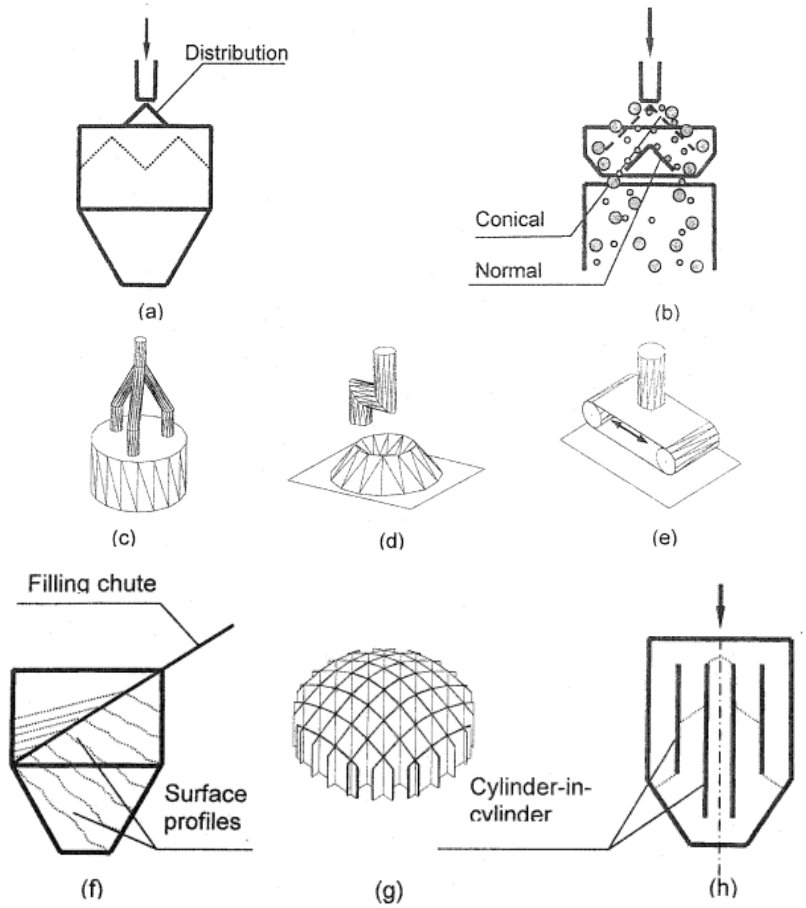

Note: (a) Conical distributor, (b) Conical sieve distributor, (c) Branch pipe distributor, (d) Rotating tube distributor, (e) Movable belt distributor, (f) Filling chute, (g) Egg-box insert, and (h) Cylinder-in-cylinder insert

Figure 2-19 Tools for minimizing segregation during filling. Reprinted from (Tang and Puri, 2004), with permission from Taylor & Francis.

2.5 Hopper discharging

2.5.1 Discharging flow patterns

Segregation of particulate solids in silos or hoppers cannot be discussed without reference to the discharge flow pattern that designates the order of withdrawal of the

contents of a silo (Engblom et al., 2012a). Segregation may be induced at silo filling, but the discharge flow pattern also affects the segregation observed at silo emptying, which is of primary interest in the majority of cases. Two main types of discharge flow patterns have been identified: mass flow and funnel flow. The concept of mass flow and funnel flow is first developed by Jenike et al. (1964). A simple illustration of different discharge flow patterns is shown in Figure 2-20.

Most of the previous and current research in the field of silo flow aimed at converting the flow pattern from funnel to mass flow, and some interesting findings in this area are discussed below.

(1) Mass flow

Figure 2-20 (a) gives a schematic illustration of mass flow. Mass flow is characterized by the movement of the entire silo contents whenever emptying occurs. The materials must be withdrawn from across the entire outlet area and can be achieved with steep and low friction hopper walls. The outstanding feature of mass flow and funnel flow is that no stagnant regions exist in the former one. Whereas the presence of dead materials regions is the unifying characteristic for all funnel flow silos.

This discharge pattern of mass flow was considered as inducing “first-in-first-out” withdrawal of the silo contents, however, this definition was not agreed by Bates et al. (1997). The reason for Bates’ postulation lied in the velocity gradients present towards the end of complete emptying in mass flow silos. Mass flow was usually associated with little or no segregation because materials from different radial positions were mixed at the outlet. Therefore, any horizontal or side-to-side segregation phenomena during filling were reoccurred for during emptying. The benefits of mass flow are to

avoid indefinite storage time, to allow materials flow through smaller outlets, to re-mix contents on discharge, to reduce the prospect of 'flushing' and to predict storage time and performance (Bates et al., 1997). But due to economic reasons or height limitation, most hoppers are not so designed.

(2) Funnel flow

Funnel flow is characterized by the presence of stagnant regions in the silo during discharge. There are several different forms. For instance, the flow can be restricted to a narrow pipe extending from the upwards outlet to the surface layers (Figure 2-20 (b)). Sometimes, the flow channel can be enlarged from the outlet and reached the silo walls below the surface of the bulk solid (Figure 2-20 (c)).

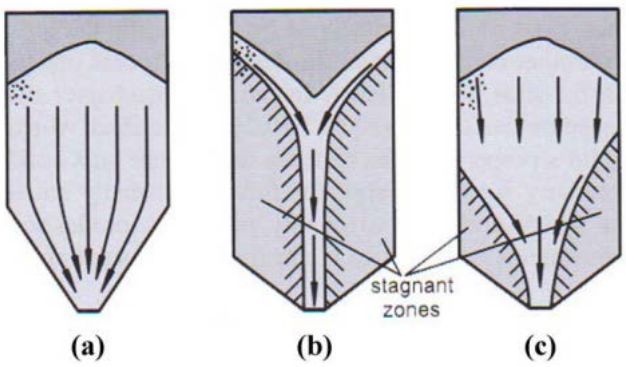

Figure 2-20 Illustration of different discharge flow patterns in silos: (a) mass flow; (b and c) funnel flow. Reprinted from (Engblom et al., 2012a), with permission from Taylor & Francis.

Funnel flow is sometimes referred to as "first-in-last-out" in order to differentiate it from the mass flow. But this is clearly an oversimplification. Compared with mass flow, funnel flow is caused by rat-holing and subsequent flooding of fine powders near the hole. With free-flowing particulate matter, the silo contents may segregate during funnel flow discharging due to the different velocities of the bulk solids.

(3) Conversion from funnel flow to mass flow

Several solutions have been proposed for achieving mass flow in silos with certain hopper angles. In the majority of cases, this is accomplished with the installation of an insert, a kind of flow obstruction, in the lower part of the silo, for examples, inverted cones, double cones, cone-in-cones. In the experiments, the tracer or marker objects have been utilized with success. These solutions reduce the requirement of headroom, but it is not a trivial task to design the inserts correctly to give mass flow.

Standish et al. (1988) examined the degree of mixing in bins in quantify level. He used the residence time distribution (RTD) to analysis mass-flow and funnel-flow patterns. Through tracer response curves and in particular, by the mean and variance of these curves, these flow patterns were readily characterised and quantified. In his experiment, hoppers with and without a flow-corrective insert were analysed respectively, as shown in Figure 2-21. From the figures, we can find that the flow pattern was completely changed with the insert placed in the bin.

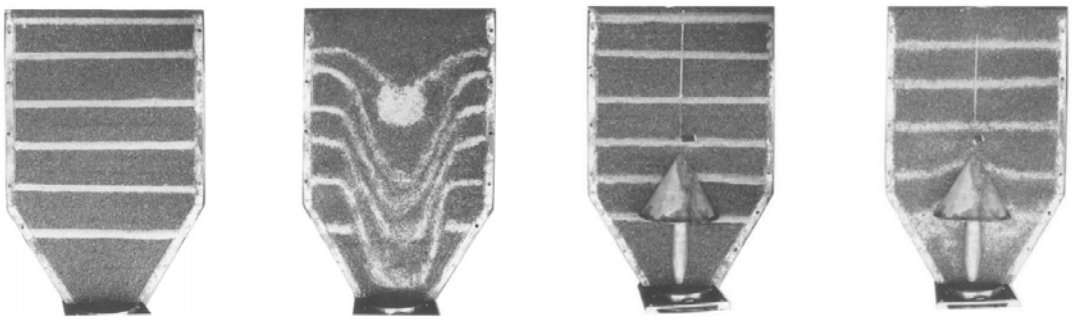

(a) (b)

Figure 2-21 Photograph of materials flow in the bin (a) without an insert; (b) with an insert. Reprinted from (Standish et al., 1988), with permission from Elsevier.

Aminaga et al. (1987) studied the effects of the flow pattern in the hopper with and without an insert on the concentration of discharged particles (Figure 2-22). Through

comparing the relative particle size to analyse the content of segregation. It was found that stone box could reduce size segregation and attribute to the improvement of solid flow during discharging.

At last, it was concluded that when aiming at the restraint of the size variation from the bunker, it is difficult to change the solid flow into plug flow during discharging by the installation of an insert in the bunker. For the restraint of the size variation from the bunker, the control of the size segregation during charging into the bunker is effective and one of the simple countermeasures is to install a stone box. The suitable size of the stone box was determined such that all of the sinters can collide with the stone box. The suitable position of the stone box was selected close to the upper surface of burden pile.

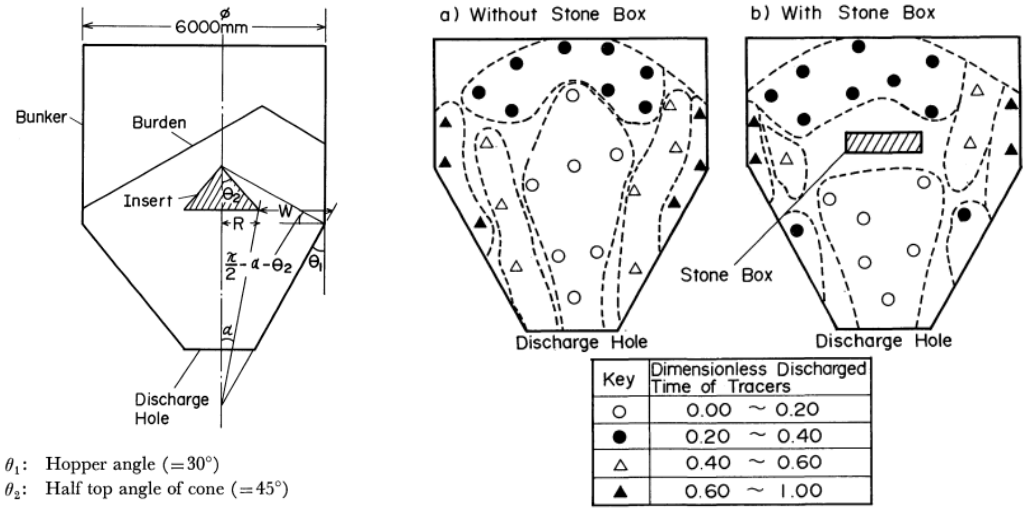

(a) (b)

Figure 2-22 (a) Design method of the suitable cone type insert in the bunker; (b) Effect of installation of the stone box on the discharge behaviour in the 1/10 scale model experiment. Reprinted from (Aminaga et al., 1987), with open access.

2.5.2 Physical experiments

As shown above, there has been significant research studied on heap formation and filling a bin or silo or hopper in last few decades. Recently, more researchers are

considering segregation appearing during the discharge of a silo or hopper through experimental methods and examine certain parameters inside.

Shinohara et al. (1970) investigated the mechanism of segregation and blending of particles when out of mass flow hoppers through calculation and experiments. A two-dimensional hopper was used for the flow test. This experiment was used to examine the screen or hypothetical-hoppers model, where small particles pass through the interspaces of large particles during flow. As a result, the patterns of segregation and blending are depending on variations in the mass flow rate and the mixing ratio with the elapse of discharge time (Figure 2-23). Mixing ratio changed with the initial mixing ratio and showed a different trend in a various weight ratio of large and small particles W_l/W_s, and diameter of small particles D_s.

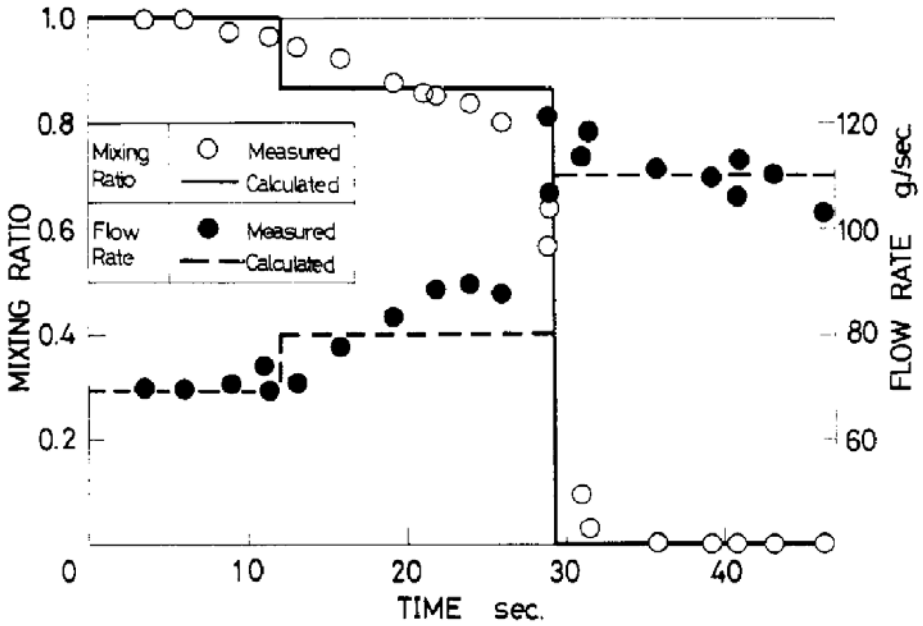

Figure 2-23 Experimental and theoretical results of mixing ratio and flow rate during discharging a two-dimensional hopper. Reprinted from (Shinohara et al., 1970), with permission from American Chemical Society.

Aminaga et al. (1987) and Kajiwara et al. (1984) investigated the particles handling process in the top bunker of a bell-less type blast furnace, including filling and discharging a hopper. Experimental apparatus is shown in Figure 2-15. In their study, it was relative particle size (RPS) rather than mixing ratio used to quantify the composition of the mixture and the content of segregation. Results showed that the influence of a stone box was little during discharging. Tanaka et al. (1988) also implemented a similar experiment with a stone box and the results were similar.

Most recently, Arteaga and Tuzun (1990, 1992) addressed a series of experiments to investigate segregation during discharging from a hopper. One (Arteaga and Tuzun, 1990) was mainly focusing on binary mixtures discharging from a mass flow hopper and funnel flow hopper. Materials they used were plastic granules, acrylic beads, turnip seeds and radish seeds every time with variable size ratios Φ_R and weight fractions X_f. Cumulative mixture discharge W/W_b normalized by expressing it in terms of a fraction of the original mass filling the hopper were used to express the discharging time. Then every kind of particles fraction was recorded at any time at both of these two flow patterns and X_i/X_f (change in the weight fraction of fines, measured concentration/ average concentration of the original fill) used to measure the extent of size segregation. Results showed that in the mass flow hopper segregation was much minimized with only a slight excess of fines during an initial transient. However, in the funnel flow hopper, segregation was much significant, with an excess of fines initially and also at the end of the discharge. Experimental results conform closely to the microstructural changes that occur within the particle bed; a transition from a coarse continuous to a fines continuous bed structure is made possible by the addition of more fines or by increasing the size ratio. A model was also developed by Arteaga and Tuzun (1990) based on the granular microstructure which delimits when segregation was feasible.

This model assumed that segregation of a binary mixture of spheres should stop once the surface area of the large spheres had been covered by small spheres, i.e. X_f was quite large, or the system becomes fines-continuous. Thus, segregation via percolation was said to only occur for fines fractions X_f less than a limiting value $X_{f,l}$, which is a function of only the particle diameter ratio Φ_D. It should be noted here that their proposed model was only available when the feasibility of segregation of spherical, free-flowing particles, and not the extent or rate at which segregation occur.

$$X_{f,l} = \frac{4}{4+\Phi_D} \tag{2-16}$$

Ketterhagen et al. (2004, 2007) performed a small experimental system with the same hopper dimensions and particle properties to validate their DEM model results. The experimental plexiglass cylindrical hoppers were shown in Figure 2-24.

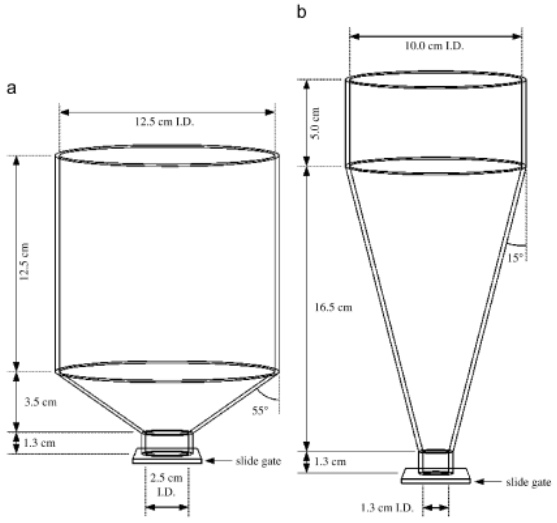

Figure 2-24 Schematic and dimensions of the experimental hoppers (a) 55 ^{o} and (b) 15^{o} for measuring sifting segregation. Reprinted from (Ketterhagen et al., 2007), with permission from Elsevier.

In this experiment, bidisperse glass spheres were utilized to test for sifting segregation. Particles were discharged from either a ‘mass-flow’ or ‘funnel-flow’ hopper design and collected transiently in equal volumes until the hopper was empty. Normalized fines

fraction was analysed with the elapse of the discharging time at both hoppers and various diameter Φ_D and initial fines fraction x_f. Last they found when filling in a hopper uniformly with bidisperse, free-flowing materials such as glass beads, these materials had an inherent tendency to segregate. For size segregation, several parameters had been shown to significantly affect the segregation during discharge and/or the internal flow pattern including the particle diameter ratio and fines mass fraction, the hopper cross-sectional shape and hopper angle, as well as the fill method and characteristics of the granular material. When investigating the regulation of normalised fines mass fraction changed with fractional mass discharged, a 'V' shape result was found for segregation.

2.5.3 Simulation methods

Ketterhagen et al. (2008) simulated the discharging process in a 2D model by DEM and the variables include fines mass fraction x_f and particle diameter ratio Φ_D, density ratio Φ_ρ, the ratio of hopper outlet width to large particle size were investigated. Only change one factor and fix others and then the trend of normalized fines mass fraction x_i / x_f with the elapse of discharging time defined here as fractional mass discharged M/M_{total}. Simply put, for various particle diameter ratios Φ_D, the composition is relatively uniform until the end of discharge where a slight excess of fines is discharged and segregation becomes more prevalent with the increase of diameter ratio, as illustrated in Figure 2-25 (a). For varying mass fraction of fines, the data shows that the extent of segregation becomes significant as x_f increases, and x_i / x_f varies in magnitude for the fines-depleted and fines-rich regions (Figure 2-25 (b)). It is approved that though percolation – a size dependent segregation mechanism – is dominant, there are no

obvious differences due to the particle density ratio. Dusting mechanism may produce a concentration profile with a large concentration of fines on the top surface.

Similarly, Yu and Saxén (2010) examined the mass fraction of fines m_f and the diameter ratio of coarse to fine. The concentration of fine particles in the system represent is low (e.g., less than 5%) the size segregation phenomena are minor, as shown in Figure 2-26. They depicted the extent of segregation by describing the mass fraction of each kind particle with the elapses of mass discharged.

The device or operational parameters that are mainly related to segregation are a shear strain, shear rate (or energy input), fall height, feed rate (filling/discharging), heap size, hopper size, hopper angle, and device surface finish. Some factors studied by DEM are shown as follows.

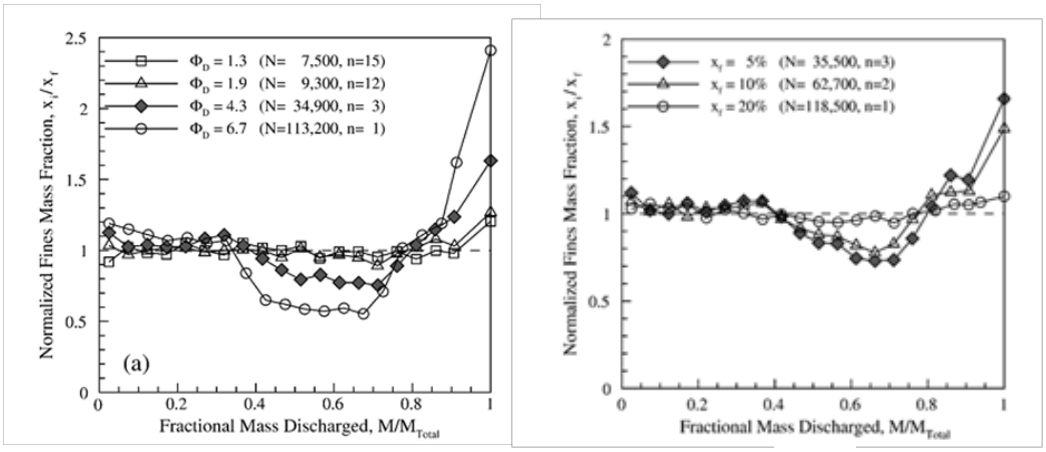

(a) (b)

Figure 2-25 Effects of materials properties on segregation. Reprinted from (Ketterhagen et al., 2008), with permission from Elsevier.

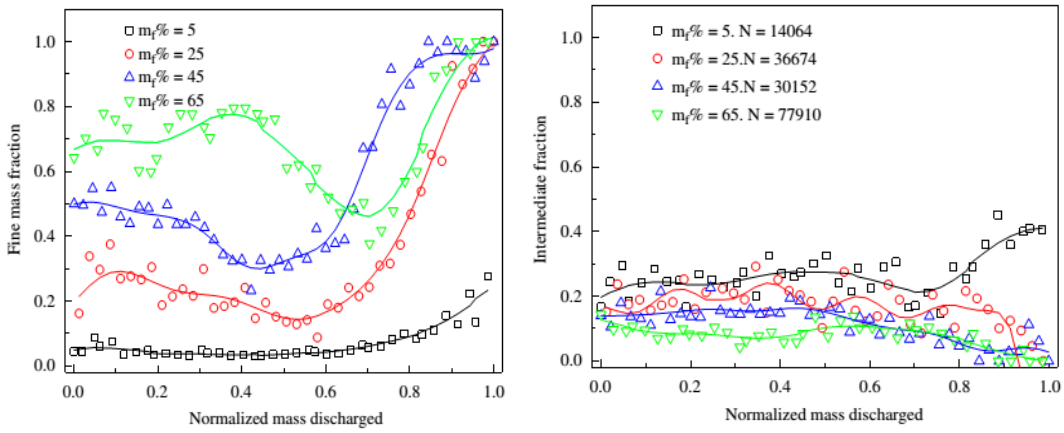

(a) (b)

Figure 2-26 Effects of mass fraction of fines on segregation. Reprinted from (Yu and Saxén, 2010), with permission from Elsevier.

Ketterhagen et al. (2008) investigated the effects of hopper wall angle, and particle diameter ratio Φ_D, density ratio Φ_ρ, the ratio of hopper outlet width to large particle size. Here the results show that making the hopper angle steep enough so that mass flow can be obtained, and therefore all the materials are induced to flow simultaneously and the velocity gradient is minimized (Figure 2-27 (a)). Next, various hopper fill heights and hopper weights are considered (Figure 2-27 (b)). The discharge is initially of uniform composition followed by a period of fines depletion and finally fines rich. Figure 2-27 (c) and (d) are about the effects of friction parameters. Smaller values of the particle-wall sliding friction tend to reduce the extent of segregation, although even with a small friction coefficient, segregation may still occur. Likewise, results show that smaller particle-particle sliding friction coefficients also reduce the extent of segregation.

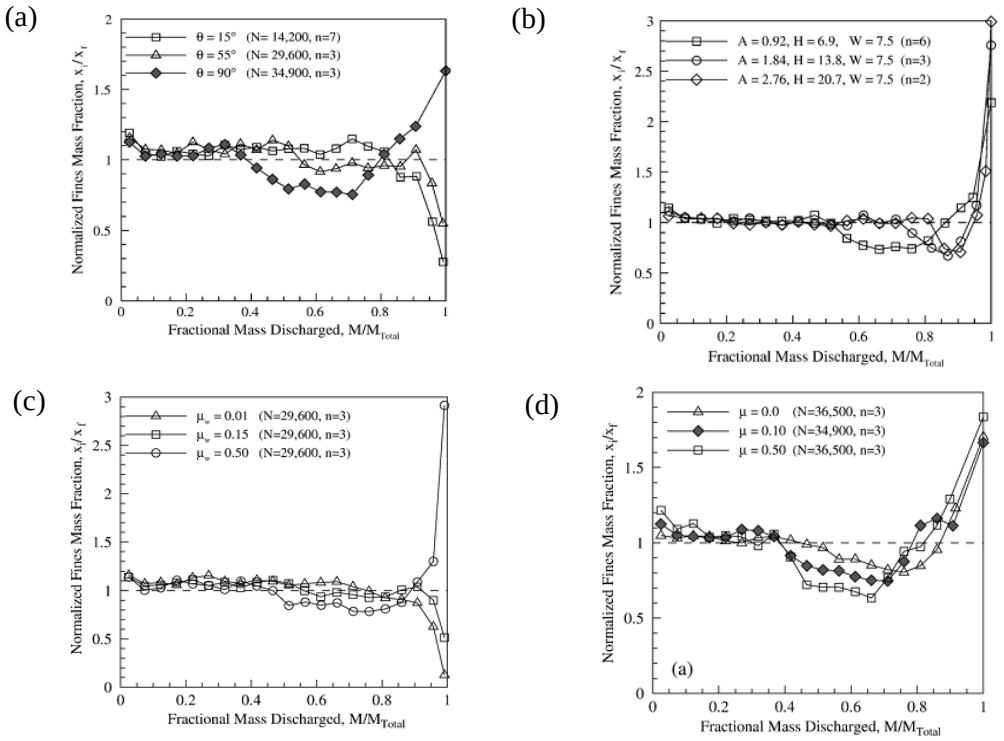

Figure 2-27 Effects of (a) hopper half angle, (b) hopper fill heights, (c) particle-wall sliding friction, and (d) particle-particle sliding friction on segregation. Reprinted from (Ketterhagen et al., 2008), with permission from Elsevier.

Yu and Saxén (2010) investigated experiment results and simulation results of three sampling methods with (1) coarse pellets in the bottom, fine in the middle and intermediate size in the top layer, (2) fine pellets in the bottom, coarse in the middle and intermediate size in the top layer, and (3) fine pellets in the bottom, intermediate in the middle and coarse pellets in the top layer. For layer-filling methods, the pellets in the bottom layer of the hopper flows out in a pattern resembling a laying 'S', while the fraction of the particles of the middle layer exhibit a W-like pattern during the discharge process, regardless of the particle size in the layer, as illustrated in Figure 2-28 (a). The outflow trend shown by the particles of the top layer is opposite that of the particles in the bottom layer. Many particle properties affect the segregation results. The extent of segregation was found to be affected mainly by wall-particles rolling and static friction (Figure 2-28 (b)). Inter-particle rolling friction has only an effect on segregation of fine

particles during the hopper discharging process. Reducing wall-particle rolling and static friction can reduce the extent of size segregation during the discharging process.

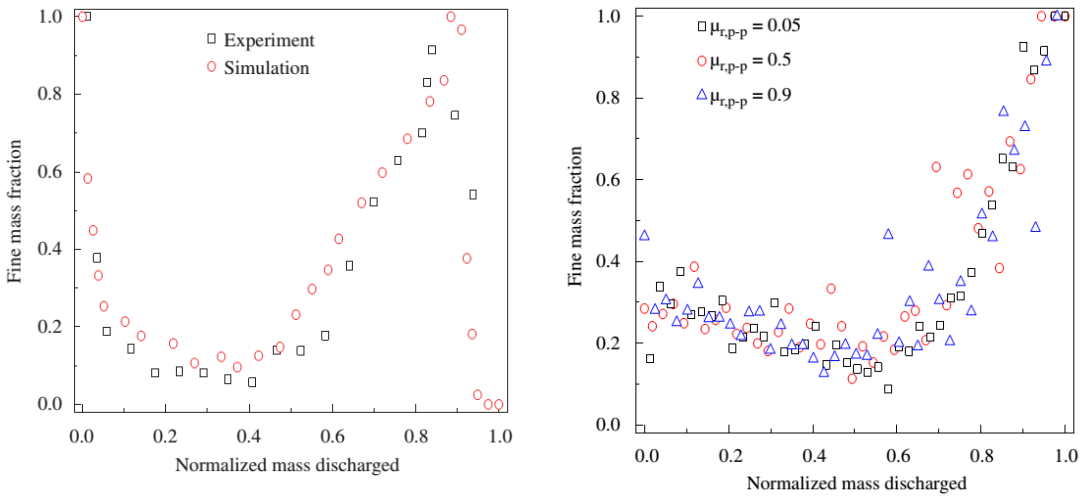

(a) (b)

Figure 2-28 (a) comparisons of experiment and simulation segregation results for hopper with filling method three, (b) Effect of inter-particle rolling friction on size segregation Reprinted from (Yu and Saxén, 2010), with permission from Elsevier.

The discharging sequence from the base hopper model is from bottom to top and from centre to wall. The sequence changes as the slope of the lower part of the hopper vary. The mass fraction of small particles in the feed and the burden apex has almost no effect on the discharging sequence.

2.6 Paul-Wurth hopper

Segregation may occur at several different parts of furnace burden system. Figure 2-29 is a schematic of Paul-Wurth (PW) top elevation of burden system. This system normally consists of parallel side by side PW hoppers discharging materials onto a rotating chute which then distributes the materials in the furnace. Both hopper and rotating chute are two primary positions where segregation occurs. In the past decades,

segregation phenomenon was reviewed by many researchers, and then mechanisms of segregation and models to predict segregation were studied. Meanwhile, some experiments were conducted to observe segregation phenomenon in a PW hopper. Recently, mathematical modelling by (DEM) was utilised to invest the essence of segregation. In the following, these contents are introduced separately.

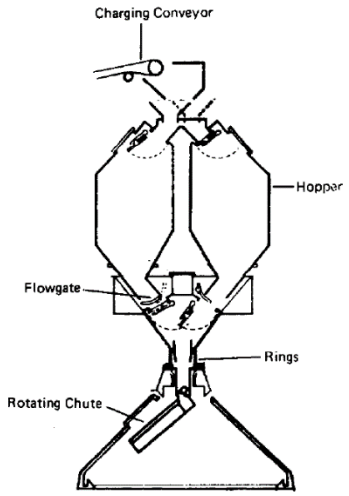

Figure 2-29 A blast furnace PW burden system. Reprinted from (Standish, 1985), with permission from Elsevier.

2.6.1 Physical experiments

For the application of a blast furnace charging system, most of the investigations focused on the effect of rotating chute (Xu et al., 2018, Xu et al., 2011, Gan et al., 2016) or the whole system by simulation methods. Only few research were carried out to study the segregation phenomenon in a PW type hopper. Standish (1985) carried out the experiments to study the segregation in a PW hopper and examined the distribution of particles in the hopper (Figure 2-30 (a)). But the filling positions were set as central and fixed, and the studies on the effects of operating conditions were not involved. For discharging process, segregation was observed with excess fines discharging initially

and coarse particles discharging later. The data showed a sinusoidal trend in the discharged fines fraction with total mass discharged, as shown in Figure 2-30 (b).

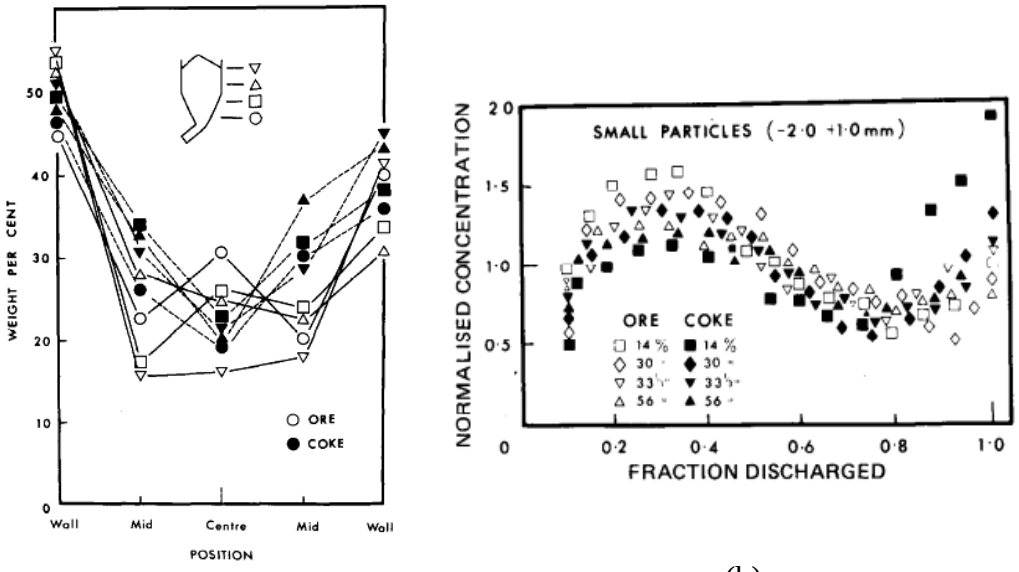

(a) (b)

Figure 2-30 (a) In-bin segregation during filling, (b) concentration at discharging process. Reprinted from (Standish, 1985), with permission from Elsevier.

Qiu et al. (2017) validated the simulation results with experimental results for mono-sized particles during the charging process of the PW hopper. When the orifice of the feeder hopper was opened, the experimentally used particles (soybean) fall into the PW hopper via the feed chute. The particles collide with the sloped wall of the hopper and flow down the bottom of the hopper at the beginning of charging process. The height of the heap increases with time until the heap with a peak is formed.

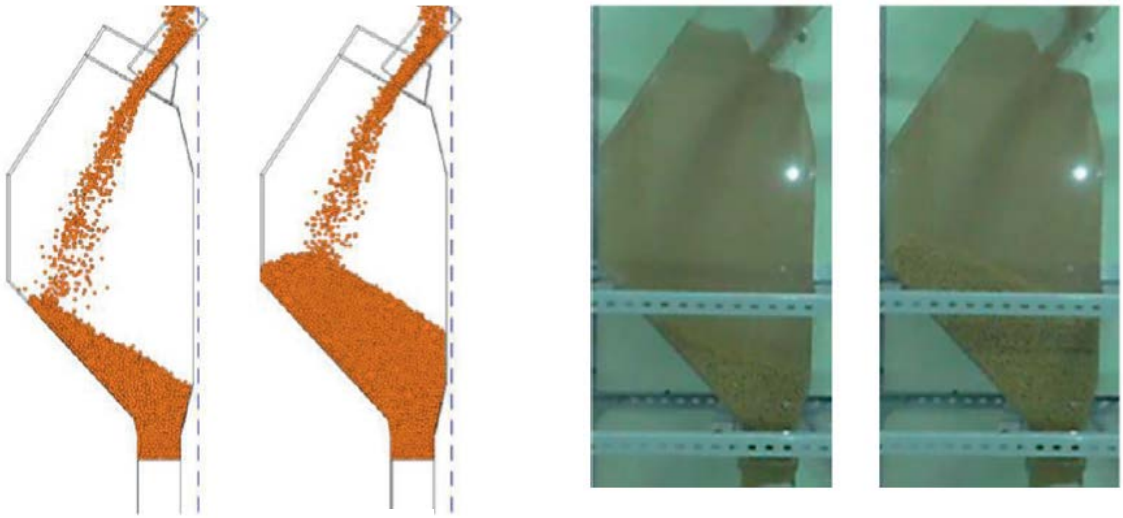

(a) (b)

Figure 2-31 Charging process in parallel PW hopper, (a) simulations; (b) experiments. Reprinted from (Qiu et al., 2017), with permission from Elsevier.

2.6.2 Simulation methods

By simulation method, most of the application of a blast furnace charging system focused on the effect of rotating chute (Xu et al., 2018, Xu et al., 2011, Gan et al., 2016) or the whole system.

Mio et al. (2009, 2010, 2012, 2017) built a simulator for the whole charging system and analysed the particle behaviour in a parallel hopper and the effect of chute angle (as shown in Figure 2-32 and Figure 2-33). They approved that the nut coke moved to the upward in the sintered ore particle layer during discharging because of the particle segregation when moving to large bell from the quad-hopper. Because the speed was large when the nut cokes began to discharge, their relative positions moved downward when they were segregated at the top. Results illustrated that the relative radial distribution of the nut coke particles was not affected by their positions in the large bell and the total mass. Thus, keeping the surrounding balance of nut coke mass in the large

bell was very important. The position of nut coke particle had a minor influence on the segregation of sintered ore and the radial distributions of relative charged mass for all conditions were similar.

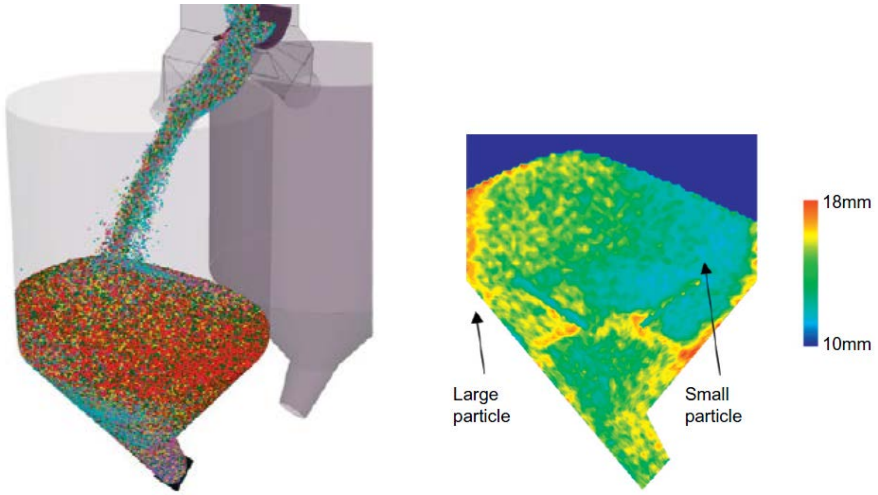

(a) (b)

Figure 2-32 (a) Snapshots of particle behaviour and (b) mapping of mass-based mean particle size in the parallel hopper. Reprinted from (Mio et al., 2012), with permission from Elsevier.

Wu et al. (2013) studied the size segregation phenomenon accompanied charging into and discharging from a Paul-Wurth type hopper at a bell-less top blast furnace. Based on the discrete element method (DEM), a three-dimensional model (Figure 2-34) is established in this work to investigate the effects of various variables on particle size segregation in and out of the hopper, as well as on the discharging sequence. Differently, the mass fraction of small particles in the feed, the burden apex, and the slope of the lower part of the hopper was the highpoint variables in this article. However, the segregation along the radial direction was not significant which might be caused by large size distribution and small particle numbers, and this was not agreed to the practical production which bears serious segregation.

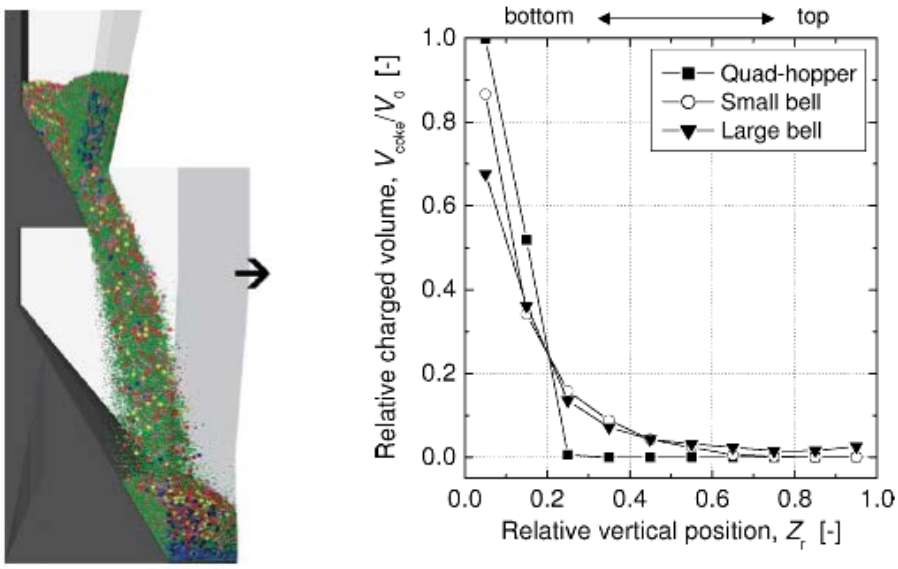

(a) (b)

Figure 2-33 (a) Snapshots of particle charging behaviour from the small bell to the large bell; (b) Relation between the relative charged volume of nut coke and the relative vertical position. Reprinted from (Mio et al., 2010), with open access.

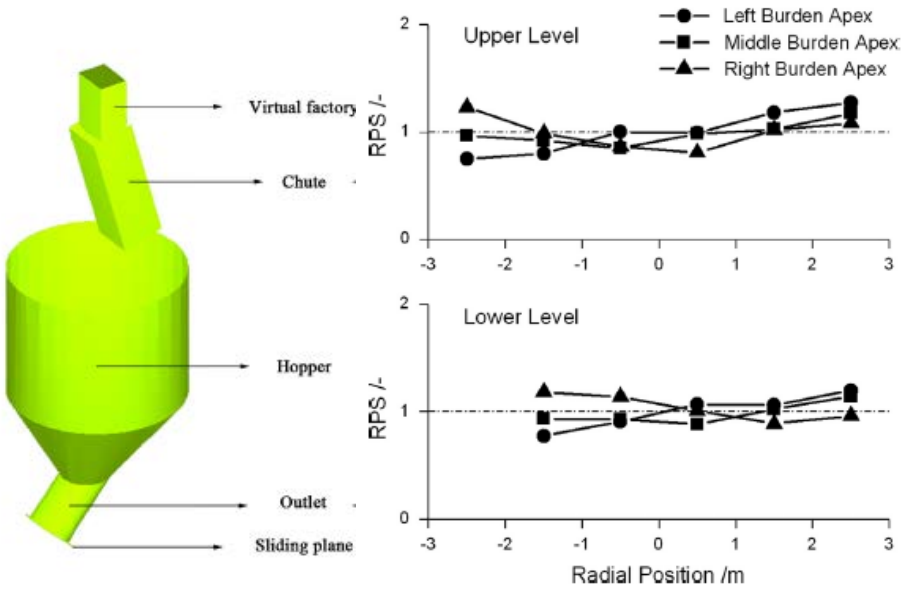

(a) (b)

Figure 2-34 (a) Schematic diagram for the simulated hopper; (b) Effect of burden apex on RPS in the hopper. Reprinted from (Wu et al., 2013), with permission from Elsevier.

2.6.3 Wall pressure

In addition, wear of the hopper concerns on the lifetime and safety products in the process. But the wall stress analysis has been studied for mono-sized particles by experiments and DEM (Qiu et al., 2017), ellipsoid particles by DEM (Liu et al., 2014) and mono-sized particles by finite element method (FEM) (Zheng and Yu, 2015, Wang et al., 2014).

Qiu et al. (2017) investigated the influence of the particle-wall sliding friction coefficient on the wall pressure. Results showed that with the increasing the particle-wall friction coefficient, the transmission of particle stresses decreases for the right side wall. A similar variation tendency of the normal and tangential forces can be observed for the left wall. Moreover, it was found that with the increase of rolling friction coefficient, the wall normal force increases.

Liu et al. (2014) calculated the wall stress as the normal contact force between particles and vertical side wall for ellipsoid particles with different aspect ratio. It could be observed (Figure 2-35 (b)) that for ellipsoids excluding the case of aspect ratio 3.0, wall stress reached the first peak (e.g. 2800 Pa) at height 0.3 m, then decreased significantly to 2100 Pa at height 0.15 m. Further, wall stress increased again sharply, they may reach the second peak. Spheres experienced the largest wall stress, and this value decreased for flat or elongated particles. This is because the ellipsoidal particles near the side wall prefer a horizontal orientation, and tend to maintain the local ordered structure.

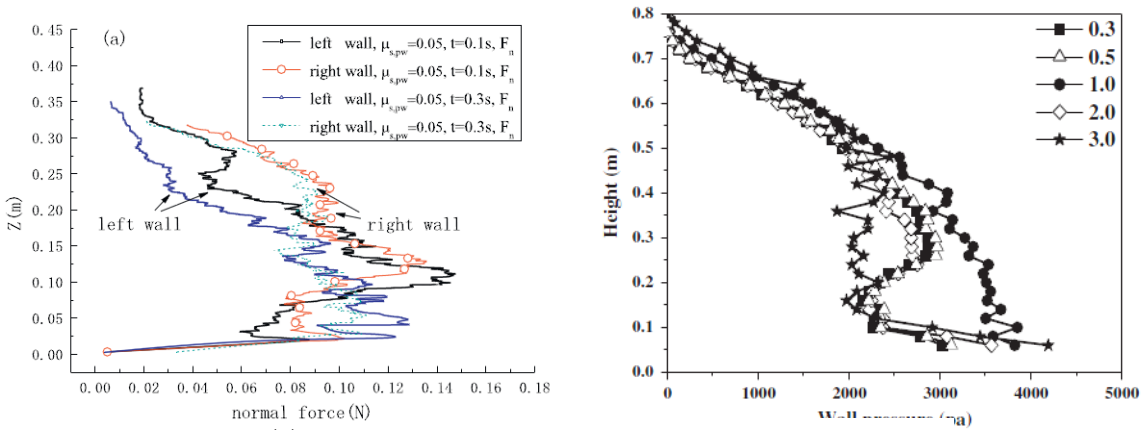

(a) (b)

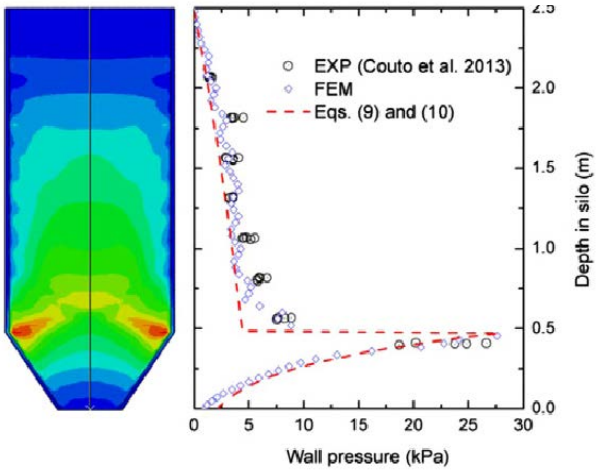

(c)

Figure 2-35 (a) Normal forces acting on the left wall as compared to the right wall during discharge for a certain sliding friction coefficient. Reprinted from (Qiu et al., 2017), with permission from Elsevier; (b) wall stress distribution with hopper height for various shapes. Reprinted from (Liu et al., 2014), with permission from Elsevier; (c) Comparison of silo pressure between experiment, current FEM simulation at discharge time of 0.5 s, and theoretical correlations. Reprinted from (Zheng and Yu, 2015), with permission from Elsevier.

It is not sure whether the wall pressure distribution is same for binary mixtures and mono-sized particles. Therefore, for the binary mixture, the factors such as operating conditions including filling positions and angles and wall stress which are related to the practical application, still need to be taken in to account to predict the size distribution

during charging and discharging a PW hopper and provide the corresponding methods to reduce segregation.

2.7 Summary

From the review on segregation both from physical experiments and numerical modelling, we can find that many factors, including materials properties, device and operation parameters, and handling processes etc. are studied in different apparatuses and various models. Although some experimental work has been investigated in last decades, the ideal materials and small-scale devices are the limits for analysing the basic mechanism of segregation, thereby numerical modelling, especially DEM, is a primary method to study this phenomenon. However, only several articles are considering segregation taking place during filling in and discharging from a hopper by DEM as the key task. To systematically examine the effect of sliding and rolling friction coefficients during filling process is still lacking. Flow of mixture with large size ratio is limited due to the computational capacity. In addition, the application guideline of DEM on filling and discharging from a PW hopper attracts our attention. Hence, extra work on segregation should be studied.

This project applies DEM approach to investigate the segregation during sandpile, hopper filling and discharging process to find the fundamental understanding of segregation. The specific objectives are as followed:

(1) Study the effects of particle properties such as sliding and rolling friction coefficients, and the moisture contents of water on piling process (chapter 3), and aim to examine the basic mechanism of the piling process and investigate the relationship of the structure and forces;

(2) Study microscopic parameters and the effects of sliding and rolling friction coefficients and volume fraction on segregation extent (chapter 4), and aim to explore the segregation phenomenon by velocity, cluster size and particle mixing index during the filling process and establish a contour plot and a correlation to illustrate of the filling process;

(3) Study the effects of size ratio and hopper angles on hopper discharging process (chapter 5), and aim to identify the percolation mechanism in the gravity system of large size ratio and to explore the influence of the structure properties, such as porosity, cluster size and the contact number ratio on particle distribution;

(4) Study the influence of different filling angles and positions on particle distribution (chapter 6) in a Paul-Wurth hopper, and aim to provide a meaningful suggestion to the industry on minimizing the segregation extent.

CHAPTER 3 NUMERICAL ANALYSIS OF SIZE SEGREGATION OF GRANULAR MATERIALS IN SANDPILE FORMATION

3.1 Introduction

When granular materials are poured onto a horizontal surface, a sandpile forms. It is one of the typical systems widely encountered in many industries dealing with particulate materials ranging from flours, coal and sinters to concretes and medicines. Sandpile is a simple particulate system for theoretical studies and much attention has been made to understand the different phenomena such as stress dip under the pile (Zhou et al., 2003, Zhou et al., 2014, Luding, 1997), stratification (Makse, 1997, Makse et al., 1997b), avalanching at the surface (Alexander et al., 2006) and self-organisation(Frette et al., 1990). In the past decades, sandpile formation process has been studied thoroughly (Makse 1997) and simulations (Meakin and Jullien, 1992). Among them, a granular dynamic simulation such as discrete element method (DEM) considers not only the geometrical factors but also the forces involved in the formation of a sandpile, and hence has been widely employed (Zhu et al., 2008). Microscopic parameters such as forces and structures, which are essential for understanding the fundamentals, can be readily obtained in the DEM simulation.

Angle of repose of a sandpile is one of the most important properties, and the investigation on the angle of repose by DEM has been implemented on mono-sized spheres (Zhou et al., 2001), ellipsoid particles (Zhou et al., 2014) and cohesive mono-sized particles (Dong et al., 2013) etc. It is generally believed that the angle of repose has the close relations with particles surface properties such as sliding friction coefficient (Lee and Herrmann, 1993, Liu et al., 2015) and rolling friction coefficient (Zhou et al., 2001), and the particle size (Carstensen and Chan, 1976) and shape (Zhou et al., 2014). However, for sandpiles composed of different species, the effect of particle properties with two different angle of repose is still not fully examined. Among them,

most of the study uses experiment and theoretical models (Shimokawa et al., 2015, Fan et al., 2012). The investigation of the effects of particle properties on the angle of repose by DEM is still lacking, particularly the piling process of particles with different sliding friction coefficients and rolling friction coefficient

On the other hand, particles are often not dry, and water or moisture content might have a significant effect on packing properties, as demonstrated in the literature (Anand et al., 2010, Yang et al., 2007, Dong et al., 2012). The cohesive force (or so-called capillary force) between particles formed by the liquid is caused by surface tension due to the liquid bridge between particles. Some experimental and theoretical studies have been conducted by Samadani and his colleagues (2001, 2002, 2005). For example, the angle of repose and segregation degree was analysed under different liquid types. Results presented that the angle of repose of the granular matter was observed to increase sharply as the volume fraction of the fluid was increased and then saturated. Meanwhile, a maximum angle of stability was proposed by Mohr-Coulomb model for a wet granular pile. However, the structure, forces and their relationship inside the pile of cohesive particles which are essential for a deep understanding of the segregation mechanism are still needed. Some attempts have been made by some researchers on rotating drums (Liu et al., 2013) and the piling process of mono-sized particles (Dong et al., 2013). The structure and forces analysis of the binary cohesive mixture on a piling process still need to be considered.

The aim of this work is to explore the changes of angle of repose in the piling process for dry particles with different sizes firstly. Then the piling processes for dry particles with different sliding and rolling friction coefficients are simulated and compared. At last, the effect of volumetric moisture content on the structures of wet particles pile is

explored. The relationship between the structure and forces is established by fitting correlations.

3.2 Theoretical treatment

3.2.1 Discrete element modelling

In a discrete element method (DEM) simulation, an explicit numerical scheme is used to trace the motion of individual particles in a considered system. A particle has two types of motions, which are the translational and rotational motion. These are described by Newton's second law of motion (Cundall and Strack, 1979). During the movement, the particles may have collisions with their neighbouring particles or the hopper wall, through which the momentum is exchanged. At any time *t*, the governing equations (Zhu et al., 2007) for translational and rotational motions of particle *i* in the system are:

$$m_i \frac{d\mathbf{v}i}{dt} = \sum_{j=1}^{k}\left(\mathbf{f}_{c,ij} + \mathbf{f}_{d,ij} + \mathbf{f}_{cohe,ij}\right) + m_i\mathbf{g} \tag{3-1}$$

$$I_i \frac{d\boldsymbol{w}i}{dt} = \sum_{j=1}^{k}(M_{t,ij} + M_{r,ij}) \tag{3-2}$$

where $\mathbf{v}_i$ and $\boldsymbol{\omega}_i$ are the translational and angular velocities respectively of particle *i* with mass m_i and moment of inertia I_i. The forces considered are gravitational and particle-particle interaction forces including elastic contact force $\mathbf{f}_{c,ij}$ and viscous damping force $\mathbf{f}_{d,ij}$ in both normal and tangential components at the contact point. The capillary force between particles *i* and *j* is also considered for a system with wet particles. The torque acting on particle *i* by particle *j* includes two components. One is generated by tangential force and causes particle *i* to rotate, $\mathbf{M}_{t,ij}$, and rolling friction torque $\mathbf{M}_{r,ij}$ generated by normal force that acts to oppose the relative rotation between the contacting particles. For a particle undergoing multiple interactions, the individual

interaction forces and torques are vectorially summed for the k_i particles interacting with particle i. Equations except for capillary force, used to calculate difference forces and torques are referred in Zhou et al. (2005)..

For wet particles, the capillary force due to the formation of a liquid bridge between two adjacent particles can be calculated by numerical solution of the Laplace-Young equation (Orr et al., 1975, Lian et al., 1993, Chen et al., 2011, Lian and Seville, 2016). However, this kind of analytical solution is complex based on different approximations. Several simple expressions are proposed by using Derjaguin approximation. One equation for unequal spheres is written as (Willett et al., 2000):

$$F_{cohe,ij} = 2\pi R_{ij}\gamma \frac{R_{ij}(1-\cos\beta)\,cos\varphi}{R_{ij}(1-\cos\beta)+2S} \tag{3-3}$$

where, R_{ij} is the harmonic mean radius of particles i and j, $R_{ij} = \frac{R_i R_j}{R_i+R_j}$. $2S$ is the distance between two particles. γ is the surface tension. φ is the contact angle. β is the half-filling angle, which can be obtained by $V = 2\pi S R^2 sin^2\beta$. V is the volume of the moisture between two particles. The relationship between V and the normalized moisture content V^* is $V = V^* \times R_{ij}^3$. The effect of particle roughness on the capillary force is complex. To simplify this process, the liquid is assumed to be distributed evenly among particles and not transferable among them. Therefore, the liquid content between each pair particle contacts is only related to the input volumetric moisture content, and by calculating a different distance, an half filling angle could be determined. Once when the distance between two particles exceeds rupture distance, the liquid bridge and capillary force be removed. This rupture distance is defined as (Willett et al., 2000):

$$2S_c = \left(1 + \frac{\varphi}{4}\left(\frac{R_j}{R_i} + 1\right)\right)\left[V^{*1/3} + \left(\frac{R_j}{R_i} - \frac{2}{5}\right)V^{*2/3}\right]R_{ij} \quad (3\text{-}4)$$

3.2.2 Simulation condition

The dimensions of the simulation domain are shown in Figure 3-1. It is a slot type rectangular box with periodic boundary condition applied in the front-rear direction, which has a thickness of 2 d_p (where d_p is the diameter of large particles). Particles are first generated from the left top region at a certain number fraction of large and small particles. Then they are packed under gravity. The particle properties used in the simulation and the geometry parameters are listed in Table 3-1. The sliding friction coefficient and rolling friction coefficients range from 0.1 to 0.9 and 0.001 d_p to 0.1 d_p, respectively. The volumetric moisture content ranges from 0.1% to 10%, which is normalized by total particle volume.

3.3 Results and discussion

3.3.1 Sandpile formation process

The sandpile flow pattern is first validated with the experimental results proposed by Benito et al. (2013). In the experiments, glass beads with size 3 mm and 1mm were poured into a bi-dimensional plexiglass cell and a pile is formed. Figure 3-2 shows the comparison of physical experimental (a) and simulation results (b). The operation conditions are similar, and the particle size ratio and the properties are same. It can be found that the angle of the pile is similar. Meanwhile, both have several strips of large particles between the junction of large and small particles, where stratification reveals. The movement of large particles on the surface is also similar, which occupy most of the surface. The slope angles are similar except for the bottom part of the pile; this might be caused by the relatively small total particle number. It can be concluded that

general good agreement confirms the validity of the present DEM model. On this basis, the DEM model can be used to examine the mechanism and the effects of different variables.

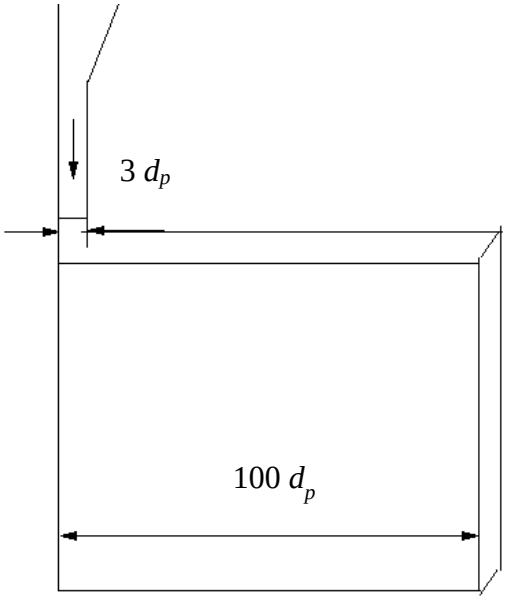

Figure 3-1 Schematic geometry of the simulation domain. Note that d_p is the diameter of large particles (3 mm).

Table 3-1 List of parameters used in DEM simulation

Parameter	**Value**
Particle size, d	3 mm, 1 mm
Particle density, ρ	1050 kg/m^3
Volume fraction	Large particles 50%, Small particles 50%
Total particle number	10392
Young's modulus, Y	1×10^7 N/m
Poisson's ratio, σ	0.3
Sliding friction coefficient,	0.1, 0.3, 0.6, 0.9
Rolling friction coefficient,	0.001 d_p, 0.01 d_p, 0.025 d_p, 0.05 d_p, 0.10 d_p
Surface tension, γ	0.72 N/m
Contact angle, φ	0^o
Volumetric moisture content, V_f	0.1%, 1%, 3%, 10%

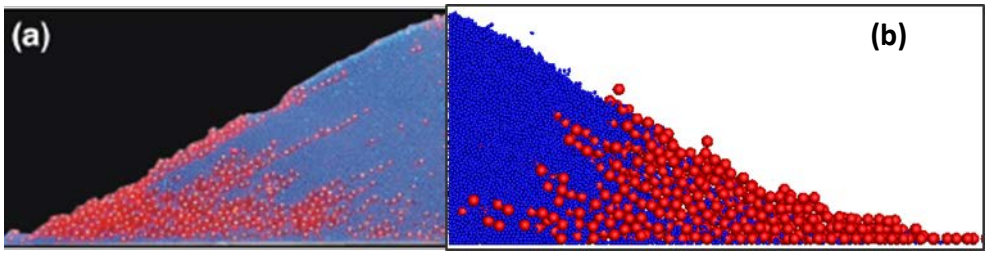

Figure 3-2 Flow patterns of (a) physical experimental results, (b) simulation results. Reprinted from (Benito et al., 2013), with permission from Elsevier.

The snapshots during the piling process are shown in Figure 3-3. Note that particles (including large and small particles) are generated at a fixed rate and fixed volume fraction in the tube (Figure 3-1), then fall by gravity and pack on the bottom surface. From Figure 3-3, it can be found that segregation happens. At the beginning t =1.72 s, some of the large particles roll far away and the remaining of them stay on the top of the small particles. The angle of the slope is around 12^{o}. With the increase of the pile height, large particles cluster appears at the edge of the pile at t =3.44 s. From then on, the slope angles keep increasing. At t =8.59 s, the surface of the pile is divided into two parts, the upper pile is the surface with a series of small particles and the lower pile is the other part with a series of large particles. Large particles cannot stay on the small particles and roll down to the lower pile.

Note that during the process, the angles of the upper pile and lower pile are different. The variation of both angles is traced during the process, and shown in Figure 3-4 (the top figure). The upper pile is smooth and the angle of repose could be obtained easily. While the lower pile full of large particles are non-smooth, with several small turning points. An estimated angle is gained here. It can be found that there are four-time points (t = 1.63 s, 6.80 s, 12.01 s, 17.80 s) where upper pile and lower pile have the same angles. At these time points, large particles occupy more surface area than other times,

showing a stratification here. It can be found that the intersection point between large and small particles changes with time. To quantify this difference, a turning point (TP) showing the distance between the left wall and the intersection point is marked and illustrated in Figure 3-4 (the bottom figure). This TP shows a similar trend in each loop. It increases at first and then decreases to a relatively small value in the adjacent area. The increase of the TP corresponds to the platform in flow pattern (an arrow in Figure 3-3). This platform appears due to the friction between the large particles and the surface and the packing of the bottom large particles. After the formation of these points, the angle of upper pile always increases a little and keeps same. The angle of lower pile always decreases a little and then increases to catch the angle of upper pile. From Figure 3-3 and Figure 3-4, it can be concluded that the whole process is a repeat of each loop.

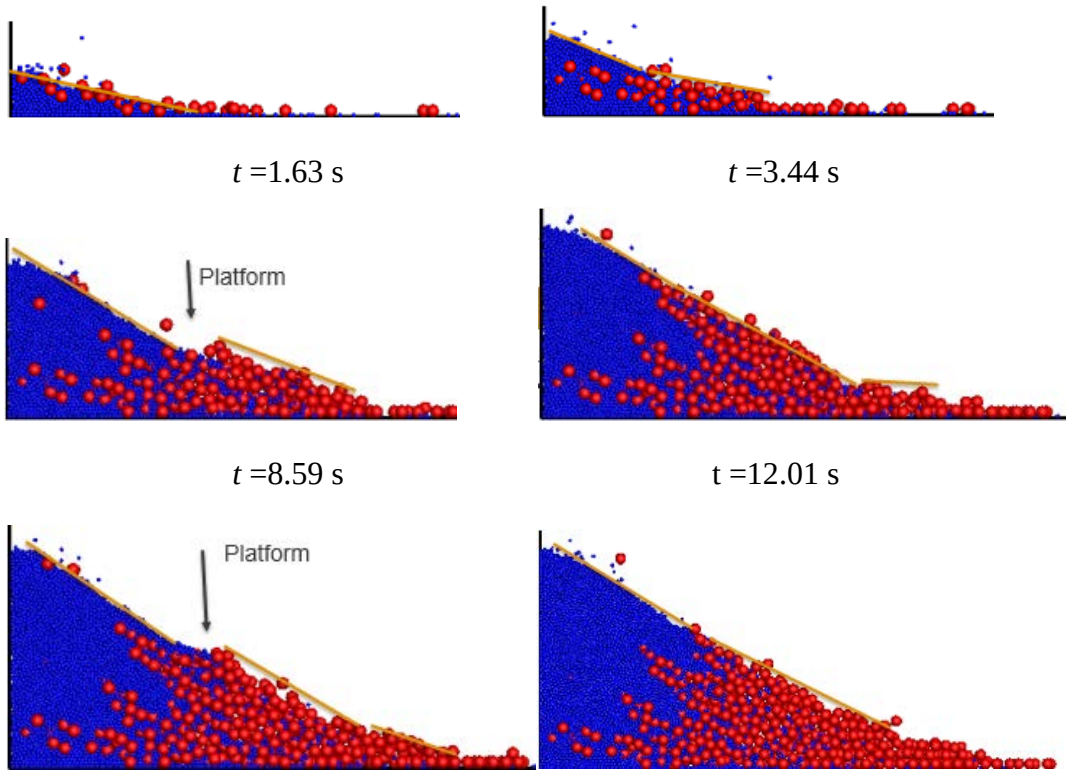

t =1.63 s *t* =3.44 s

t =8.59 s t =12.01 s

T =13.73 s t =17.80 s

Figure 3-3 Flow patterns of sandpile formation process for two types of particles with different sizes.

One loop from t =12.01 s to 17.80 s is chosen for a further analysis of segregation and stratification occurrence in sandpile formation process. The particles packing could be seen from the coloured particle ID number, as shown in Figure 3-5. The particles ID number shows the sequential order of particles generated. It can be found that most of the small particles are in the left part and the upper slope. Four layers of different colours are regularly distributed. Different from small particles, large particles have irregular distribution. Three-layer particles are like a base, supporting the last layer on its top, where the large particles stripe appears. Large particles behaviour is the main reason for segregation and stratification.

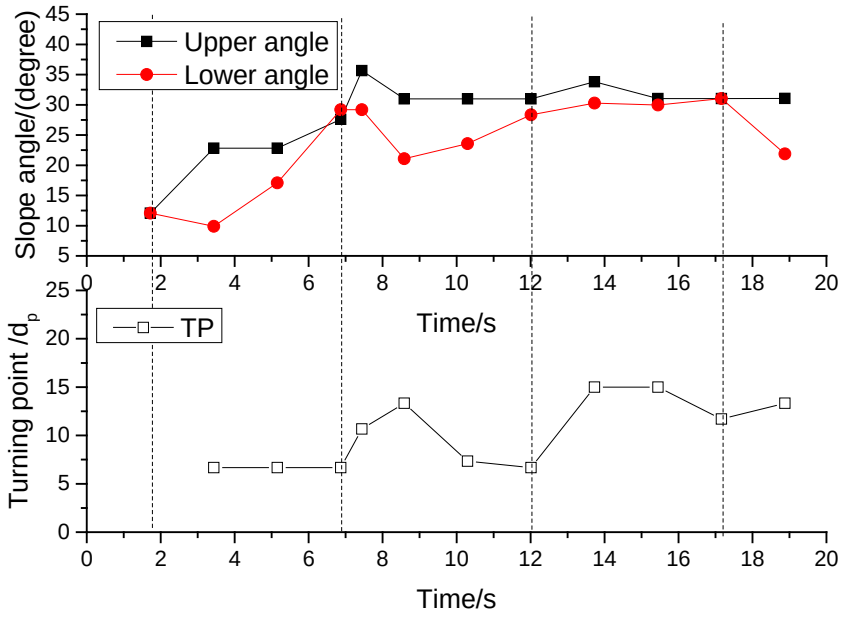

Figure 3-4 The slope angle of the upper pile and lower pile change with time (top) and the distances to the left wall of turning points 1 and 2 (bottom).

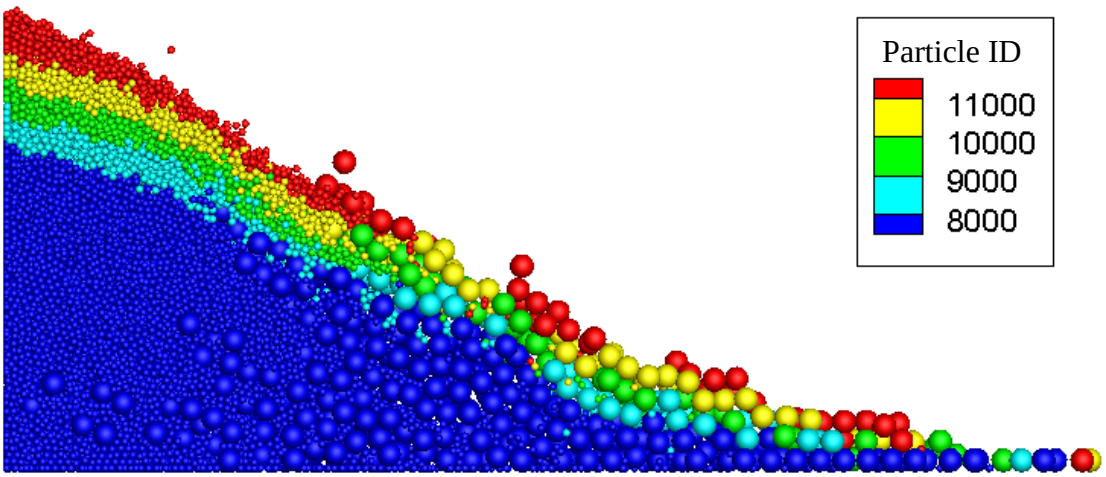

Figure 3-5 Coloured particles pattern showing the flowing sequence during t = 12.01 s to 17.80 s.

To see how large particles travel and stop during the process, the trajectories of several large particles and their clusters are drawn in Figure 3-6 and Figure 3-7. Note that the cluster is defined as the group of particles in contact with the core particle at stopping time. Two particles (ID=8532, and 8586) are randomly chosen as examples. From the trajectories in Figure 3-6 (a) and (b), it can be found that both particles roll down the upper slope at the initial stage (t_{a1} and t_{b1}). When they first encounter a platform formed by large particles, which is a suitable place with a deep turning curve to make particles steady, particle 8532 stops (t_{a2} and t_{a3}) due to a collision with another large particle on the platform. On the contrary, particle 8586 climbs over the small hill and continue rolling down until another platform to stop (t_{b2} and t_{b3}). This is because of its initial velocity. It means that it is not only the difference between slope angles and particle angle of repose which determines the particles' movement but also the initial status such as its velocity. This is different from the theory proposed by Maske et al. (1997a) and Boutreux et al. (1998), which mainly consider the effect of the angle difference. It can be concluded that when the slope has a platform generated by steady particles, a

moving large particle might stop depending on its velocity at that time. With small velocity and suitable support, particles would stop (t_{a2} and t_{a3}, t_{b4} and t_{b5}). On the contrary, with large velocity, particles would bounce higher along the easiest movement direction related to the geometrical mechanism proposed by Dasgupta et al. (2011).

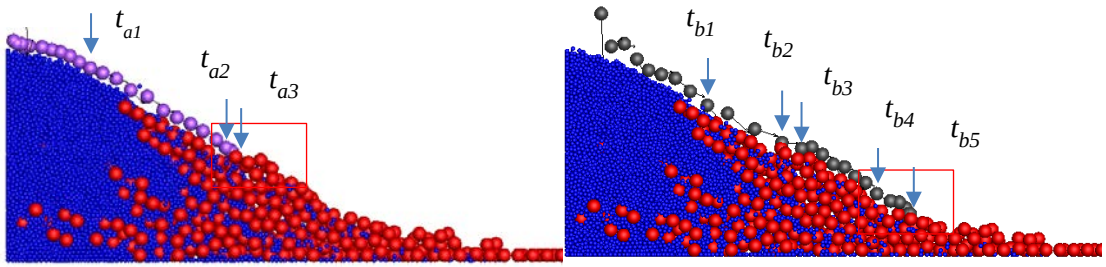

(a) Particle 8532 trajectory (b) Particle 8586 trajectory

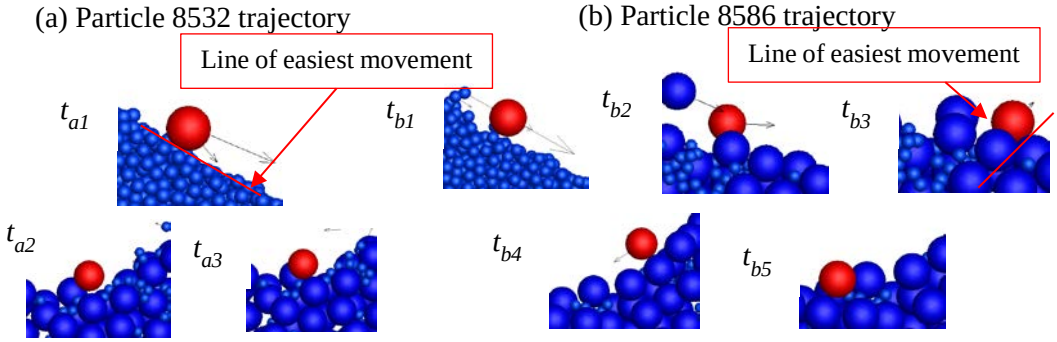

(c) Demonstration of velocity vectors and slope structure at different time steps. (Note that t_{a2} and t_{a3}, t_{b4} and t_{b5}, are the back view of XZ direction)

Figure 3-6 (a) and (b) the trajectory of two randomly chosen large particles; (c) demonstration of velocity vectors and slope structure at different time steps.

When the particles stop, the structure of the clusters providing support is similar. A turning curve shown as a platform can be found from both flow pattern and the force chain (shown in Figure 3-7 (a) and (b)). It can be observed that most of the branches of the force chains are leaking to left, the direction of the fill-in positions, illustrating how particles are packed during piling process. The number of particles contacting with the core one is three, and the shape of force network is a tetrahedron, as shown in Figure 3-7 (c) and (d). This is a 3D representation of stable position with necessary supports. It can be found that only when the slope has a turning curve, where the moving particle

could have a collision with the steady particle, and then the moving particles turn to the steady particles. The other large particles have similar moving principles.

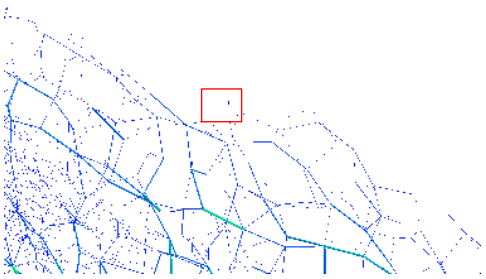

(a) Force chain in Figure 3-6 (a) square

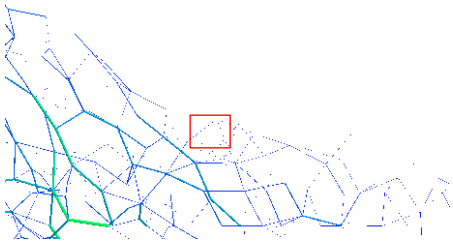

(b) Force chain in Figure 3-6 (b) square area

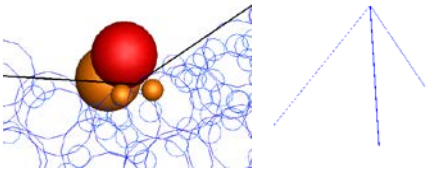

(c) Core particle 8532 cluster and force network when it stops (180°

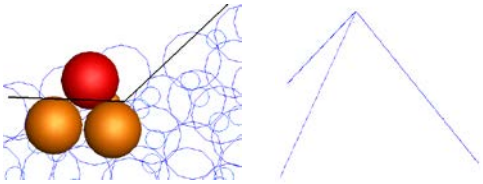

(d) Core particle 8586 cluster and force network when it stops (180°

Figure 3-7 (a) and (b) force chain of the marked area in Figure 3-6; (c) and (d) the 3D representation of the cluster showing the contacts neighbour at stopping time.

3.3.2 Effect of particle property on segregation

The analysis above is based on the assumptions that particles have the same properties such as sliding friction and rolling friction coefficients. Experimental results show that mixtures with a different angle of repose depict various flow patterns, which might be stratification. However, in DEM simulation, sliding and rolling friction coefficients are two significant parameters for the formation of a sandpile, which significantly affects the angle of repose. The contact between spheres results in a rolling resistance due to elastic hysteresis losses or viscous dissipation, which are characterized by sliding and rolling friction coefficients in the force calculation in the simulation. However, the

effect of surface property for binary mixture on segregation phenomenon by DEM is still lacking.

The relationship between the angle of repose and the sliding friction coefficient and rolling friction coefficients is examined for mono-sized particles, as depicted in Figure 3-8. The result is consistent with Zhou et al. (2001) that with the increasing of rolling friction coefficient, the angle of repose rises from 23^o to 30^o. Similarly, the angle of repose also increases with sliding friction coefficient. The property of large particles keeps same as $\mu_{s,\ large} = 0.6$, $\mu_{r,\ large} = 0.05\ d_p$ and then the sliding friction coefficient of small particles $\mu_{s,\ small}$ is changed from 0.1 to 0.9, the rolling friction coefficients $\mu_{r,\ small}$ is from 0.001 d_p to 0.1 d_p, respectively. The results are shown in Figure 3-9. It can be found that segregation is serious at a large sliding friction coefficient and large rolling friction coefficient, where small particles have a large angle of repose. A more quantitative comparison is achieved by cutting the research area into several grids (grid size is 2 d_p) and the concentration of large particles and small particles in each grid is calculated. It can be found that the number ratio of grids full of large particles and small particles to the total grid numbers, where the volume fraction of small particles and large particles is above 0.9, are big for $\mu_{s,\ small} = 0.9$, and these number ratio decreases slightly with sliding friction decrease, as shown in Figure 3-10 (a). This is because when the sliding friction of small particles is tiny, their energy lost is less, and then small particles roll further. When these small particles have contacts with large particles, large particles have more chance to stop earlier due to larger energy lost than small ones. On the pattern snapshot, it seems that more large particles spread on the surface of small particles. Due to small particles' good flowability, there is little segregation at the bottom. The distribution of different rolling friction coefficients is similar, but with a slight decrease of large particle number ratio at 0.10. For small rolling friction of small

particles, to balance the effects of both size and flowability, little segregation can be found there.

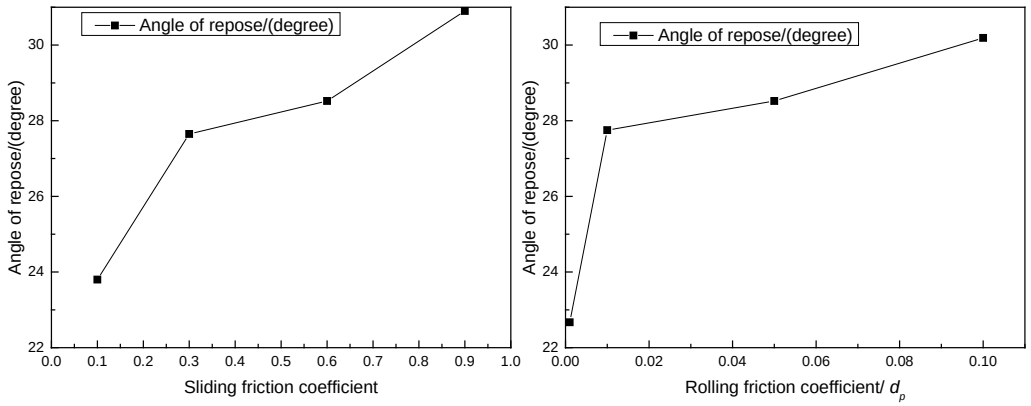

(a) (b)

Figure 3-8 Angle of repose for mono-sized particles at (a) different friction coefficients, with same rolling friction coefficient 0.025 d_p and (b) different rolling friction coefficients, with same sliding friction coefficient 0.6.

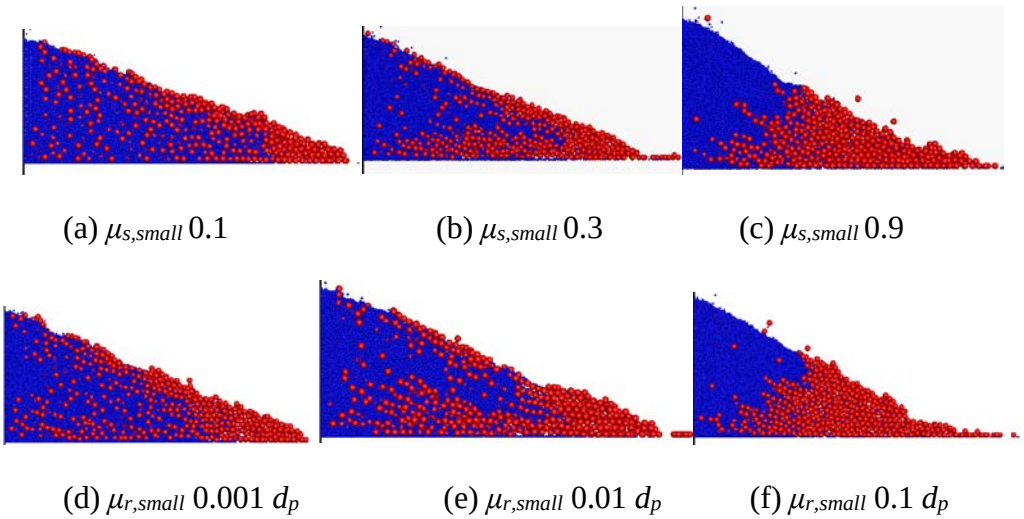

(a) $\mu_{s,small}$ 0.1 (b) $\mu_{s,small}$ 0.3 (c) $\mu_{s,small}$ 0.9

(d) $\mu_{r,small}$ 0.001 d_p (e) $\mu_{r,small}$ 0.01 d_p (f) $\mu_{r,small}$ 0.1 d_p

Figure 3-9 Flow patterns of sandpile under different sliding friction coefficients $\mu_{s,small}$ and rolling friction coefficients $\mu_{r,small}$ of small particles

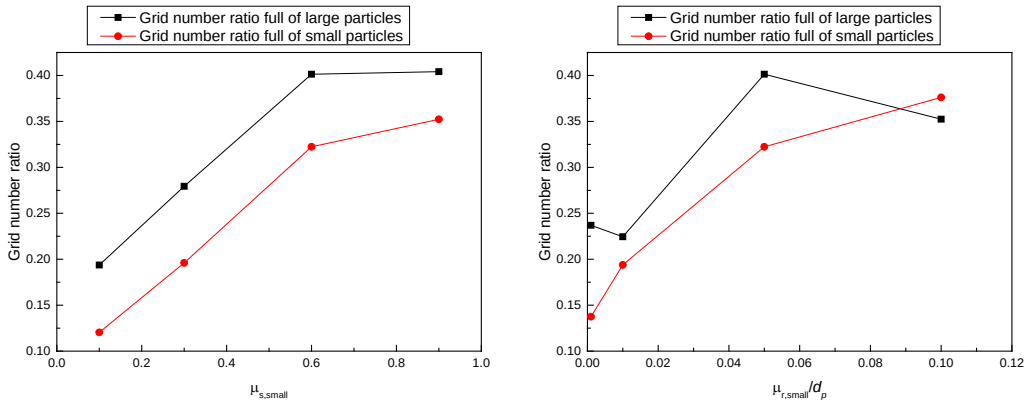

Figure 3-10 The number ratios of grids full of large particles and small particles at (a) different sliding friction coefficients $\mu_{s,\,small}$ and (b) rolling friction coefficients $\mu_{r,\,small}$ of small particles.

Similarly, the properties of small particles keep same as $\mu_{s,\,small} = 0.6$, $\mu_{r,\,small} = 0.05\ d_p$, and the sliding friction and rolling friction coefficient of large particles changes from 0.1 to 0.9 and 0.001 d_p to 0.1 d_p respectively. The grid number ratio and the flow patterns are illustrated in Figure 3-11 and Figure 3-12. Different with Figure 3-10, the trend of all the lines in Figure 3-11 is gentle, which means the segregation extent does not differ much. This means that the effect of particle size is more significant than the effects of sliding and rolling friction coefficients of large particles. The segregation is distinct for all the cases, as shown in Figure 3-12. It is because if the small particles have a relatively large angle of repose, the large particles roll down easily along the upper slope formed by the small particles, and at that time, the surface properties of large particles play a minor effect on packing patterns.

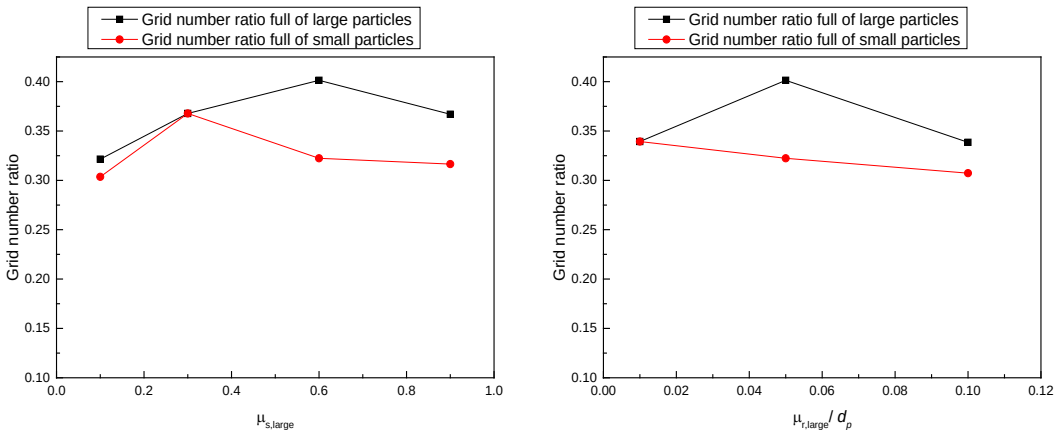

(a) (b)

Figure 3-11 Number ratios of grids full of large particles and small particles at (a) different sliding friction coefficients $\mu_{s,\,large}$ and (b) rolling friction coefficients $\mu_{r,\,large}$ of large particles.

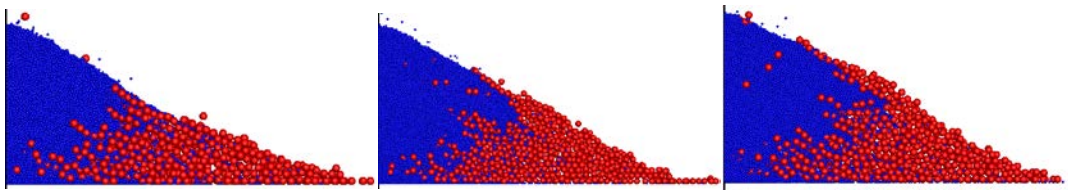

(a) $\mu_{s,large}$ = 0.3 (b) $\mu_{s,large}$ = 0.9 (c) $\mu_{r,large}$ = 0.10

Figure 3-12 Flow patterns of sandpile under different sliding friction coefficients $\mu_{s,\,large}$ and rolling friction coefficients $\mu_{r,\,large}$ of large particles.

3.3.3 Effect of moisture content on segregation

A capillary force is considered as the cohesive force for the mixture. The added liquid is water and the volumetric moisture content V_f ranging from 0.1% to 10% are examined. Note that the moisture content is a volumetric fraction and is normalized by total particle volume. The parameters and assumptions are listed in Section 3.2.1. The flow patterns of different volumetric moisture contents are depicted in Figure 3-13. It can be found that the segregation is serious for all the cases, but the angle of repose of upper

pile formed by small particles and the lower pile angle formed by large particles differ much under different V_f. For (c) and (d), when the volumetric moisture contents are large, the newly-generated small particles have large capillary force with its neighbors, which leading to steep slope in the flow pattern. More intuitive analysis is shown in Figure 3-14, showing the slope angle change trend and the grid number ratio which is full of large and small particles respectively. The slope angle is determined by the straight part in the middle area. It can be found that the angle of repose of small particles shows a sharp increase for small V_f from 0.1% to 1%, then it becomes steady for larger V_f =3%. This angle change trend of the lower pile is different from that of the upper pile, which shows a gentle drop with the increasing of V_f. The number ratios of grids full of large particles and small particles show a drop first at small V_f, then a steady increase at large V_f, meaning that segregation is more serious with the increasing of V_f, and the interaction between large and small particles are less at a large V_f.

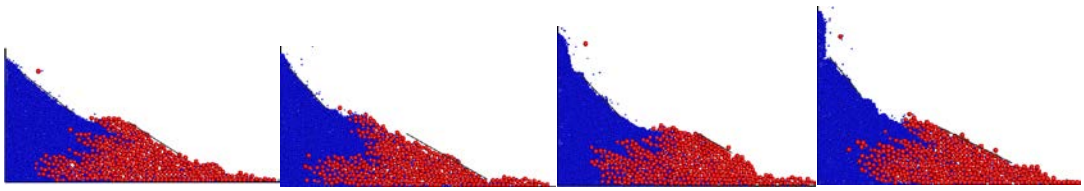

(a) (b) (c) (d)

Figure 3-13 Flow patterns at different volumetric moisture contents (a) 0.001, (b) 0.01, (c) 0.03, (d) 0.1

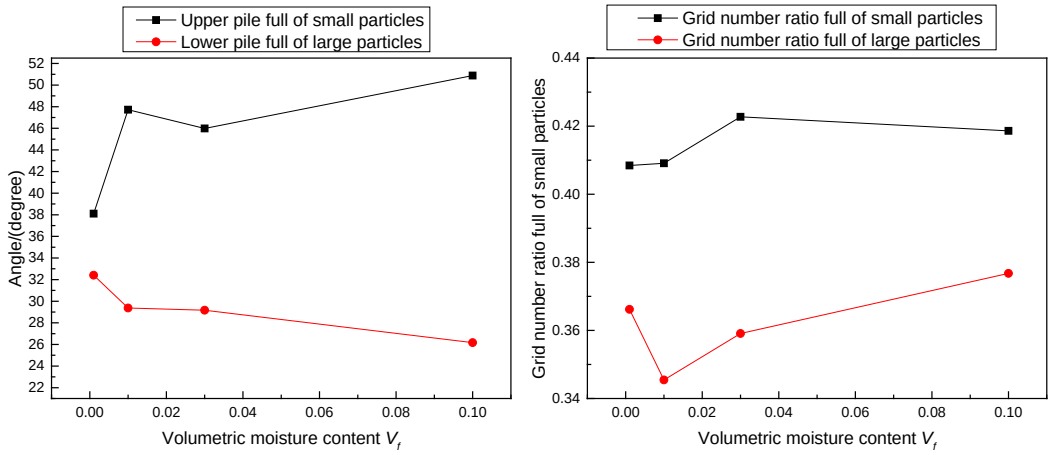

(a) (b)

Figure 3-14 (a) Trend of slope angles change with V_f; (b) grid number ratio full of large and small particles with V_f.

The behaviour of granular materials is the collective outcome of individual particles, which is controlled by the forces between them. Therefore, the analysis of forces clarifies the mechanism of the moisture content. Mono-sized particle behaviour under different volumetric moisture contents is analyzed by Dong (Dong et al., 2013), but the binary mixture behaviour is still lacking. Hence, the numbers of liquid bridges and average capillary forces between large and large (L-L), small and small (S-S), and large and small (L-S) is illustrated in Figure 3-15. It can be found that with the increase of the moisture content, the ratio of average capillary force and gravity, which is Bond number, is largest at small V_f for L-S contacts. For L-L and S-S contact, the ratio of average capillary force and gravity are steady. Then, the average number of liquid bridges are normalized by the same type of contact number. It can be found that the average liquid bridge numbers of all three kinds of contacts have an increasing trend. The number of L-L and S-S are smaller than L-S ones, same with the force ratio.

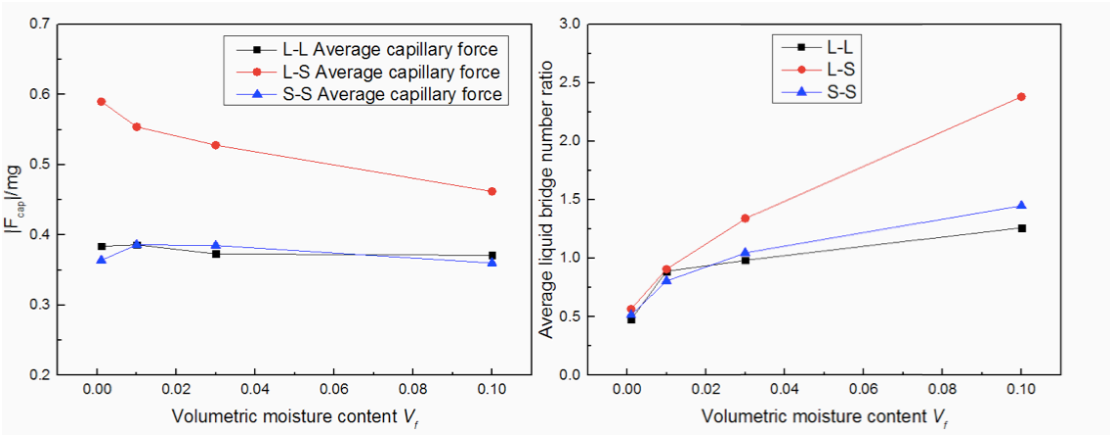

(a) (b)

Figure 3-15 (a) Average capillary force and (b) average liquid bridge numbers between large and large (L-L) particles, large and small (L-S) particles and small and small (S-S) particles.

The relationship between the angle of repose and porosity, which are two important structural characterization properties shows a linear correlation for the mono-sized cohesive system (Dong et al., 2013). The porosity is calculated by cutting the study area into several small grids, and the volume of large and small particles are considered to get the porosity by $\varepsilon = (V_{grid}-V_{(large+small)})/V_{grid}$). The values at the pile surface are abandoned due to blank parts in the grid. For a binary cohesive system, the relationship of the angle of repose θ and porosity ε is also fitted by a linear correlation, where the correlation is $\theta = 139.25\ \varepsilon + 5.51$ (R square is 0.74). It presents that a large porosity leads to a large angle of repose, as shown in Figure 3-16. This correlation is based on the data obtained at size ratio 3:1 and $\mu_s = 0.6$, $\mu_r = 0.05\ d_p$.

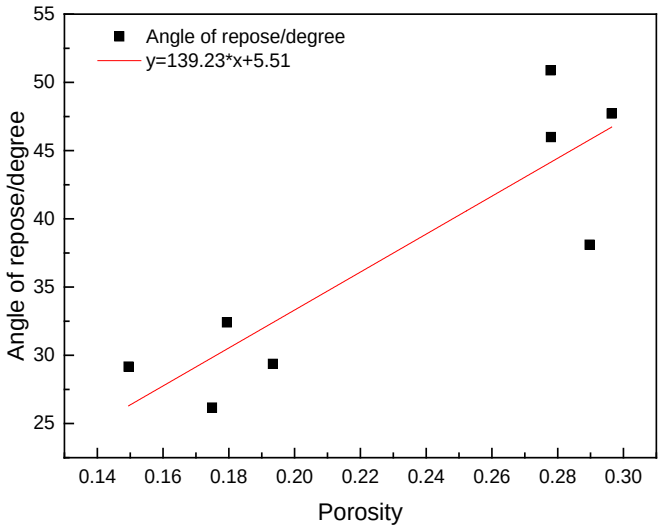

Figure 3-16 Angle of repose as a function of porosity for different piles.

As a force characterization factor, a force ratio χ_i defined as the sum of the cohesive forces on a particle to its effective gravity is chosen here, written as $\chi_i = \sum_j |F_{ij}^c|/mg$. It can be affected by both the magnitude of a pair of force between each of two particles as well as the number of force pairs, and also related to the porosity for the packing of cohesive particles (Yang et al., 2007, Dong et al., 2012). Therefore, it includes local structural information, hence it is more accurate compared with a Bond number, which is the cohesive force between two particles to the weight of a particle, usually used to characterize the packing density, maximum angle of stability and flow rate(Nowak et al., 2005, Nase et al., 2001). As shown in Figure 3-17, this relationship between the porosity and force ratio can be fitted as a correlation as:

$$\varepsilon = \varepsilon_0 - \alpha \exp(\beta \chi_i) \tag{3-5}$$

where ε_o=0.31847, α=0.23077 and β =- 0.56885 (R-square is 0.95). ε_o could be treated as a mono-sized particles porosity, and α and β are related to particle properties. Because of the different filling method and the boundary conditions, these fitting

parameters might be different from those used in the packing of cohesive particles. Then combined the correlation obtained from Figure 3-16, the relationship between the angle of repose and the force ratio can be written as:

$$\theta = k(\varepsilon_0 - \alpha \exp(\beta \chi_i)) + m \tag{3-6}$$

where k=139.23, m=5.51, which are obtained in Figure 3-16. The fitting curves are also illustrated in Figure 3-17. These results reveal the relationship between the sandpile structure including its porosity, force ratio with the angle of repose and other properties.

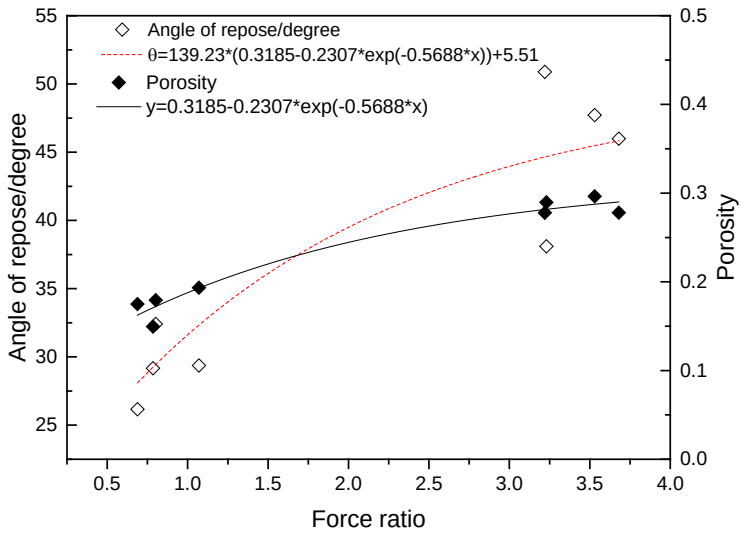

Figure 3-17 Angle of repose and porosity as a function of <χ_i>. Solid and dash lines are predicted results.

3.4 Conclusion

Sandpile formation process with different particle sizes has been analysed by means of DEM. The flow patterns simulated are validated by experimental results first, then the flow process is demonstrated and the effects of particle surface properties and the water

content are examined. The main conclusions drawn from the present work are listed below.

- The different slopes of the upper and lower piles are the main reason for particles stratification. It means that the local structure determines the following packing patterns and is the reason for the repeat loop of piling process. In terms of a large particle, only when its force chain is like a tetrahedron, the supporting particles form a cage to trap the moving particle and its velocity is tiny enough at that time, it can reach a steady state.

- The angle of repose of the pile is decided by the particles surface properties. Small sliding coefficient and rolling friction coefficient decreases particles flowability and leads to a small angle of repose. Mixtures with both different surface properties and size show various mixing patterns. When particles with a large size and smooth surface, segregation is most serious. A small particle with little sliding friction and rolling friction has least grid number full of large and small particles.

- When particles are wet, the volumetric moisture content has a huge effect on the packing structure. The relationships between porosity, force ratio and angle of repose have been fitted by several correlations. It reveals the structural and force characteristics of sandpile formation process. The angle of repose of large particles increase with the moisture content and then saturate at V_f =3%. The average capillary force decreases for all three types of particle contacts.

This page is intentionally blank

CHAPTER 4 SIZE-INDUCED SEGREGATION OF GRANULAR MATERIALS DURING FILLING A QUASI-THREE-DIMENSIONAL HOPPER

4.1 Introduction

Granular materials are prone to segregate spatially with different sizes, densities, shapes or particle resilience (Williams, 1976). It is generally accepted that particle size difference is by far the most important cause of segregation, and consequently, extensive attention has been paid in the literature to size-induced segregation. This is also a commonly encountered problem in a variety of industries, including pharmaceuticals, food and agricultural processing, chemical and metallurgical industries. Segregation might render undesirable blend quality and also induce flow problems. For example, in an ironmaking blast furnace, multiple hoppers, conveyors and transfer points are involved in the charging equipment. Particles in such processes experience segregation, which directly affects the burden distribution and smooth operation of the process.

A hopper is one of the most significant granular handling devices. Many researchers have studied the size segregation experimentally during the hopper filling process over the preceding decades (Bridgwater, 1976, Standish, 1985, Kajiwara et al., 1988, Hastie and Wypych, 2000, Engblom et al., 2012b). Different materials and various vessel shapes have been examined, and macroscopic results including flow and segregation patterns have been described. Meanwhile, several models including the ‘minimal’ model (Samadani et al., 1999), ‘screening’ model (Boutreux and deGennes, 1996) and ‘void filling’ model (Shinohara et al., 1972) and other theoretical analyses using continuous methods (Gray and Kokelaar, 2010, Fan et al., 2014) were proposed to predict segregation. However, the models generally have assumptions to simplify the initial conditions and complex flow processes. Therefore, they could predict the concentration distribution under certain conditions only with approximate results. Most

of the experimental and theoretical analyses could not capture the microscopic information such as particle scale velocity and stress, which however are significant in understanding the size-induced segregation.

More recently, computer simulation using discrete element method (DEM) has become a popular tool to examine hopper charging processes. Many articles (Tanaka et al., 1988, Langston et al., 1997, Cleary and Sawley, 2002, Zhu and Yu, 2004, Balevičius et al., 2008, Ketterhagen et al., 2008, Ketterhagen et al., 2009) have been published on the flow of mono-sized particles in hoppers. However, only a few researchers focused on binary and ternary mixture charging. For example, Rahman et al. (2011) used DEM to validate the screening model proposed by Shinohara et al. (1972) in forming a conical pile. They examined the mixing ratio at different distances from the centre along the pile line at different initial size ratios and feed rates. Wu et al. (2013) utilised relative particle size to examine the effects of the small particle mass fraction, the burden apex and the lower hopper slope on segregation. Mio et al. (2012) built a DEM model for blast furnace bell-less type charging process, showing that large particles are located in the wall boundary during the hopper filling process. Although the efforts made, as shown above, microscopic properties such as velocity, cluster size and particle mixing index are not fully analysed to develop a further understanding of segregation mechanism. The effects of some key variables including sliding friction and rolling friction are not well addressed in the literature, which however is important as they are closely related to particle properties such as particle shape and particle surface roughness.

Therefore, the objective of this paper is to analyse the segregation details of binary mixtures during the hopper filling process. The model is validated first, and then a

particle scale mixing index which is related to coordination number (CN) is used to quantify the segregation degree. The velocities and trajectories of large and small particles in binary mixtures are traced for understanding the segregation. In addition, effects of parameters used in DEM including sliding friction coefficient and rolling friction coefficients are examined and shown by a contour plot. Finally, a correlation is also proposed to quantify the segregation extent for the various volume fraction of small particles.

4.2 Model description

4.2.1 Discrete element modelling

In DEM, granular materials are modelled based on a finite number of discrete, semi-rigid particles interacting by contact or non-contact forces. The translational and rotational motion of every particle in a system is described by Newton's law of motion. For simplicity, we only consider spherical particles and the most dominant forces and torques. Therefore, the governing equations for the translational and rotational motion of a particle *i* interacting with another particle *j* can be written as (Zhou et al., 2008):

$$m_i \frac{d\mathbf{v}i}{dt} = \sum_{j=1}^{k}\left(\mathbf{f}_{c,ij} + \mathbf{f}_{d,ij}\right) + m_i\mathbf{g} \tag{4-1}$$

$$I_i \frac{dwi}{dt} = \sum_{j=1}^{k}(M_{t,ij} + M_{r,ij}) \tag{4-2}$$

where $\mathbf{v}_i$ and $\boldsymbol{\omega}_i$ are the translational and angular velocities respectively of particle *i* with mass m_i and moment of inertia I_i. The forces considered are gravitational and particle-particle interaction forces including elastic contact force $\mathbf{f}_{c,ij}$ and viscous damping force $\mathbf{f}_{d,ij}$ in both normal and tangential components at the contact point. The torque acting on particle *i* by particle *j* includes two components. One is generated by

tangential force and causes particle *i* to rotate, $\mathbf{M}_{t,ij}$, and rolling friction torque $\mathbf{M}_{r,ij}$ generated by normal force that acts to hinder the relative rotation between the contacting particles. For a particle undergoing multiple interactions, the individual interaction forces and torques are summed for the k_i particles interacting with particle *i*. Equations used to calculate difference forces and torques are summarized in Table 4-1, and detailed description can be referred in Zhou et al. (2005).

Table 4-1 Components of forces and torque acting on particle *i*

Forces and torques	Symbols	Equations
Normal elastic force	$\mathbf{f}_{cn,ij}$	$-4/3E^*\sqrt{R^*}\delta_n^{3/2}\mathbf{n}$
Normal damping force	$\mathbf{f}_{dn,ij}$	$-c_n\left(8m_{ij}E^*\sqrt{R^*\delta_n}\right)^{1/2}\mathbf{V}_{n,ij}$
Tangential elastic force	$\mathbf{f}_{ct,ij}$	$-\mu_s\lvert\mathbf{f}_{cn,ij}\rvert(1-(1-\delta_t/\delta_{t,\max}{}^{3/2})\hat{\delta}_t$, $(\delta_t<\delta_{t,\max})$
Tangential damping force	$\mathbf{f}_{dt,ij}$	$-c_t\left(6\mu_s m_{ij}\lvert\mathbf{f}_{cn,ij}\rvert\sqrt{1-\lvert\mathbf{v}_t\rvert/\delta_{t,\max}}/\delta_{t,\max}\right)^{1/2}\mathbf{V}_{t,ij}$, $(\delta_t<\delta_{t,\max})$
Coulomb friction force	$\mathbf{f}_{t,ij}$	$-\mu_s\lvert\mathbf{f}_{cn,ij}\rvert\hat{\delta}_t$, $(\delta_t\geq\delta_{t,\max})$
Torque by tangential forces	$\mathbf{M}_{t,ij}$	$\mathbf{R}_{ij}\times(\mathbf{f}_{cn,ij}+\mathbf{f}_{dt,ij})$
Rolling friction torque	$\mathbf{M}_{r,ij}$	$\mu_{r,ij}\lvert\mathbf{f}_{n,ij}\rvert\hat{\boldsymbol{\omega}}_{t,ij}^n$

where R* is the reduced radius of the particle *i* and *j* at the contact point. $1/m_{ij}=1/m_i+1/m_j$, $E^*=E/2(1-\nu^2)$, $\hat{\boldsymbol{\omega}}_{t,ij}=\boldsymbol{\omega}_{t,ij}/\lvert\boldsymbol{\omega}_{t,ij}\rvert$, $\hat{\boldsymbol{\delta}}_t=\boldsymbol{\delta}_t/\lvert\boldsymbol{\delta}_t\rvert$, $\delta_{t,\max}=\mu_s(2-\nu)/2(1-\nu)\cdot\delta_n$, $\mathbf{V}_{ij}=\mathbf{V}_j-\mathbf{V}_i+\boldsymbol{\omega}_j\times\mathbf{R}_{c,ji}-\boldsymbol{\omega}_i\times\mathbf{R}_{c,ij}$, $\mathbf{V}_{n,ij}=(\mathbf{V}_{ij}\cdot\mathbf{n})\cdot\mathbf{n}$, $\mathbf{V}_{t,ij}=(\mathbf{V}_{ij}\times\mathbf{n})\times\mathbf{n}$. Note that tangential forces ($\mathbf{f}_{ct,ij}$+$\mathbf{f}_{dt,ij}$) should be replaced by $\mathbf{f}_{t,ij}$ when $\delta_t\geq\delta_{t,\max}$.

4.2.2 Simulation condition

The filling process of granular materials into a conical hopper is the research target in this work. To reduce the computational time, periodic boundaries and a GPU-based

simulation code are used. Periodic boundaries permit simulation of a section of the full physical domain by treating particles moving out of the simulation domain across one boundary as moving back into the simulation across the other parallel boundary (Yang et al., 2014). In the simulation, particles are generated randomly in the upper hopper and then flow through a steep angle cone. Followed by a gravitational setting process, the particles are discharged at a relatively stable rate from the upper hopper's outlet into the lower hopper under gravity. The materials properties and DEM parameters used are listed in Table 4-2.

Table 4-2 Materials properties and DEM parameters used in the present simulations

Variables	Base value	Parameters range
Particle properties		
Particle shape	Spherical	
Particle number	81,283	
Particle diameter, d_p	5 mm (large) 2 mm (small)	
Size ratio, φ	2.5	
Small volume fractions, χ	50%	(25%-95%)
Particle density, ρ_p	900 kg/m^3	
Young's modulus, E	1.0×10^7 Pa	
Poisson ratio, ν	0.3	
Time step, Δt	2.25×10^{-5} s	
Interaction parameters		
Particle-particle sliding friction, $\mu_{r,pp}$	0.6	(0.1-0.8)
Particle-wall sliding friction, $\mu_{s,pw}$	0.6	(0.1-0.8)
Rolling friction coefficient, μ_r	0.025 d_p	(0.001-0.2 d_p)
Damping coefficient	0.3	(0.1-0.4)
Dimensionless hopper geometry		
Width, W	40 d_p	
Depth, Z	4 d_p	
Upper hopper outlet orifice, W_0	2 d_p	(1.0-4.0)

4.3 Results and discussion

4.3.1 Model validation

To verify the DEM model, simulations corresponding to physical experiments by Hastie and Wypych (2000) were conducted. The experiments were carried out in a two-dimensional bin using rape seeds (1.0 to 2.0 mm) and white plastic pellets (3.8 to 5.6 mm). The width and height of the bin is 1000 mm and 1500 mm respectively. The hopper is 30^{o} inclined with vertical direction and has a 150 mm outlet. 20 litres of well-mixed mixtures were discharged from a feed bin under fixed opening size. After filling process was completed, the granular distribution pattern in the lower hopper was captured by a camera, and the proportion of rapeseed in each sampling grid square was determined to assess the segregation. In the simulation, particle sizes are set as 5 mm for large particles and 2 mm for small particles giving a size ratio of 2.5. Because of the limitation of computational capacity, a one-fifth scale size hopper is used. The total particle number used is 81,238, and the volume fraction of small particles is 50%.

Figure 4-1 shows a comparison of size segregation between the physical experiments and the DEM simulation, indicating macroscopically consistent results. The shape of the heap formed in the central top and the distribution of large particles are similar, with a thick layer of large particles gathering near the side walls. The volume fraction of small particles in the radial direction (dimensionless x) at different heights (z) is calculated, (the centre of the hopper bottom is (0,0)), and quantitative comparisons with experiments are shown in Figure 4-2. It can be observed that at each height, both experimental results and DEM data show a minimum value near the hopper boundary and a large difference between the hopper centre and the boundary. This difference of

simulation result is larger than that of experimental results at the low height of 16.65 d_p. This is caused by the relative small scale of simulation condition. In the same lateral direction, especially in the lower part of the hopper, the number of particle is rather small, and the particle distribution is more easily effected by the wall boundary than that under experimental conditions. Particles mixed well in a larger equipment. But this difference between simulation and experimental results is weaken at higher heights. The volume fraction of small particles has a peak at dimensionless x = 10.0 d_p, at high dimensionless heightsfor both experimental results and simulation results. The magnitude of this difference is largest at the low height of 16.65 d_p. The volume fraction of small particles has a peak at x = 10.0 d_p, especially at high heights, but not obvious at a lower height. The generally good agreement between the simulation and the measurement shown in Figure 4-1, either qualitative or quantitative, confirms the validity of the present DEM model. On this basis, the DEM model is used to examine the effects of different variables and investigate size segregation during the hopper filling process.

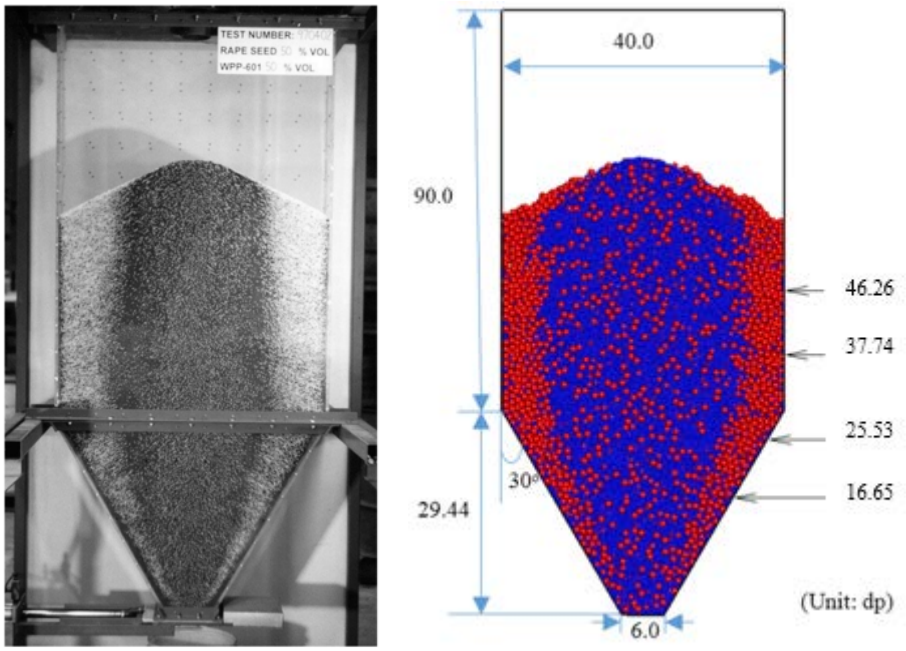

(a) (b)

Figure 4-1 Flow patterns obtained from (a) physical experiments. Reprinted from Hastie and Wypych (2000), with permission from Springer Nature. (b) DEM simulation in this work

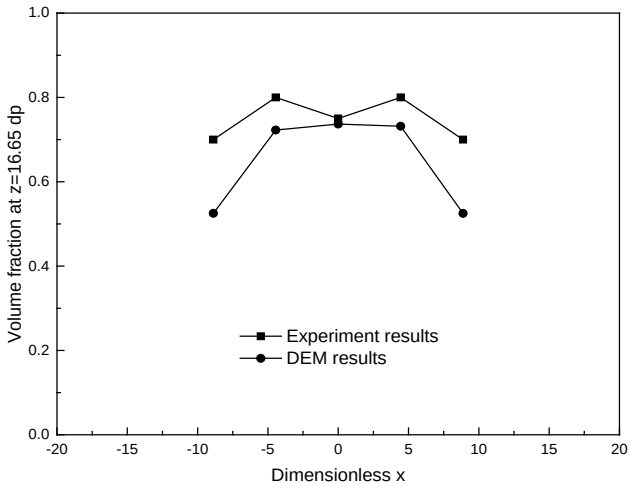

(a)

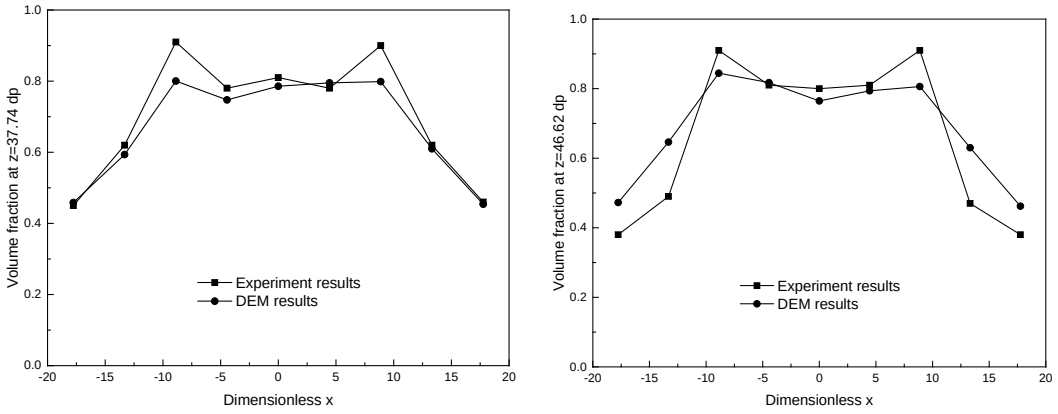

(b) (c)

Figure 4-2 Volume fraction distribution of small particles at different heights: (a) z = 16.65 d_p; (b) z = 37.14 d_p; and (c) z = 46.62 d_p (Note that the experiment results are from Hastie and Wypych (2000)).

4.3.2 Hopper filling process analysis

4.3.2.1 Flow regimes

The solid flow patterns are examined first to generate a visual understanding of the segregation process (Figure 4-3). Here, different particle sizes are represented by different colours (red for large particles, and blue for small particles). After particles start to be discharged from the upper hopper, the whole filling process can be divided into three stages. The first stage is the formation of an initial well-mixed region at the bottom of the conical hopper, and the heap has not been formed yet (t = 1.81 s). Segregation at this stage is not obvious and particles are well-mixed. After that, the mixing degree declines gradually, and segregation emerges. This is 'pile-up stage' ranging from t = 8.13 s to 14.45 s as shown in Figure 4-3. Then the 'steady filling process' starts. At this stage, the heap increases steadily and large particles are able to roll down the heap surface to the bin boundary due to the size difference. At t = 27.09 s, the filling process finishes. Clearly, a thick layer of large particles is formed near the

side walls. The concentration of small particles in the central region does not change much.

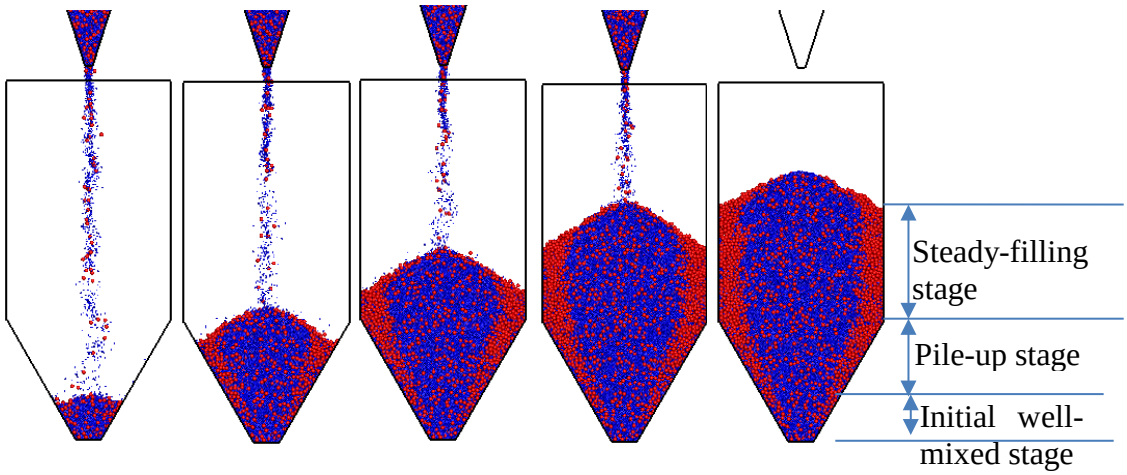

Figure 4-3 Snapshots of solid flow patterns at different times during the hopper filling process.

To visualise the motions of particles, trajectories of a number of large and small particles are traced and shown in Figure 4-4 (a). It can be observed that both large and small particles at the initial stage fall straight down regardless of particle size. However, during the steady-filling stage, the trajectories are quite different. Most of the large particles, represented by solid lines in Figure 4-4 (a), can travel long distances in the radial direction and stop near the side walls. Small particles, represented by dashed lines, however, come to rest quickly around the central region. Figure 4-4 (b) presents the concentration of small particles along the radial direction at various heights (z). The height of $z = 4\ d_p$ is within the initial stage, with a slight concentration difference along the radial direction. The height of $z = 12\ d_p$ is in the area corresponding to the pile-up stage. Concentration differences become more obvious between the hopper centre and side wall. The distributions in other heights of 34 d_p, 42 d_p and 50 d_p are quite similar,

which is the characteristic of bin steady-filling stage. The concentration of small particles near the side walls is very low, almost 0, indicating that most of the particles near the wall are large ones. The concentration of small particles in the range of $x < 10$ d_p is almost constant at 65% which is much larger than the initial fraction of 50%.

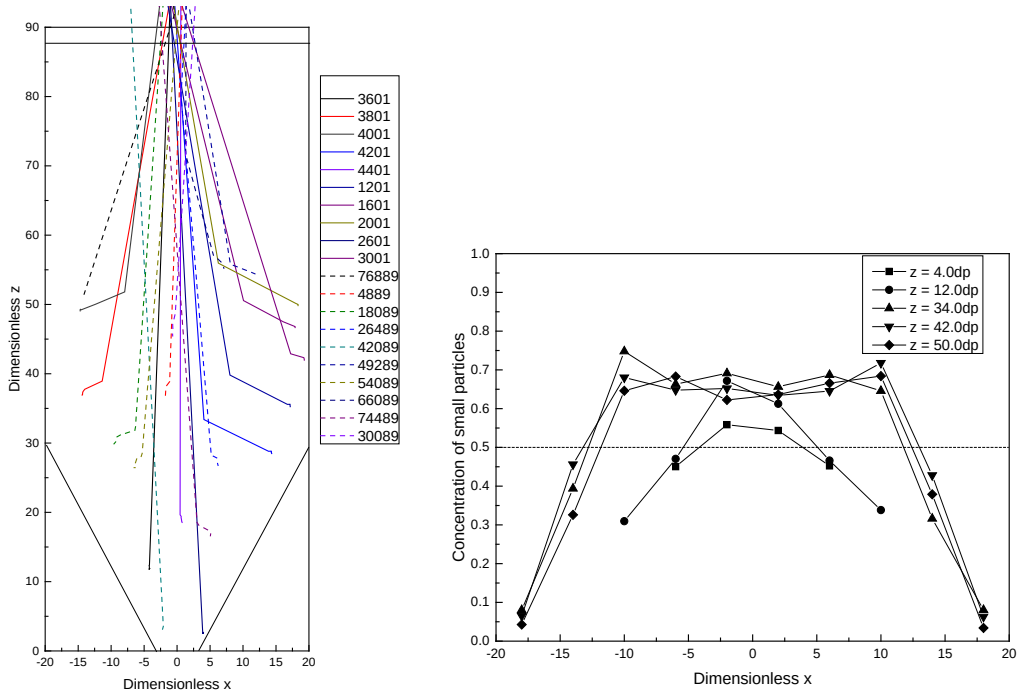

(a) (b)

Figure 4-4 (a) Trajectories of 20 large and small particles (note that solid lines are for large particles, and dash lines are for small particles); (b) concentration of small particles in the radial direction at different heights.

Mixing index is commonly used to quantify the segregation degree. Here, the particle-scale mixing index (PSMI) proposed by Chandratilleke et al. (2012)is used. PSMI is determined based on coordination number (CN) which can be obtained from DEM simulation. Briefly, PSMI is defined by analogy to Lacey's mixing index (Lacey, 1954) and given by $M = (S_0^2 - S_t^2)/(S_0^2 - S_r^2)$, where S_0^2 is a fully segregated state at time t_0, S_r^2 is a fully mixed state, and S_t^2 is the standard deviation of the fraction of the largest

quantity of particles in samples at time t. PSMI = 0 means that mixtures are fully segregated, and PSMI = 1 represents well-mixed mixtures.

The PSMI distribution as a function of height from the hopper bottom and distance from the hopper centre D_c are obtained and shown in Figure 4-5. It can be seen that PSMI shows a downward trend with the increase of the height from 0 to 30 d_p. This illustrates that the segregation increases with the height of the lower hopper. At heights larger than 30 d_p, PSMI remains approximately constant within the range of 0.5 ~ 0.6, indicating that segregation extent does not vary significantly with height in the upper bin. PSMI variation with D_c in the radial direction is also examined at the heights of 35 d_p to 50 d_p, and shown in this figure. It can be seen that PSMI is high near the centre, and starts to drop sharply at D_c = 10 d_p until almost zero at D_c = 18 d_p. This indicates that at the side wall region, significant segregation exists, and in the hopper centre, large and small particles are well mixed.

4.3.2.2 Segregation analysis at bin steady-filling stage

In the three stages identified during the whole hopper filling process, size segregation is the most stable at the bin steady-filling stage. Therefore, an assembly of particles at this stage is tracked to investigate how segregation occurs, and the results are shown in Figure 4-6. Here, 2829 small particles (in blue) and 187 large particles (in yellow) are marked and tracked from the time t = 11.74 s (Figure 4-6 (a)). The tracked particles fall and hit the heap, with most of the large particles moving towards the heap edge, and only a few remaining in the centre. Correspondingly, most of small particles are enclosed by large particles. Whereas several small particles bounce to the side walls. Finally, the tracked particles come to rest at the time of 14.56 s (Figure 4-6 (e)).

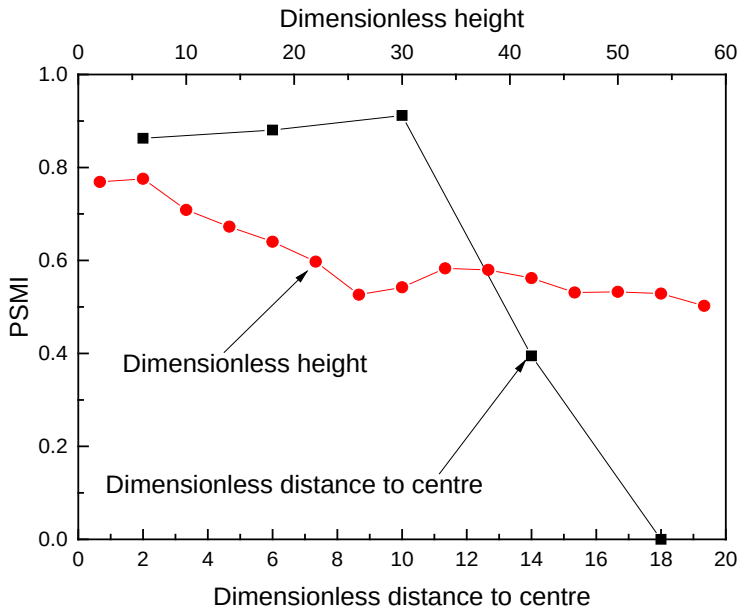

Figure 4-5 PSMI variation with height and distance to the hopper centre.

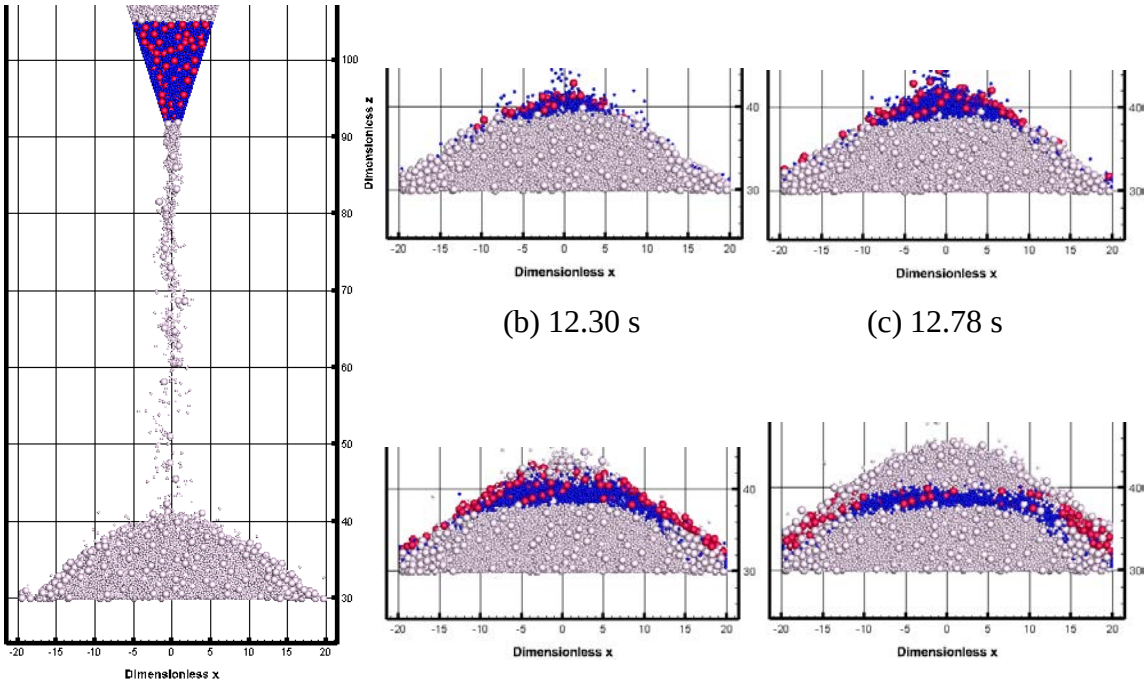

(a) 11.74 s (b) 12.30 s (c) 12.78 s (d) 13.43 s (e) 14.56 s

Figure 4-6 Flow patterns of traced particles at different times showing size segregation process.

The stopping position of moving particles is determined by the neighbour particles in contact and their respective rolling and sliding interactions. To further address this issue, eight particles are chosen with various distances (D_c) to the hopper centre and different sizes to examine their velocity variation with time. For example, Figure 4-7 shows the velocity variation with time for one particle (marked in red, and its contacting neighbours marked in blue) at $D_c = 17.5\ d_p$. Note that here one parameter called cluster size, defined as the current neighbour particles in contact is used to analyse its effect on trajectory, as shown by blue particles in Figure 4-7. It can be observed that after contacting the heap at t = 12.64 s, the red particle has no neighbours and its velocity is large. It travels a long distance and then has the first contact at t = 12.76 s. Its velocity decreases as the cluster size increases at t = 13.09 s. Finally, the cluster size reaches 7, meaning that the red particle is surrounded by the seven particles, and comes to rest.

Figure 4-8 and Figure 4-9 show the variations of velocity and cluster size of four large and four small particles during the filling process. These particles are chosen from different final radial positions at $D_c = 17.5\ d_p$, $12.5\ d_p$, $7.5\ d_p$ and $2.5\ d_p$, respectively. As shown in Figure 4-8, the particle movement history can be divided into three stages by the horizontal velocity v_x or the vertical velocity v_z. The first stage is the period before the initial contact with the heap (in the free fall) where v_z reaches the maximum in magnitude. After that, the particles hit the heap with v_z decreasing to near zero and then fluctuate, illustrating repeated collisions during its motion down the heap surface. During this stage, the particles roll along the heap surface before becoming embedded. Once particles come to rest, they become part of the heap. The second stage is critical in affecting particle trajectory and distribution. The horizontal velocity v_x variation indicates that the maximum value occurs when the particles just hit the heap, and this

value varies with D_c, being slightly smaller for small D_c. The travelling time from the initial impact to fully embed is also shorter for small D_c due to the short travelling path.

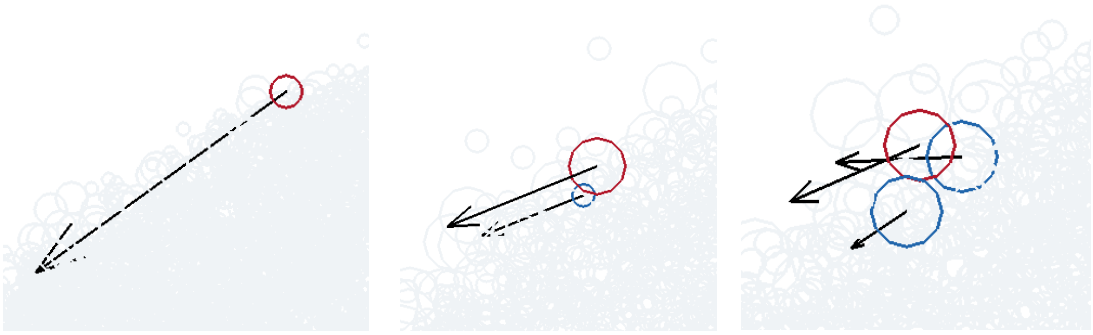

t = 12.64 s t = 12.76 s t = 12.88 s

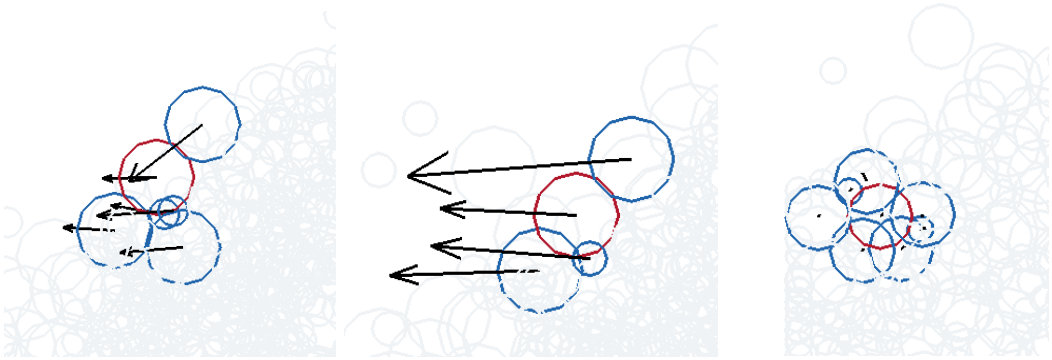

t = 13.09 s t = 13.21 s t = 14.11 s

(a)

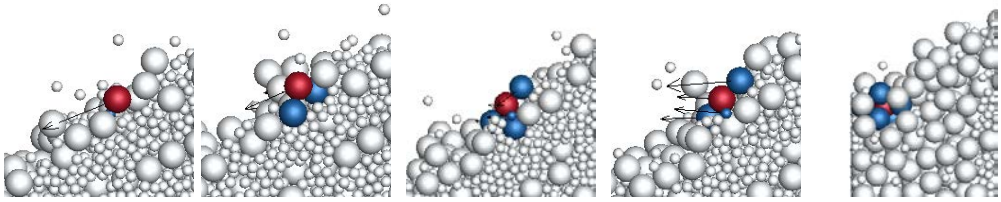

t = 12.76 s t = 12.88 s t = 13.09 s t = 13.21 s t = 14.11 s

(b)

Figure 4-7 Demonstration of velocity vectors for one large particle located in the position of D_c =17.5 d_p, (a) schematic illustration; (b) rendering of the particles in the hopper.

Figure 4-8 also shows the variation of cluster size with time and particle position. During the rolling period, the cluster size increases rapidly. For example, particles at D_c = 17.5 d_p and 12.5 d_p have cluster size below 10, while cluster size for particles at D_c = 7.5 d_p and 2.5 d_p is above 10. This reveals the local segregation pattern that for large D_c, large particles have more contacts with other large particles, hence smaller cluster size. Correspondingly, the large particle cluster size in the centre is larger than that at the side wall region. Particles, which have larger initial v_x and smaller cluster size, bounce more easily due to their large potential energy and low energy loss through neighbour interactions. Particles, which have smaller v_x and larger cluster size, become embedded due to their small initial potential energy and cluster interactions. Small particles show a similar trend as large particles for v_x, travelling time and cluster size, as shown in Figure 4-9. The absolute value of v_x at D_c = 17.5 d_p and 12.5 d_p are larger than that at other positions and large particles, reaching almost 0.05 m/s. The travelling time is shorter than large particles. This is due to small particles spending less time in bouncing to the wall boundary with large velocities.

Note that Figure 4-8 and Figure 4-9 only show the flow properties of individual particles chosen from different radial positions. To give a more general analysis, the average flow properties including travelling time, maximum velocity in the radial direction $v_{x,\,max}$, and cluster size for different D_c at both the second and the third stages are shown in Figure 4-10. Results are similar with those shown in Figure 4-8 and Figure 4-9. It can be observed that with the distance from the centre (D_c) increasing, the particle travelling time increases first then decreases at D_c = 17.5d_p. It illustrates that both large and small particles near the side walls have small travelling time and large $v_{x,\,max}$ (Figure 4-10 (a)). Meanwhile, cluster size at initial stages is small compared to other radial

positions (Figure 4-10 (b)). Therefore, it can be concluded that bouncing is the main mechanism for small particles, and rolling for large particles.

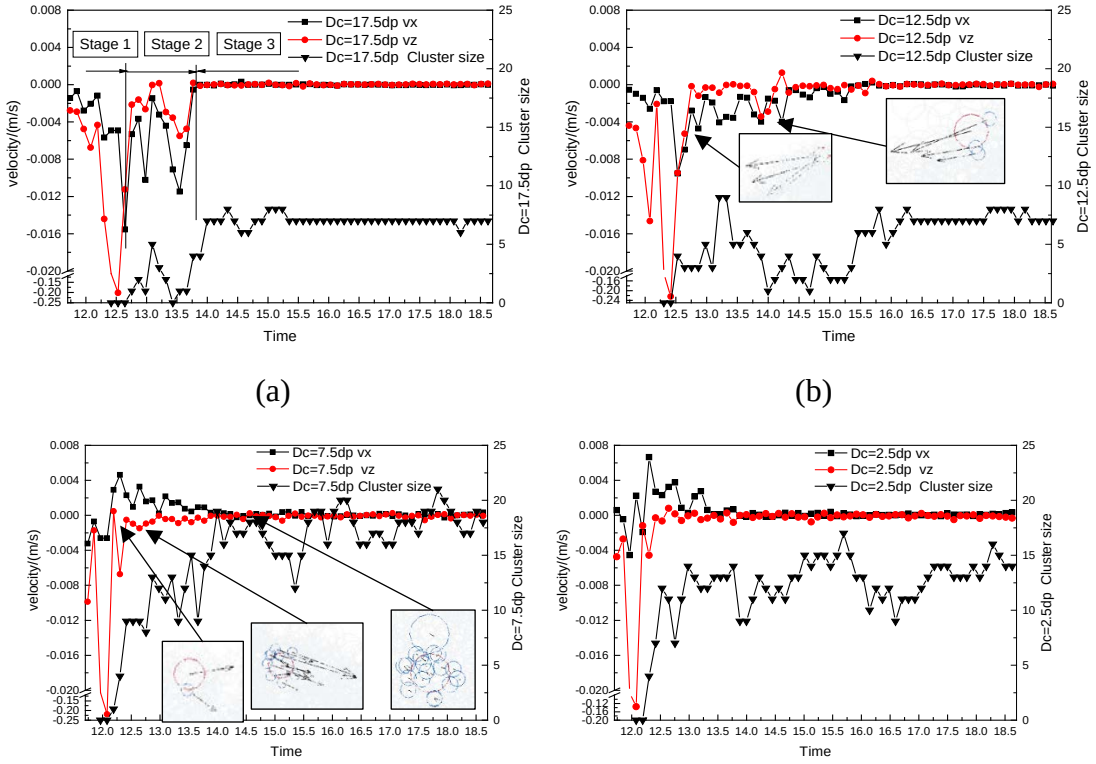

Figure 4-8 Variation of velocities (v_x and v_z) and cluster size of four large particles at different radial positions with time, (a) D_c = 17.5 d_p; (b) D_c = 12.5 d_p; (c) D_c = 7.5 d_p; and (d) D_c = 2.5 d_p. Note that: stage 1 - before hitting the heap; stage 2 - rolling or embedding process; and stage 3 - steady state.

Particles in the radial positions less than 12.5 d_p have large $v_{x,\,max}$ and small initial cluster size, and travel further and need a longer travelling time. This is because they are embedded into the heap after hitting, then pushed by the flowing particles. This can also be verified by the force network shown in Figure 4-11. Both the stick thickness and colours represent the contact normal force magnitude between particles. Large forces are observed at the location of initial impacts. The green network under the filling point is the embedding area. Compared large and small particles, it can be found that

regardless of radial positions, all small particles have shorter travelling time and larger $v_{x,\,max}$ compared with large ones. Small particles also have small cluster size.

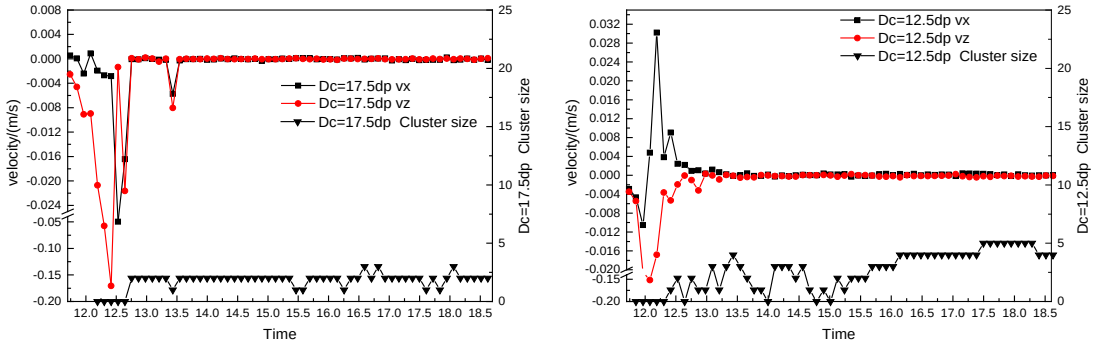

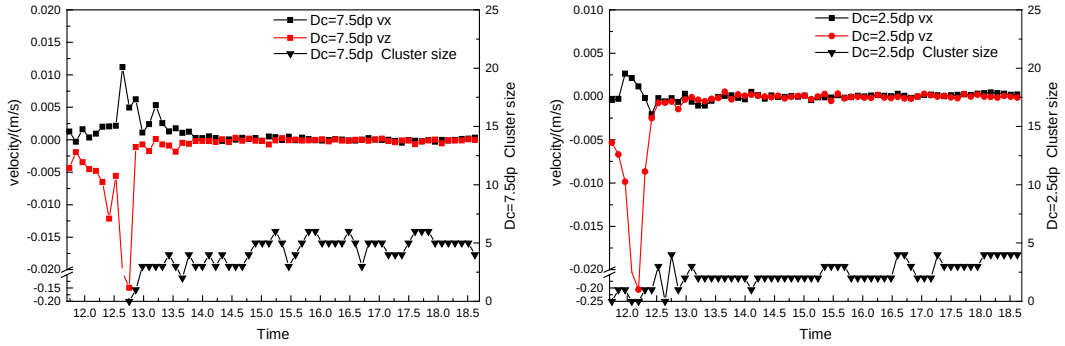

Figure 4-9 Variation of velocities (v_x and v_z) and cluster size of four small particles at different radial positions with time, (a) D_c = 17.5 d_p; (b) D_c = 12.5 d_p; (c) D_c = 7.5 d_p; and (d) D_c = 2.5 d_p.

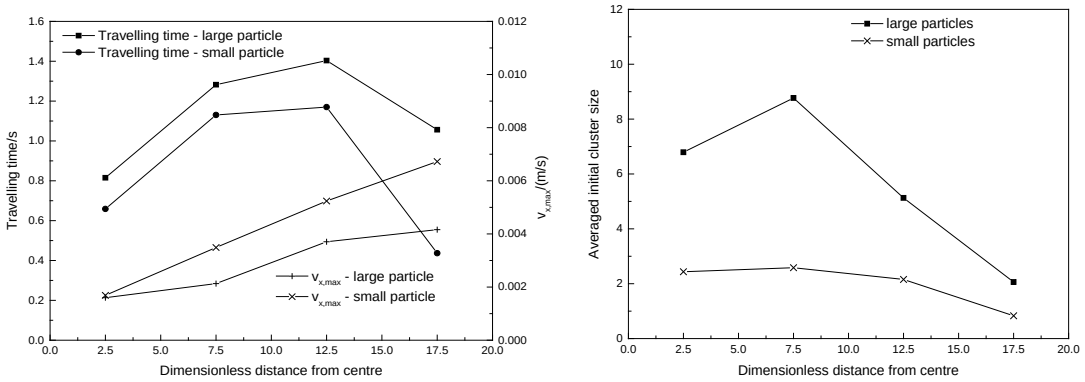

(a) (b)

Figure 4-10 (a) Average travelling time and average velocity $v_{x,\,max}$; (b) average initial cluster size for all large and small particles stopping at a certain D_c.

(a)

(b)

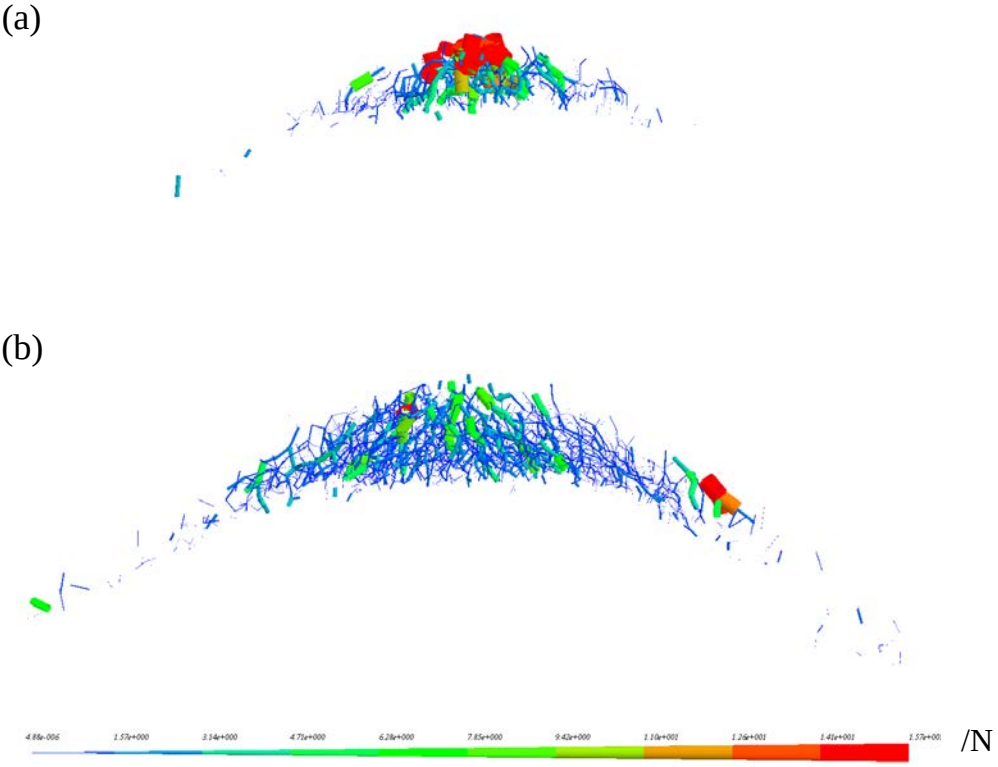

Figure 4-11 Normal force network of traced particles at (a) initial hitting process and (b) the next embedding process in the central top part.

4.3.3 Effect of friction coefficients on segregation

Sliding friction and rolling friction coefficients are two important variables related to materials properties such as particle surface roughness and particle deformation. In practice, different materials such as rape seeds and plastic pellets used in experiments, or coke and ore used in the ironmaking process, have different properties which may affect the segregation. Simulation results show that PSMI at different particle-wall sliding friction coefficients does not change much compared with particle-particle sliding friction coefficient ($\mu_{s,pp}$) and particle-particle rolling friction coefficient ($\mu_{r,pp}$) as shown in Figure 4-12. Hence, only results of $\mu_{s,pp}$ and $\mu_{r,pp}$ are examined and used to obtain a contour plot.

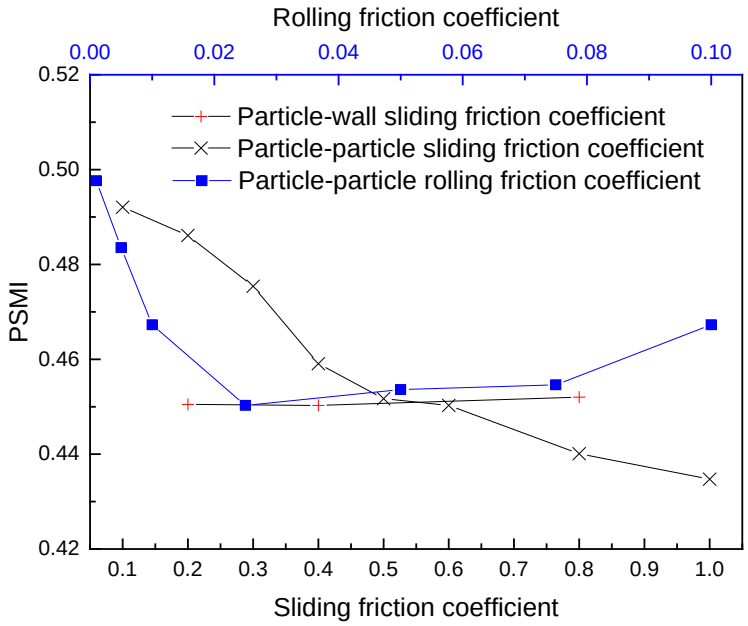

Figure 4-12 PSMI at different particle-wall and particle-particle sliding friction coefficients, $\mu_{s,pp}$, (with χ =50%, φ =2.5 and $\mu_{r,pp}$=0.025) and particle-particle rolling friction coefficients, $\mu_{r,pp}$, (with χ =50%, φ =2.5 and $\mu_{s,pp}$=0.6).

A matrix of rolling and sliding friction coefficients are examined and several typical flow patterns are depicted in Figure 4-13. The base case is the one used in Sections 3.1 and 3.2 with the sliding friction coefficient 0.6 and rolling friction coefficient 0.025 d_p. Figure 4-13 (a) shows the flow patterns of different particle-particle sliding friction coefficients, increasing from 0.1 to 1.0. It can be observed that the segregation degree varies significantly with $\mu_{s,pp}$. With the increase of $\mu_{s,pp}$, the slope of the heap becomes steeper and the differences between the centre and side walls are distinct. The segregation is more serious and more large particles gather at the side wall region. Figure 4-13 (b) shows the flow patterns of various rolling friction coefficients $\mu_{r,pp}$, ranging from 0.001 d_p to 0.2 d_p. It can be found that large particles gather at the side wall region with increasing $\mu_{r,pp}$ from 0.001 d_p to 0.025 d_p. After this, segregation becomes less pronounced at $\mu_{r,pp}$ = 0.2 d_p.

The angular difference between large and small particles and a contour plot of segregation degree (quantified by PSMI) for a series of combinations of various sliding and rolling friction coefficients is shown in Figure 4-14. Smaller PSMI means more significant segregation in the hopper, and larger PSMI means more uniform mixtures. The PSMI contours are approximately parabolic with the minimum value at $\mu_{r,pp}$ = 0.025d_p *-0.05*d_p, in which the angular velocity difference is larger than other rolling friction coefficient (Figure 4-14 (a)). At fixed rolling friction coefficient, PSMI drops with the increasing of sliding friction coefficient. When sliding friction coefficient $\mu_{s,pp}$ is large, the mixing index is affected by rolling friction coefficient significantly. As shown in Figure 4-14 (a), the angular difference between large and small particles is more significant of sliding friction coefficient 0.8 than that of 0.3, leading to serious

segregation. The smallest PSMI appears when $\mu_{s,pp}$ is 1.0 and $\mu_{r,pp}$ is 0.025 d_p. This effect decreases at the small sliding friction coefficient $\mu_{s,pp}$, meaning that PSMI keeps steady at around 0.7 when $\mu_{s,pp}$ is 0.1.

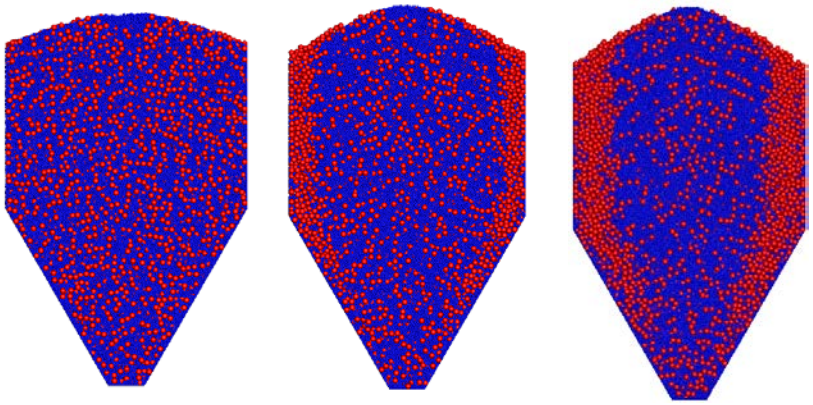

$\mu_{s,pp}$ = 0.1 $\mu_{s,pp}$ = 0.3 $\mu_{s,pp}$ = 1.0

(a)

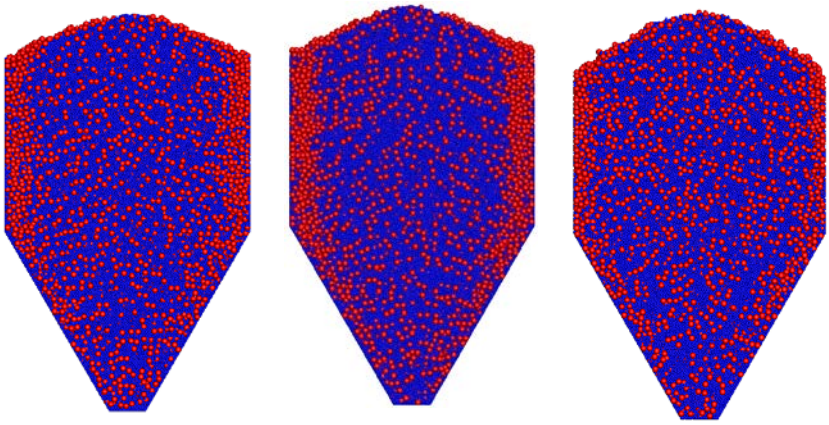

$\mu_{r,pp}$ = 0.001 d_p $\mu_{r,pp}$ = 0.005 d_p $\mu_{r,pp}$ = 0.2 d_p

(b)

Figure 4-13 Flow patterns under different conditions: (a) different particle-particle sliding friction coefficients $\mu_{s,pp}$, and (b) different rolling friction coefficients $\mu_{r,pp}$.

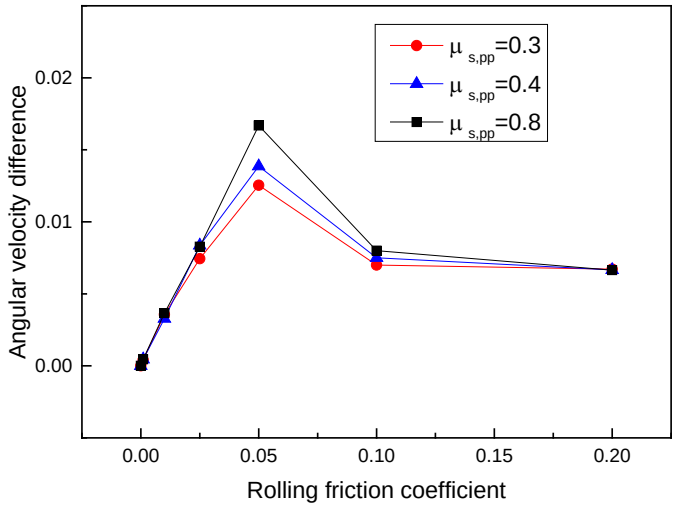

(a)

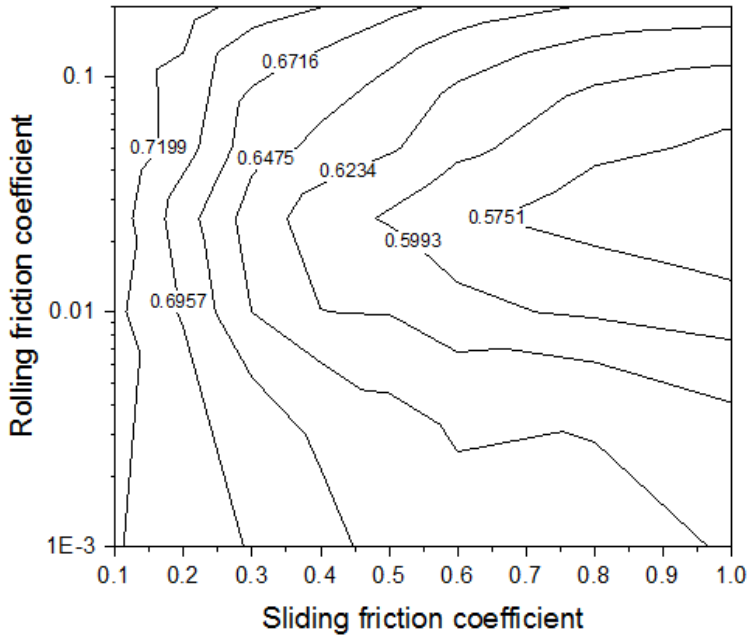

(b)

Figure 4-14 (a) Angular velocity difference between large and small particles under different $\mu_{s,pp}$, and $\mu_{r,pp}$, (b) Contour plot illustrating particle scale mixing index at various sliding and rolling friction coefficients when size ratio is 2.5 and the mass fraction of small particles is 50%.

4.3.4 Effect of the volume fraction of small particles on segregation

The small particle volume fraction χ of the mixture is another important factor which influences the segregation degree, as shown in Figure 4-15, where the volume fractions of small particles are 25%, 50%, 75% and 90%, respectively. At 25%, large particles are dominant (Figure 4-15 (a)), and small particles fill the voids among the large ones and mostly gather in the middle part. When the small particle volume fraction dominates at 75% and 90% (Figure 4-15 (c) and (d)), large particles are dispersed inside the hopper but still show a tendency to gather at the side walls. To further quantify the segregation, the distribution of small particle concentration at various radial positions is compared under different χ. In each half hopper, three sections are divided by their distance to the centre: the side wall section, the mid-radius section and the centre (see the inset in Figure 4-16).

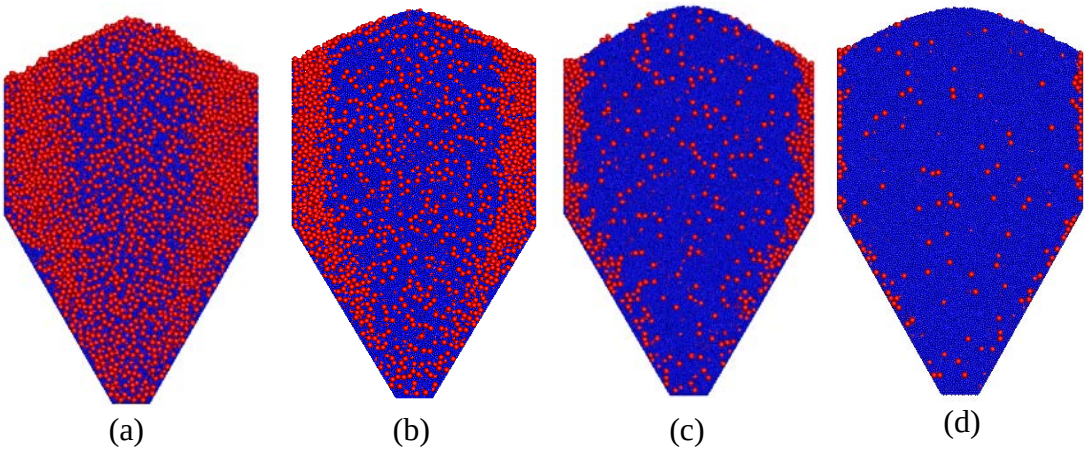

Figure 4-15 Flow patterns of different small particle volume fraction χ: (a) 25%, (b) 50%, (c) 75%, and (d) 90%.

The volume fraction of small particles in each section is obtained and plotted in Figure 4-16. The *x*-axis is the initial concentration (C_0) of small particles in the feed, and the

y-axis is the concentration of small particles (*C*) at different radial positions of the hopper. Connecting the points of the concentration of small particles at the same sections but different initial concentration χ, it can be found that each curve can be fitted by a polynomial correlation,

$$C = (1\text{-}A)\, C_o + AC_o^2 \tag{4-3}$$

The fitting parameter *A* is 1.119, -0.495 and -0.636 for the side wall, the mid-radius and the centre, respectively. The parameter A can present the segregation extent. When $A > 0$, it means that $C > C_0$. The concentration of small particles is larger than the initial concentration, which can be called positive segregation (Standish 1985). For the concentration at the mid-radius section and the centre, $A < 0$ hence $C < C_0$. The concentration of small particles is smaller than the initial concentration, named as negative segregation. Different values of *A* indicate different segregation extents. The larger the absolute value, the stronger the segregation extent.

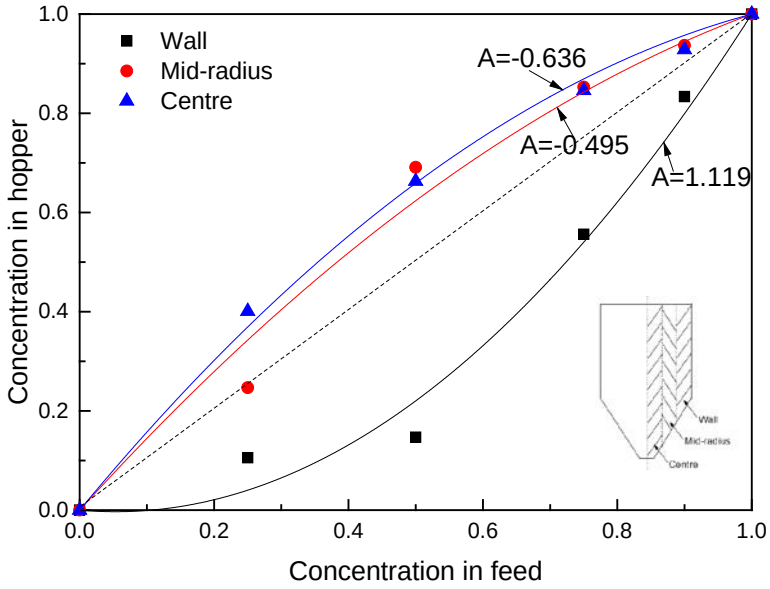

Figure 4-16 Concentration of small particles as a function of feeding concentration in three sections of side wall, mid-radius and centre.

4.4 Conclusion

Particle size-induced segregation during filling a hopper is investigated by DEM in this work. The simulation results are firstly confirmed by the physical experiments, which verifies the feasibility of DEM. The detailed conclusions are listed below.

- The simulation results confirm that during the hopper filling process, large particles tend to travel further along the slope surface and stop at the side walls while small particles tend to remain in the central region. The analysis of particle velocities, travelling time, cluster size and force networks is made in detail to obtain an understanding of particle segregation mechanisms. Both large and small particles at the side walls (e.g., D_c = 17.5 d_p) have short travelling time, high velocity and small cluster size, which verifies the bouncing mechanism for

small particles and rolling mechanism for large particles. Some particles are embedded into the bed due to cluster interactions and smaller initial potential energy with low velocity and large cluster size, then stay in the central region. Some particles with relatively large velocity and small cluster size travel further to $D_c = 12.5\ d_p$. But they spend more time because the mechanism here is being pushed by the embedded particle layer.

- A contour plot is drawn by particle scale mixing index to quantify the effects of particle sliding and rolling friction coefficients. The PSMI contours are approximately hyperbola reaching the minimum value when $\mu_{r,pp} = 0.025\ d_p$. Larger sliding friction leads to serious segregation. The smallest PSMI appears when sliding friction coefficient is 1.0 and rolling friction coefficient is 0.025 d_p.
- A correlation is fitted for the concentration of small particles at the side wall, the mid-radius and the centre. Results show that the parameter A is positive and has large absolute value in the side wall region, meaning that segregation is positive and significant. The segregation in the mid-radius section and the centre is negative ($A < 0$) and weak.

CHAPTER 5 PARTICLE SCALE MODELLING OF SIZE SEGREGATION OF GRANULAR MATERIALS DURING DISCHARGING A HOPPER

5.1 Introduction

Granular materials with different particle properties may segregate. Segregation is a common phenomenon and can occur during handling and transport process of granular materials, such as particle flow in a hopper which is widely used as a storage container to dispense or collect granular materials in engineering. However, industries are often troubled with the problem of non-uniform mixtures and hence products when particles with different sizes are discharged from a hopper. It can impact the effectiveness of medicine in pharmaceutics, and poor long-term durability for the concrete structure and uneven coke or ore distribution in an ironmaking blast furnace. Therefore, the understanding the segregation during the discharging process is important and should be paid more attention to.

Particle flow in a hopper is a long-standing research topic due to its practical application across a wide range of real-world problems. For example, the discharging rate from a hopper was firstly investigated by Beverloo et al. (1961) and improved later by others (Anand et al., 2008, Nedderman et al., 1982, Arteaga and Tuzun, 1990, Langston et al., 1995, Unac et al., 2012, Liu et al., 2014). The arching phenomenon near the orifice was also extensively examined (Reisner, 1968, Luding, 1997, Matuttis et al., 2000, Zhou et al., 2004). Most of these studies are based on mono-sized particles and focused on the flow dynamics. For mixtures with different sizes in a hopper, only limited studies have been conducted (Arteaga and Tuzun, 1990, Samadani et al., 1999, Ketterhagen et al., 2007, Anand et al., 2008, Engblom et al., 2012b, Wu et al., 2013, Yu and Saxen, 2014, Shinohara et al., 1970). By physical experiments, Arteaga and Tuzun (1990) investigated the microstructure of binary mixtures which were related to particle size ratio in mixtures and fraction ratio and modified the Beverloo et al. (1961) discharge

rate correlation to incorporate particle size ratio and mass fraction. Shinohara et al. (1970) analysed the mechanism of segregation and blending of binary mixtures for particles flowing from a mass-flow hopper based on the screen or hypothetical-hoppers model, where small particles pass through the interspaces of large particles during flow to predict the mass flow rate and the mixing ratio during the discharge. Samadani et al. (1999) explained that segregation occurs mainly on the surface of the hopper such as inclined surface flow and then large particles gather at the core area. Standish (1985) experimentally showed the concentration of small particles when discharged from a parallel bin ironmaking blast furnace hopper. Engblom et al. (2012b) proposed a correlation by sum of least squares on the basis of a large number of experiments to describe the concentration of fine particles at the walls. Recently, the simulation method such as discrete element method (DEM) has been a popular approach to analyse the microscopic parameters and visualize the internal flow properties. Ketterhagen et al. (2008, 2007) studied the changes of the mass fraction of fine particles with time during discharging process by a quasi-3D and a 3D model and validated with their experimental results under various particle properties and hopper geometries. Yu and Saxen (2010, 2014) investigated the concentration of particles in a ternary mixture during the discharging process and validated with experiments. Wu et al. (2013) also examined the segregation in a Paul-Wurth hopper for mixtures with particle size distributions.

However, most of the studies above focus on the mixtures with size ratios ranging from 1.5 to 5.0. Study of segregation during hopper discharge for mixtures with large size ratios during hopper discharging process is still lacking. Generally, percolation is the main segregation mechanism for large size ratio mixtures. But note that if two particles

have very different sizes, small particles drain through the voids of large particles simply due to the influence of gravity. This is normally termed spontaneous inter-particle percolation. Such percolation is a common phenomenon in nature and industry. Scott and Bridgwater (1976) and Cooke et al. (1978) investigated such percolation in a shear box. Jha and Puri (2010) explored the percolation under different strain rates. Zhu et al. (2009) and Rahman et al. (2008) examined the percolation velocity, residence time distribution and radial dispersion under various restitution coefficients and particle size ratios for the case with a layer of 171 small particles percolating through a packed bed. However, it is not clear how the moving of large particles, e.g. during the hopper discharging process, affects the segregation of different size ratios, particularly when the size ratio is very large.

Therefore, in the present work, the simulation is first validated by the experimental results referred in Shinohara et al. (1970) for a large size ratio. Then the microscopic parameters, including the velocity of small particles, the porosity of large particle and force structure are analysed for understanding the percolation and segregation during the hopper discharging process. Finally, the effects of size ratio and hopper geometry on segregation are also investigated.

5.2 Theoretical treatment

5.2.1 Simulation method

Please refer to Section 4.2 in Chapter 4.

5.2.2 Simulation condition

A two-dimensional hopper (Figure 5-1) is used in our simulation, which is the same as the geometry used in the experiment (Shinohara et al., 1970). It has an apex angle of 30°, which is small enough for each particle size to flow through in mass flow. The thickness, T used in the simulation is 2 d_p where d_p is the diameter of large particles. Because the width used in experiment is 17 d_p, therefore, periodic boundary conditions are also applied to reduce the effect of front and rear walls (Yang et al., 2015). The slit outlet width of the hopper is D = 0.52 cm, which is 3 d_p in our simulation, same as the value used in the experiment. This width increases to 4 d_p for small size ratio case, because arching happens at when particles have small size difference. Different cone apex angles ranging from 60° to 180° are also used to examine the effect on the percolation.

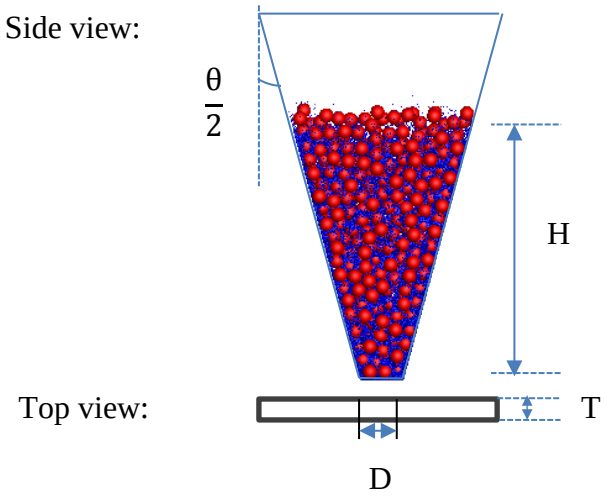

Figure 5-1 Geometry of the two-dimensional hopper in experiments and simulation.

The particles are generated at random location above the hopper at a higher height. To avoid the percolation segregation, the outlet is opened soon when some of particles

have settled, not all the particles, and packed at a height of *H* and then are discharged through the slit outlet. The detailed mixture properties and parameters used in DEM simulation are listed in Table 5-1. Mixtures with different size ratios are examined in our study. Due to the large size ratio, multigrid contact detection method (He et al., 2007) and GPU-besed code (Gan et al., 2016) are used in DEM simulation. Note that the number of large particles and hence their volume is the same in all simulation cases, and the number of small particles varies with the size ratio for each simulation.

Table 5-1 Materials properties and parameters range used in DEM simulation

Variables	**Base value**	**Parameters range**
Particle properties		
Particle shape	Spherical	
Particle number	97,768 (large: 299, small: 97469)	2,394 - 67,174 (large particle number and size are fixed.)
Particle diameter, d_p	17.05 mm (large); 1.19 mm (small)	
Size ratio, φ	14.3:1	10:1, 8:1, 6:1, 4:1, 3:1
Volume fractions of small particles, χ	10%	
Particle density, ρ_p	2520 kg/m^3	
Young's modulus, E	1.0×10^7 Pa	
Poisson ratio, ν	0.3	
Interaction parameters		
Particle-particle sliding friction, $\mu_{r,pp}$	0.6	
Particle-wall sliding friction, $\mu_{s,pw}$	0.6	
Rolling friction coefficient, μ_r	0.025 d_p	
Damping coefficient	0.3	
Dimensionless hopper geometry		
Outlet slit, D	3 d_p	4 d_p (when arching happens)
Thickness, T	2 d_p	
Apex cone angle θ	30^o	60^o, 120^o, 180^o

5.3 Results and discussion

5.3.1 Model validation & size segregation analysis

In the simulations, mixtures of large and small particles are discharged from the hopper by gravity. The discharging time is normalized by the fully discharged time, giving the normalized discharging time (NDT), which is defined as NDT = instantaneous discharge time/fully discharged time. The snapshot of flow patterns during the discharging process is shown in Figure 5-2. It can be clearly seen that small particles are discharged out first due to the percolation through the voids formed by large particles and the small particles near the side wall region are discharged slower than that at the centre.

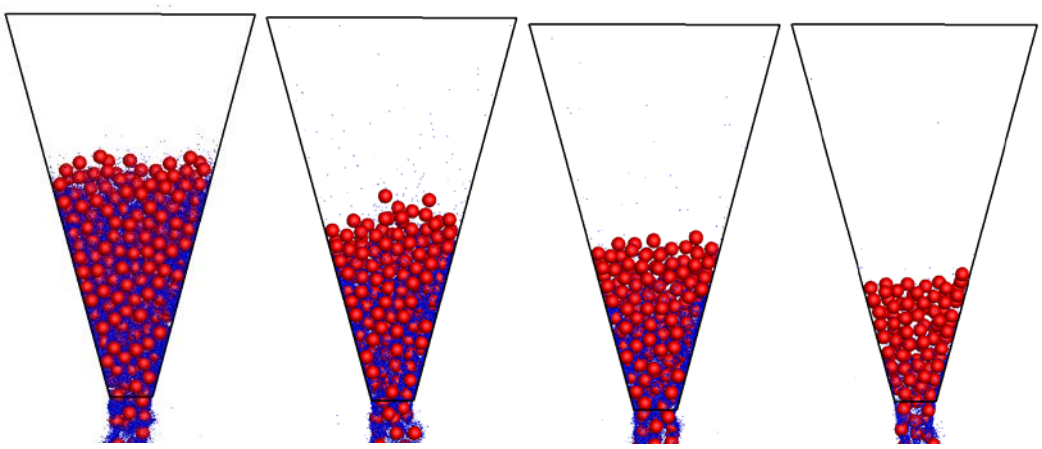

(a) NDT=0.13 (b) NDT= 0.22 (c) NDT=0.48 (d) NDT= 0.60

Figure 5-2 Snapshots of particle flow patterns at different NDT

During the discharging, the concentration of large particles discharged at the outlet in a fixed running time by considering the particles remaining in the hopper is recorded, and the results are compared with experimental values, and shown in Figure 5-3. It

illustrates that at the initial stage, both results show that an initial discharge concentration of large particles at outlet is around 0.85, indicating the small-particles-dominated flow compared with the initial overall large particles concentration of 0.9. Then from NDT= 0.5, the concentration of discharged mixture changes from a small-particles-concentrated value to a large-particles-concentrated value, a concentration of large particles at around 1.0. Afterwards, small particles are fully discharged first and only large particles are left at NDT= 0.7. Hence, the Small particle Fully Discharged Time (SFDT) is 0.7 in the simulation. In experiments, after NDT= 0.7, the volume concentration of large particles are bigger than 0.98, which is very close to 1.0.

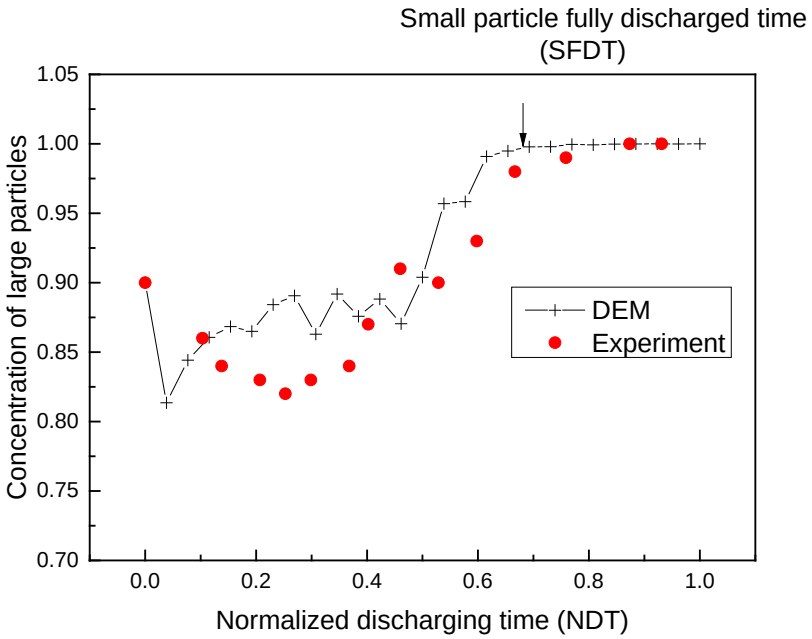

Figure 5-3 Concentration of large particles during the discharging process (The experiment data are from (Shinohara et al., 1970)),

To quantify the different behaviour of large and small particles in the hopper, the velocity of both large and small particles from different positions are analysed. Four regions, marked by different colours, are shown in Figure 5-4 (a): the right sidewall

(RW), the left sidewall (LW), the central higher positon (CH) and the central lower position (CL). The average resultant velocities of large and small particles in these regions are calculated during discharge, and shown in Figure 5-4 (b). It can be found that the particles from both RW and LW discharged over a longer period compared with the particles in the CH, indicating that the sidewall has a significant effect on the flow of granular materials in the hopper. Meanwhile, large particles have longer discharging time than small particles in all four regions. It shows that small particles have a larger relative velocity in order to pass through the voids formed by large particles. This observation provides a quantitative insight into the gravitational percolation mechanism. Particles at CL have the largest absolute average velocity among these eight curves, meaning that they have the largest potential trend for discharging. This is because they are above the outlet, there is no obstacle reaching the outlet under gravity.

It can be found that the particles from both RW and LW discharged over a long period compared with the particles in the CH, indicating that the side wall has a significant effect on the flow of granular materials in the hopper. Meanwhile, large particles have longer discharging time than small particles in all four regions. It shows that small particles have a larger relative velocity in order to pass through the voids formed by large particles. This observation provides a quantitative insight into the gravitational percolation mechanism. Small particles marked as red have the largest absolute average velocity among these eight curves, meaning that they have the largest potential trend for discharging. This is because they are near the outlet, the effect of the side wall is tiny compared with other regions. Both large and small particles have relatively large velocity. The particles here have loose packing which leads to large porosity at CL.

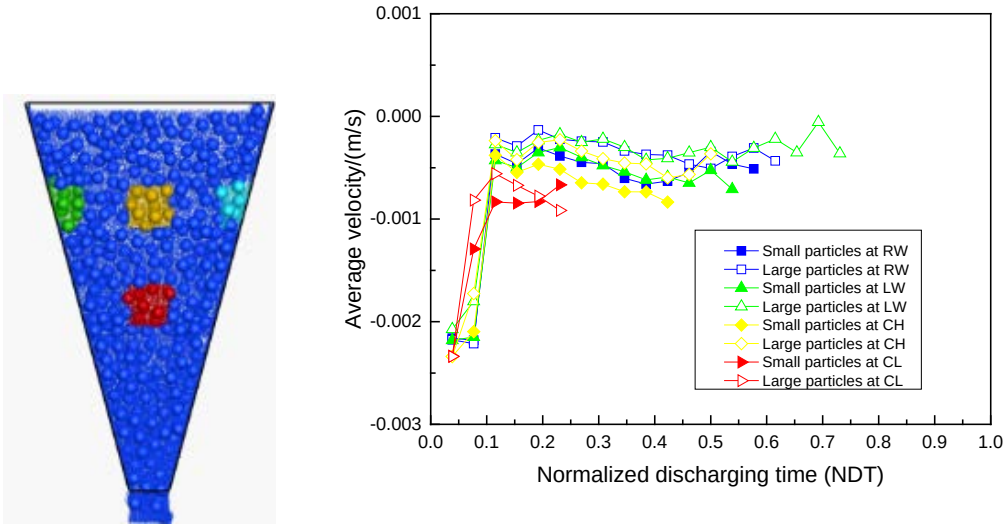

(a) (b)

Figure 5-4 (a) Coloured four regions (yellow – the centre higher position (CH), red – the centre lower position (CL), green – the left side wall (LW), and light blue – the right wall (RW)), and (b) the average velocity of both large and small particles in the four regions.

At NDT = 0.2, the flow pattern snapshot showing the movement of particles in four regions and the velocity probability density distribution of small particles in each region is shown in Figure 5-5. The particles in the red region have formed a narrow elongated shape compared with other three regions. The probability density distribution of CL is a linear trend which is different from other three regions, which are Gaussian distribution. Half of the particles in CL have large absolute velocities, at around -0.85 mm/s, and this leads to the slim shape. On the contrary, particles at the same height of RW, LW and CH show similar probability density function. Most of the particles have velocities varying from -0.15 mm/s to -0.35 mm/s and their density distributions are analogous to a Gaussian distribution. Comparing the probability density of small particles with a large absolute velocity above 0.5 mm/s, it can be found that this density of RW and CH is larger than that of LW. It agrees with the coloured particles

distribution from Figure 5-5 (a), where small particles drop faster. It might be caused by the jamming at the outlet, leading to the unsymmetrical distribution of RW and LW.

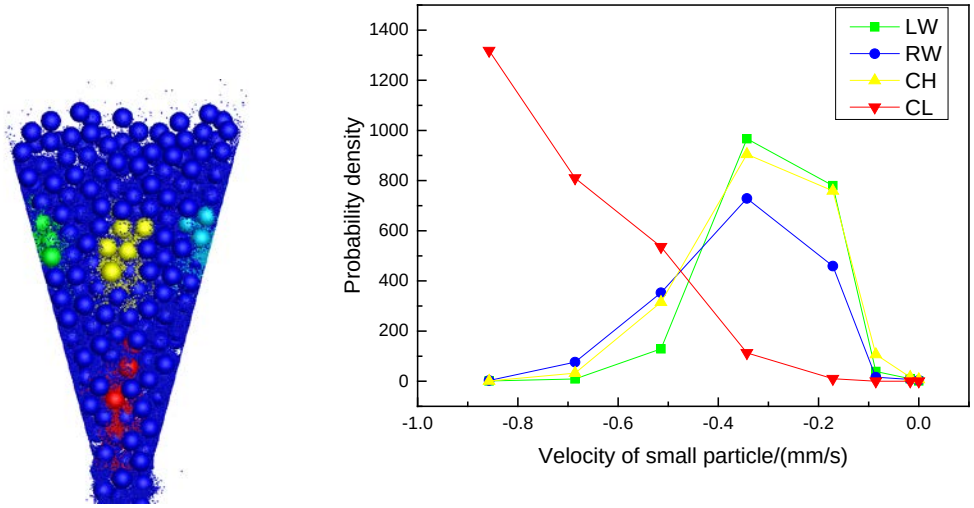

(a) (b)

Figure 5-5 (a) flow pattern snapshot of four coloured regions at NDT = 0.2; and (b) the velocity probability density distribution of small particles in each region at NDT = 0.2

This distribution is closely related to the voids distribution which is presented by porosity. To decrease the effect of boundary and segmentation of large particles when computing porosity on rectilinear grids, a 3D Voronoi tessellation is used to segment the domain based on the large particles, ignoring the small particles inside the voids between the large particles. The porosity of large particles (only considering large particles by ignoring the small particles inside) in these four regions at NDT= 0.2 is obtained and shown in Figure 5-6. It can be found that large particles at the centre regions CH and CL have large porosity than particles from the side wall RW and LW. It means that more voids exist in the centre and therefore, small particles have more opportunities to percolate through the voids among large particles. Information about the distribution of small particles can be derived from the number of small particles in

each large particle Voronoi cell N_s and the number of small particles in contact with each cell's core large particles N_{sc} is also illustrated in Figure 5-6. It shows that in the voids among large particles, the distribution of small particles is different in the four coloured regions. The CH region has the lowest number of small particles in each Voronoi cell. For small particles in contact with the core large particles, the CH also has the smallest number, which implies that small particles may flow through the large voids without interaction with the adjacent large particles. This can also explain why velocity difference between large and small particles are large in the centre. Due to the congestion of small particles at the hopper outlet, the number of small particles and the contacts number with the core large particles is largest in the CL among these four regions. The number ratio N_{sc}/N_s is larger than other regions, meaning more interactions between large and small particles. The number of small particles and the contact number are similar in RW and LW and have a relatively large value. It means that small particles aggregate at the side wall. After their percolation through the voids, small particles cannot find a direct way to the outlet because of the effect of inclined wall, leading to the high concentration of small particles around the side wall.

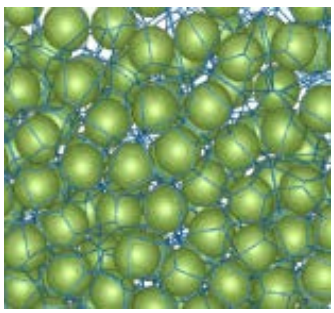

(a)

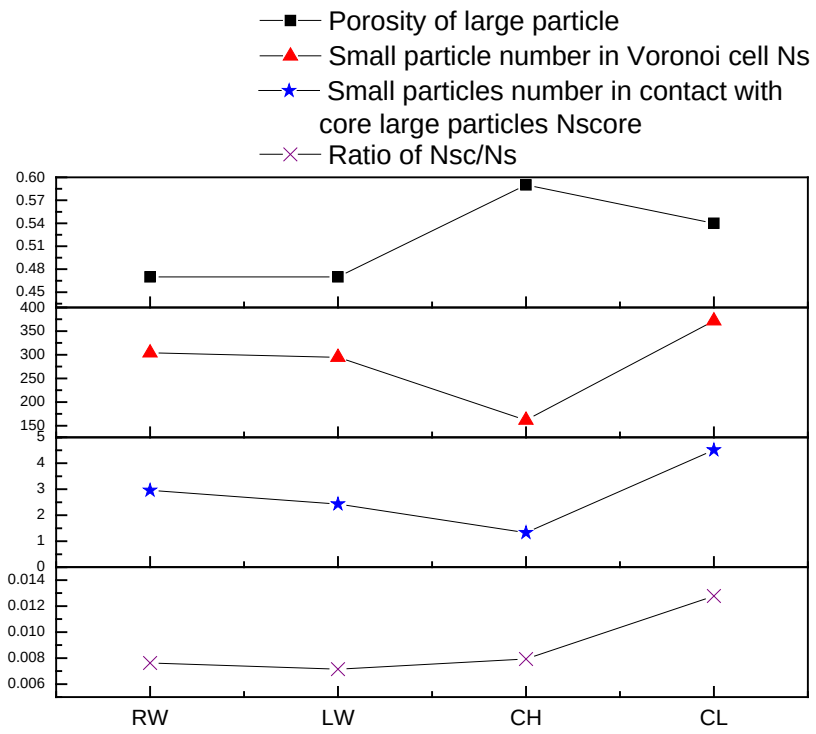

(b)

Figure 5-6 (a) Voronoi diagram; (b) porosity of large particles, number of small particles in Voronoi cell, number of small particles in contact with core large particles and their ratio in different positions at NDT=0.2.

The distribution of large and small particles can be further understood in terms of particle-particle interaction forces, mainly the contact force. Figure 5-7 shows spatial distribution of the normal contact forces in the hopper. The cylinder length represents the contact type, for example, the small-small contact (the contact of small particles to small particles) has the shortest length, large-large contact the longest, and small-large contact medium length. The diameter represents the force magnitude. It can be found that the force chains have various patterns at different regions. In the CH, most of the samples show umbrella frames, where the core is occupied by large particles and the frames are the forces caused by small particles falling and contacting with the core large particle, as shown in Figure 5-7 (b). Note that most of the small particles in CH do not produce a contact of sufficient magnitude to be seen here because their interaction with

large particles is limited to flow collisions and they do not transmit sustained contact forces through the bulk packing. This explains that why percolation is easy for small particles in this area. Then at the side wall, most of the chains are small, indicating that small particles accumulate here. The umbrella frame at CL is denser compared with CH, meaning that small particles are blocked to some extent, but the block is not serious and most of them still percolate or are discharged from the hopper with a high speed.

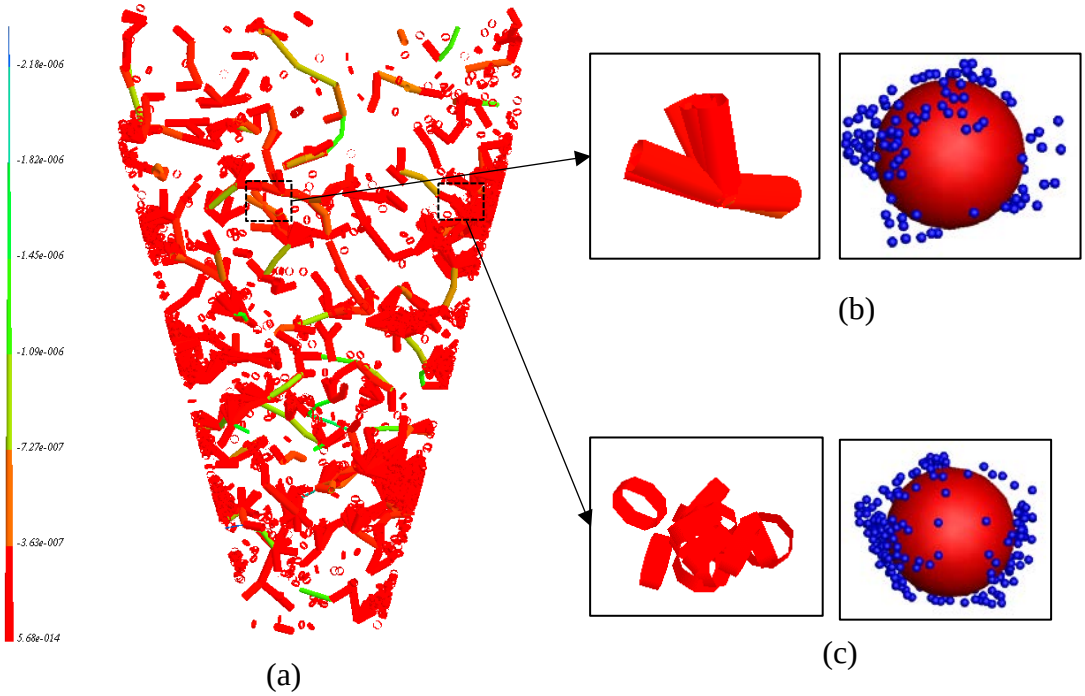

Figure 5-7 (a) Contact force network in the hopper; (b) an umbrella frame and pattern in CH, and (c) the pattern of small particles at the side wall.

5.3.2 Effect of size ratio on discharging process

For the large size ratios, the results show that percolation is the main flow mechanism for small particles and their fully discharged time is primary related to the voids concentration. The voids concentration might differ significantly with a size ratio of particles in mixtures. To understand the effect of size ratio on the void concentration

and the spatial distribution of small particles, mixtures with different size ratios from 4.0 to 14.0 are examined.

The concentration of large particles discharged from the hopper at different times is shown in Figure 5-8. The small particles fully discharged time (SFDT) can also be seen for different size ratios. These results show that for all size ratios, at the initial stage, it is a small-particle-concentrated period where the concentration of large particles is around 0.88. Then at NDT= 0.5, it becomes a large-particles-concentrated period, where almost all values are larger than 0.9. However, for small size ratios such as 4.0 and 6.0, the large particles concentrated period is longer than large size ratio until small particles are fully discharged. The SFDT is similar for size ratios of 10 and 14, which is the smallest due to the significant difference of size ratio. Percolation is the main mechanism in these cases, and small particles have fewer interactions with large particles and drop quicker in the voids. For smaller size ratios, the mechanism might be different which leads to a late SFDT.

It is known that large particles and small particles have different velocities in the hopper, as shown in Figure 5-4 and Figure 5-5. The difference between these two kinds of particles determines the SFDT. It can be seen from Figure 5-9 that the velocity difference increases with size ratio increasing. The velocity difference is larger for particles from the central region (CH and CL) than particles from the side wall region (RW and LW). For size ratios of 4 and 6, the difference between various regions is almost same and very small, which means that particles in the hopper move in a similar pace, and percolation is not serious in these situations. Mixtures with size ratio larger than 8, the velocity difference at CH is significant, showing that small particles percolate through the voids formed by large particles. It can be concluded that when

the velocity difference is smaller than 0.07 mm/s, where size ratio is lower than 6.0, percolation does not play a dominant role in segregation. Considering the particle size, this turning velocity difference could be written as 0.041 d_p/s.

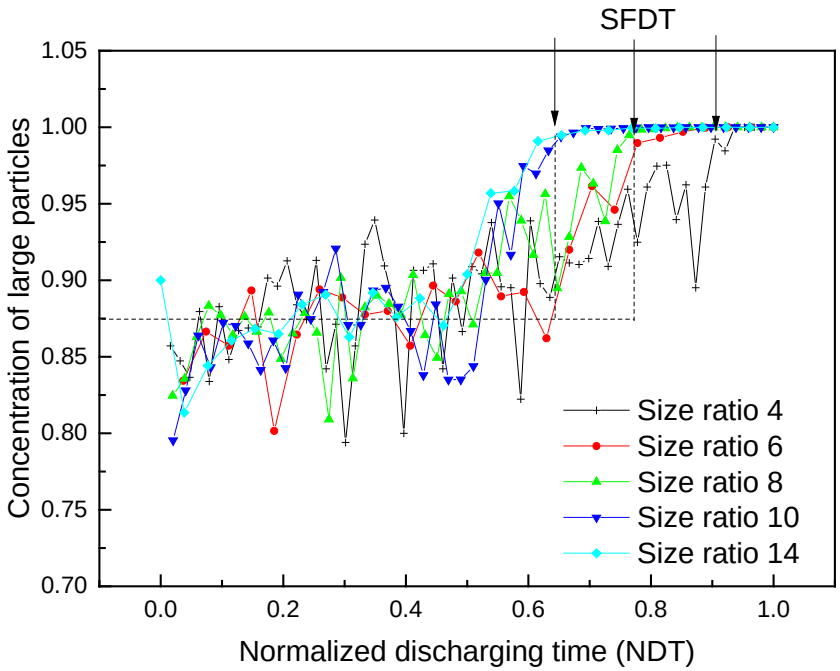

Figure 5-8 Concentration of large particles during the discharging process at different size ratios

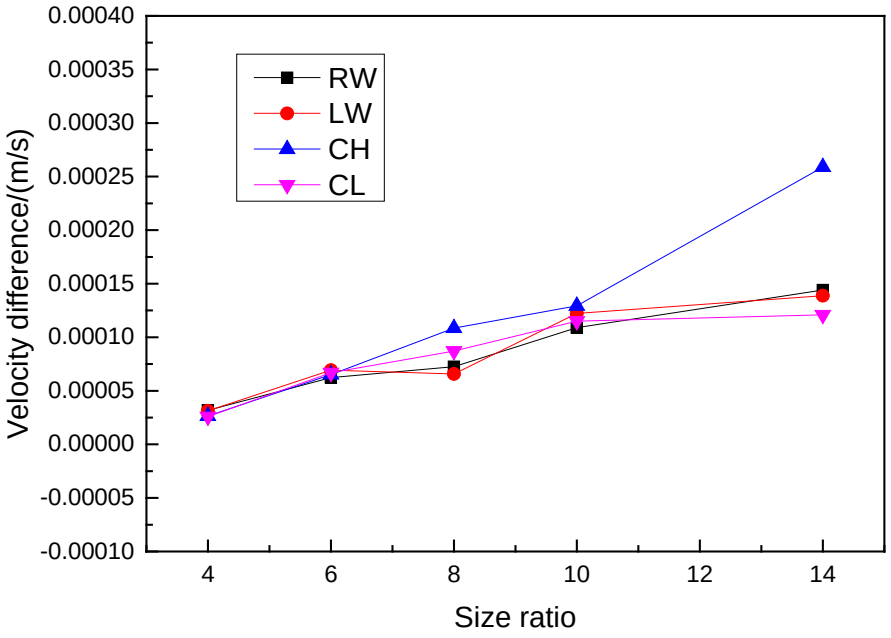

Figure 5-9 The velocity difference between large and small particle at various positions under different size ratios

Further comparison on the porosity of large particles, the volume of small particles, and the ratio of number of small particles in contact with core large particles N_{cs} to the number of small particles in this grid N_s are obtained from a 7 d_p × 7 d_p grid chosen from the hopper centre at NDT= 0.45 and shown in Figure 5-10. It can be found that porosity of large particles decreases with the increase of size ratio, and is largest at smallest size ratio of 3. This is because for large size ratio, small particles spread in the voids formed by large particles. But for small size ratio, small particles push the large ones and makes the porosity of large particles small. In the meantime, the volume of small particles is large at this time. However, if most of the small particles are in contact with large ones, they cannot percolate smoothly. Therefore, the ratio N_{cs}/N_s is a significant value, which can reflect the small particle distribution in the discharging process. This ratio decreases with size ratio increasing. Interestingly, when size ratio is

3, the outlet size is 3 d_p, and an arch forms at the outlet. Thus, for the case with a size ratio of 3, the outlet size is set as 4 d_p and the arch disappears. The concentration of large particles and the porosity are checked for this case. Compared with other size ratios at the same outlet size, it can be found that a large number of small particle in the mixture can decrease the possibility of the arch formation.

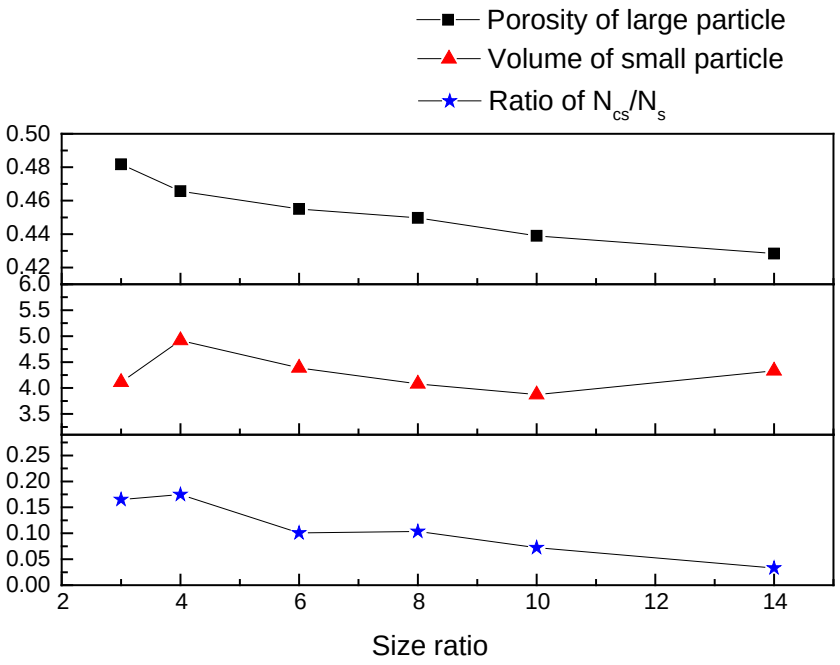

Figure 5-10 Porosity of large particles, the volume of small particles in the chosen grid and the number ratio N_{cs}/N_s (from top to bottom) in the centre hopper for different size ratios.

The difference caused by size ratio can be further seen from the flow patterns and the normal contact force, as shown in Figure 5-11 and Figure 5-12. For large size ratios such as 10 and 14, the number of small particles is huge, therefore, the umbrella frame in normal contact force has more branches. The force networks formed by large particles at different size ratios are similar. However, for the same voids, smaller size particles are free to fall through. Hence, besides the particles which are in contacts with

core large particles, the number of free ones are still large. This is the reason for the velocity difference between large and small particles and the main cause of percolation occurrence.

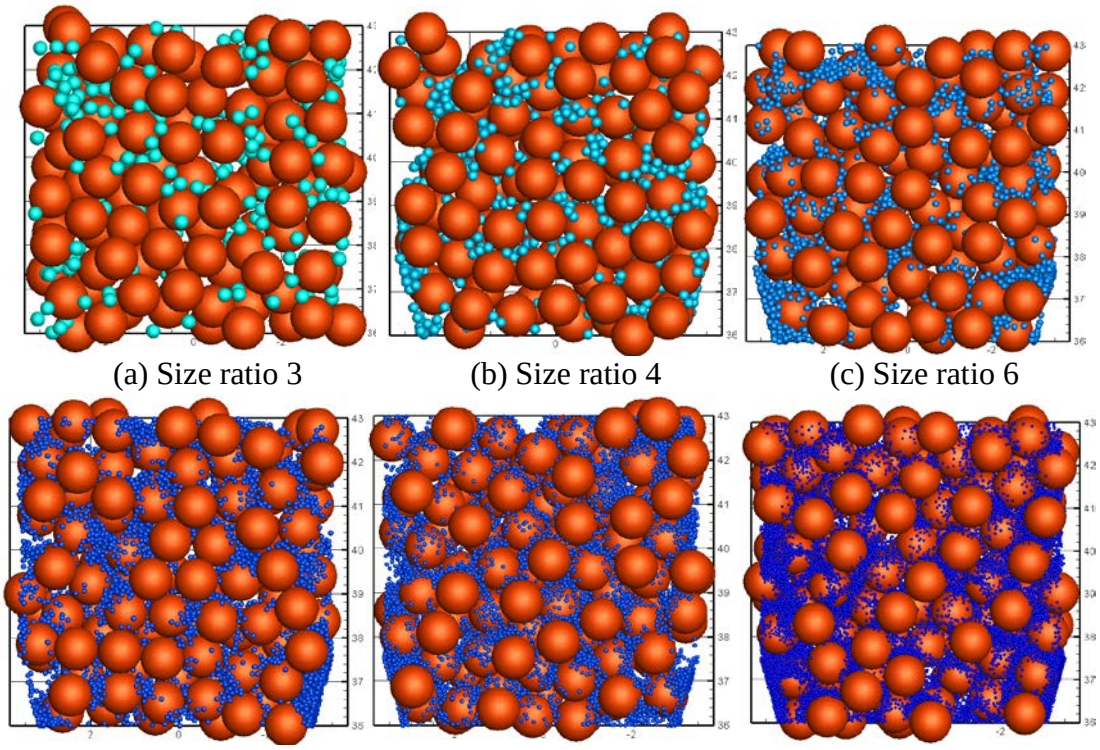

(a) Size ratio 3 (b) Size ratio 4 (c) Size ratio 6

(d) Size ratio 8 (e) Size ratio 10 (f) Size ratio 14

Figure 5-11 Flow patterns of different size ratios in chosen 7 d_p × 7 d_p grid at the unit discharging time of 0.45.

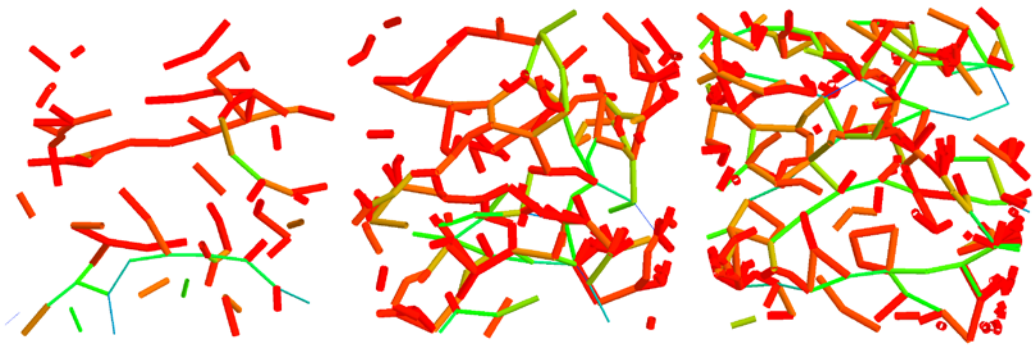

(a) Size ratio 3 (b) Size ratio 4 (c) Size ratio 6

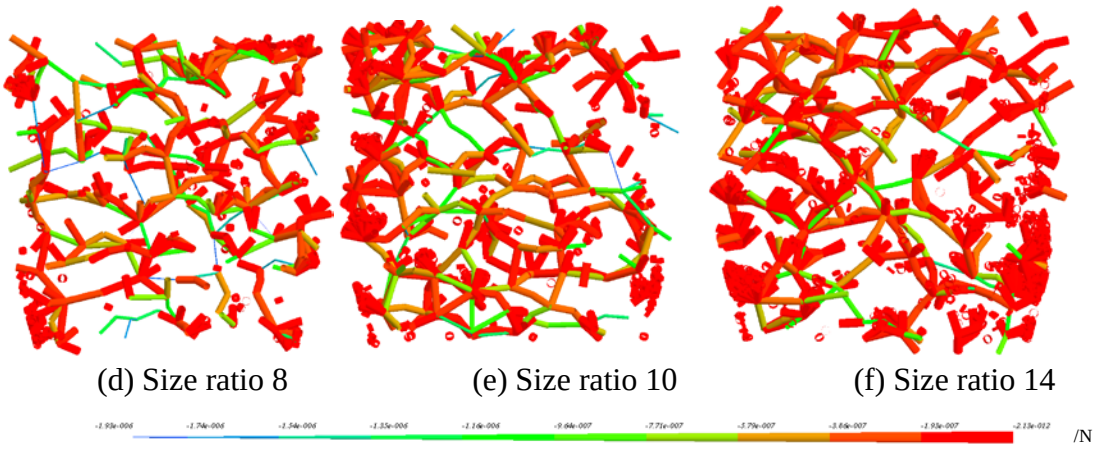

(d) Size ratio 8 (e) Size ratio 10 (f) Size ratio 14

Figure 5-12 Contact force network in the chosen grid for different size ratios

5.3.3 Effect of cone angle on discharging process

The hopper shape is also a significant factor influencing the discharging process. In this section, the hopper cone angle varies and its effect on segregation is examined based on mixture properties used in Table 5-1. The discharge snapshots of flow patterns for different cone angles at the initial stage and the mass discharged at 40% are shown in Figure 5-13. The concentration of large particles in the mixture discharged is shown in Figure 5-14. Because of the hopper shape difference, the flow rate differs significantly, therefore, the mass discharged fraction is used here to show the discharging process time.

From Figure 5-13 (b), it can be observed that the distribution of small particles varies significantly for different cone angles. Due to the same large size ratio, all small particles at different cone angles percolate through the voids formed by large particles and discharge from the hopper quickly. Therefore, a region of only large particles remains in the upper part of the hopper for all the cone angles. However, small particles are distributed uniformly and discharged together with large particles evenly for $\theta = 30^{o}$ and 60^{o}, which are flat and smooth curves shown in Figure 5-14. On the other hand, for

θ =120º and 180º, small particles are percolated in large cross section, but most of them are gathered at the side wall hence cannot be discharged smoothly. Therefore, the concentration of large particles reaches 0.9 at θ =120º and 180º faster than that at θ =30º and 60º. But the concentration at θ =120º spends more time in reaching 1.0, where the slope of the turning point line is small, compared with that at θ =30º and 60º. For θ =180º, almost half of the mixtures are blocked at the corner, and small particles near the side wall have small chance to fall out.

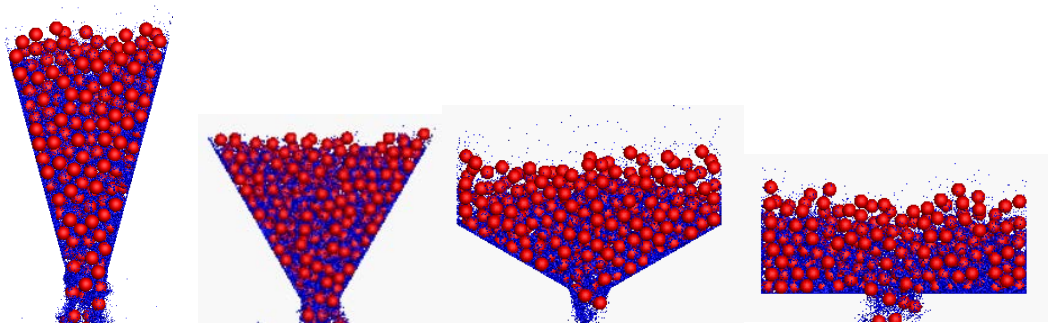

θ =30º θ = 60º θ =120º θ = 180º

(a) Initial stage

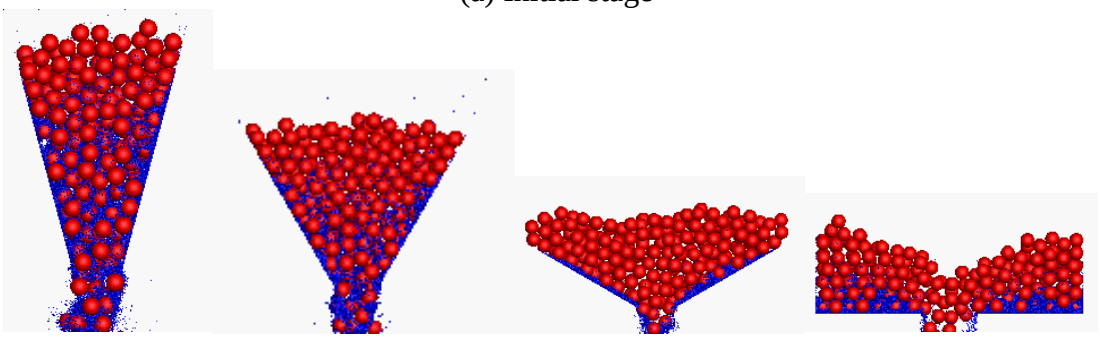

θ =30º θ = 60º θ =120º θ = 180º

(b) Mass discharged fraction 40%

Figure 5-13 Snapshots of the flow patterns at different discharging angles

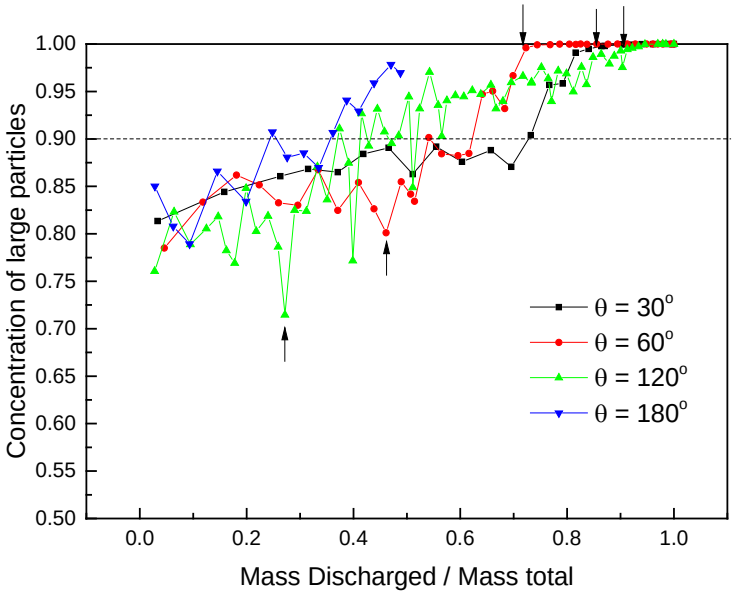

Figure 5-14 Variation of the concentration of large particles with discharged fraction at different hopper angles.

When small particles are gathered at the side wall, their movement is determined by the adjacent large particles. This can be found from the normal contact force network in Figure 5-15. The force chains between small particles are among the network of large particles, then the small particles wait for the chance to percolate and drop down. For example, the kink points at 60 º and 120 º are when small particles at the side wall are pushed out. Therefore, for large cone angle hopper, which is commonly used in industry, to control the movement of large particles around the bottom of the hopper is meaningful. In addition, when the cone angle is 180 º, arching is formed at the outlet even the outlet size is same as other cone angles. Similar with small size ratio, the movement of small particles between the large particles can decrease the chance of arch formation.

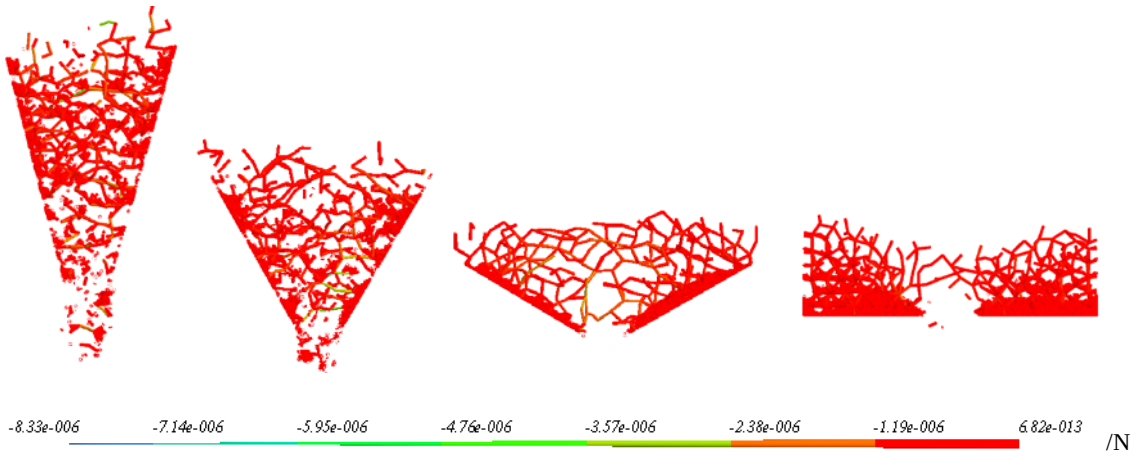

Figure 5-15 Contact force network at different discharging angles

5.4 Conclusion

The mixture with large size ratio (14.3:1) is discharged from a hopper and the concentration of large particles discharged is validated by physical experiment from literature data. The results show a quantitative agreement. The following conclusions can be drawn from the present work.

- The velocity difference, (an indicator of percolation mechanism), between large and small particles is significant in the centre at the upper hopper. In addition, particles in the centre travel faster than that at the side wall. This difference is related to the porosity of large particles and the number ratio of small particles which indicates the fraction of free drop particles. Results show that mixtures with large porosity and a large amount of fraction of free small particles ($1 - N_{cs}/N_s$) easily segregate and has a large small particle fully discharged time.

- Mixtures with different size ratios also have various SFDT. For small ratio size, the velocity difference between large and small particles are small. This is

caused by a small fraction of free small particles. In the present study, when the velocity difference is below 0.07 mm/s and the number ratio N_{cs}/N_s is above 0.10, percolation is not the dominant mechanism, and the segregation is not obvious.

- For different hopper geometries, the SFDT is related to the cross-section of the hopper. When the cone angle is large, the wide cross-section leads to fast percolation of small particles. But because of the wall and the relatively small outlet slit width, small particles are gathered at the side wall and are taken along by the movement of large particles.

CHAPTER 6 EFFECT OF OPERATION CONDITIONS ON SIZE SEGREGATION OF PARTICLES DURING CHARGING AND DISCHARGING A PAUL-WURTH HOPPER

6.1 Introduction

In an ironmaking blast furnace, burden materials (coke, sinter, pellets and fluxes) are weighed from bins in the stock-house and delivered to the furnace top bins before discharged into the furnace by the burden distribution system. Several bell-less top charging systems have been developed by Paul Wurth, including the serial-hopper type and parallel hopper type. The latter one is innovative which can achieve flexible burden distribution and control segregation to some extent, therefore, named as Paul-Wurth (PW) type hopper, and has been widely used in practice. The ferrous batch with sinter, lump ore, pellets, limestone and a small coke, representing a very wide range of sizes, shapes, and densities, is likely to segregate. Further, the batches pass through the rotating chute and deposit on the stock-line. Hence, understanding how size segregation happens during charging into or discharging from the PW hopper is significant for the smooth operation of a blast furnace.

Most of the segregation studies in a hopper by experiments (Shinohara et al., 1972, Arteaga and Tuzun, 1990, Jha and Puri, 2009, Engblom et al., 2012b) and simulation (Ketterhagen et al., 2007, Yu and Saxén, 2010, Zhu et al., 2009) in the past decades focused on conical shape, which is more symmetrical and fundamental. However, for the application of a blast furnace charging system, most of the investigations focused on the effect of rotating chute (Gan et al., 2016, Xu et al., 2011, Xu et al., 2018)or the whole system. For example, Zhang, et al. (2014) studied the flow behaviour in a conical hopper and effect of the chute inclined angle. Mio, et al. (2009, 2010, 2017) built a simulator for the whole charging system and analysed the effect of chute angle. Only few research were carried out to study the segregation phenomenon in a PW type hopper. Standish (1985) carried out the experiments to study the segregation in a PW

hopper and examined the distribution of particles in the hopper. But the filling positions were set as central and fixed, and the studies on the effects of operating conditions were not involved. Yu et al. (2014) found that the effect of particle shape on segregation was insignificant. Wu, et al. (2013) found that the segregation along the radial direction did not significantly affect by burden apex which might be caused by large size distribution and small particle numbers, and this was not consistent with the practical production which bears serious segregation. Qiu, et al. (2017) investigated the velocity, force chain for mono-sized particles when discharging a PW hopper. In addition, wear of the hopper concerns the lifetime and safety products in the process. But the wall stress has been studied for mono-sized particles by experiments and simulations such as DEM for spheres (Qiu et al., 2017) and ellipsoid particles (Liu et al., 2014) and finite element method (Zheng and Yu, 2015, Wang et al., 2014). Results show that the largest wall pressure happens in the upper part of the conical hopper. The wall stress analysis has been studied for mono-sized particles by experiments and DEM (Qiu et al., 2017), ellipsoid particles by DEM (Liu et al., 2014) and mono-sized particles by finite element method (FEM) (Zheng and Yu, 2015, Wang et al., 2014). However, It is not sure whether the wall pressure distribution is same for binary mixtures and mono-sized particles. Therefore, for the binary mixture, the factors such as operating conditions including filling positions and angles and wall stress which are related to the practical application, still need to be taken in to account to predict the size distribution. What's more, in order to predict the size distribution during charging and discharging a PW hopper and provide the corresponding methods to reduce segregation, the operation conditions including filling positions and angles, and wall stress which are related to the practical application, still need to be taken into account.

To address this, in present work, a quasi-three-dimensional PW model based on a No.5 blast furnace in BlueScope is built by DEM to study the effects of filling operation and filling angles on the size segregation during charging and discharging a PW hopper. Then the degree of segregation is used to quantify the segregation extent during charging and discharging. Further, the contours during discharging and the wall stress distribution are drawn to further discuss the segregation mechanisms.

6.2 Theoretical treatment

6.2.1 Discrete element modelling

Please refer to Section 4.2 in Chapter 4.

6.2.2 Simulation condition

The geometry of the quasi-3D rectangular cross-sectioned PW hopper used in this work is shown in Figure 6-1 (a), which is one critical part of the parallel Paul Wurth hopper in the burden charging system (as shown in Figure 6-1 (b)). In the charging system, particles fill through a tilting chute and then are charged into a PW hopper. After this, particles are discharged out and fall into the furnace. Therefore, as a transition vessel in the system, the segregation during filling and discharging out the hopper is significant to the distribution of particles in the blast furnace. In our simulation, particles are generated randomly in a feeder hopper and then discharged out through an inclined surface, which replaces the moving of particles from the belt in a real system. The angle and the endpoint of this inclined surface can be adjusted for parameter study. The feeder hopper is set conical to make particles flow as close as mass flow pattern, and then particles are more uniform when filling into the PW hopper. Then particles stack in the PW hopper and pile up. Here, periodic boundaries are used to reduce the

effect of front and rear walls (Yang et al., 2014). Particle properties used in this work are listed in Table 6-1.

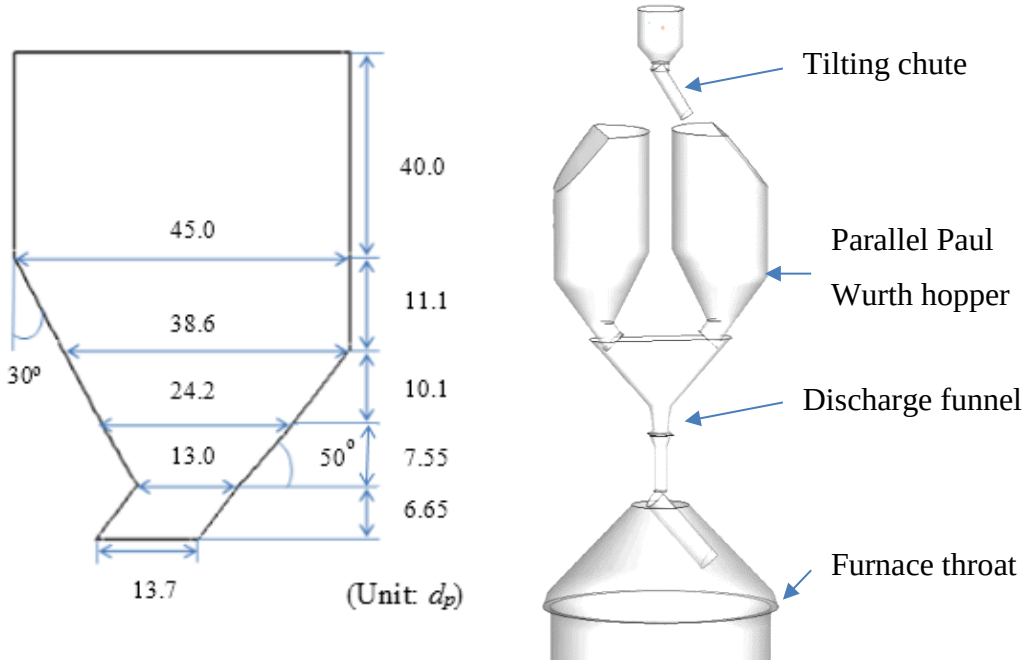

(a) (b)

Figure 6-1 Schematic illustration of (a) the geometry of a quasi-3D hopper used in current work; (b) burden charging system above a blast furnace.

Table 6-1 Materials properties and parameters used in the simulation

Parameter	**Value**
Particle size, d	80 mm, 20 mm
Particle density, ρ	900 kg/m^3
Volume fraction	Large particles 50%, Small particles 50%
Total particle number	148968
Young's modulus, Y	1×10^7 N/m
Poisson's ratio, σ	0.3
Sliding friction coefficient,	0.6
Rolling friction coefficient,	0.025 d_p

6.3 Results and discussion

6.3.1 Charging in a Paul-Wurth hopper

6.3.1.1 Segregation flow patterns for different filling positions

The filling positions affect the particle distributions in a hopper significantly. Different filling positions including the left side wall (P1), ¼ of hopper width from the left side wall (P2), the centre (P3), ¾ of hopper width from the left side wall (P4) and the right side wall (P5) are studied. The flow patterns and the spatial distribution of the concentration of small particles after charging in a PW hopper at corresponding filling positions are shown in Figure 6-2. It can be found that the filling positions of P1 and P5 gather most of the large particles compared with the filling positions of P2 and P3 (Figure 2 (b) and (c), respectively), which is marked as light blue colour in Figure 6-2 (i). It can be found that when the filling positions of P1 and P5 gathers most of the large particles compared with positions of P2 and P3 (Figure 6-2 (i) (b) and (c), respectively), which is marked as light blue colour in Figure 6-2 (ii). Meanwhile, the area at the left side wall is filled with small particles. It is similar with the right filling position P5, regardless the shape of PW hopper. Large particles gather at the side wall which is opposite to the filling position. This might be because the left and right filling positions (P1 and P5) allow a longer slope for particles to roll down. Therefore, segregation happens in this rolling process and is more distinct under these filling positions. The area of the concentration of small particles below 0.1 decreases from P1 to P3, the same with the red region, where the concentration of small particles is above 0.9. This is attributed to the different distances of filling positions to the side wall. For P1, the centre

of the slope is at the left part of the hopper, then particles roll down from the filling point. Therefore, the slope where particles rolling down is longer than other two situations P2 and P3. It is known that mixtures are distributed due to the competition of large particles rolling down and mixtures embedding in when filling in the hopper. When the slope is longer, large particles have more time to roll down rather than pushing away. The left side wall also influences the small particles gathering. (b) and (d), (a) and (e) are axisymmetric. The only difference is the directions of large particles gathering area, therefore, it determines what kind of particles are first discharged out at the discharging process. Then consider the small particle gathering area, which is the place under the filling place. The concentration of small particles in P1 at x = 20 d_p is almost 1.0, and this number keeps high and above 0.9 until dimensionless x = 15. d_p It means that the small particle gathering area of P1 occupies 5/45 of the whole hopper width. This number decreases for the 1/4 filling (P2) and central filling (P3) cases. This also gives a quantitative value evaluating the particle distribution in the hopper. More quantitative data on the concentration of small particles can be found in Figure 6-3. It shows the distribution along the radial position of the average concentration of small particles at dimensionless z at 35-45 d_p and 15 d_p.

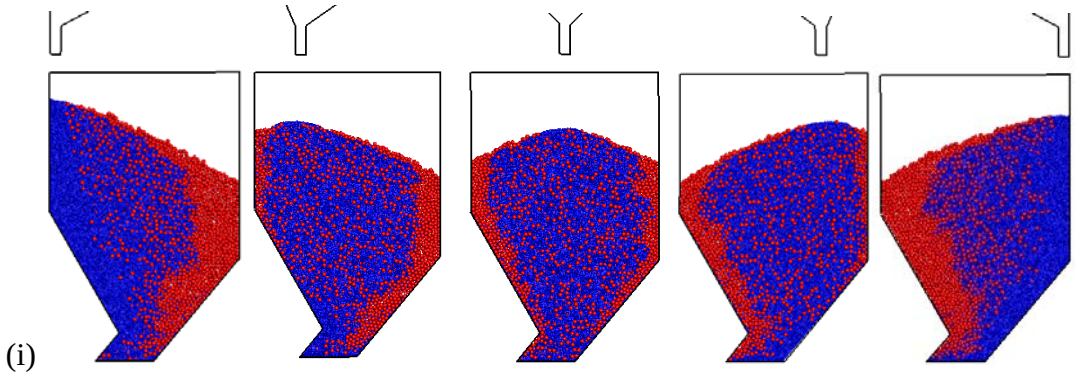

(i)

(a) (b) (c) (d) (e)

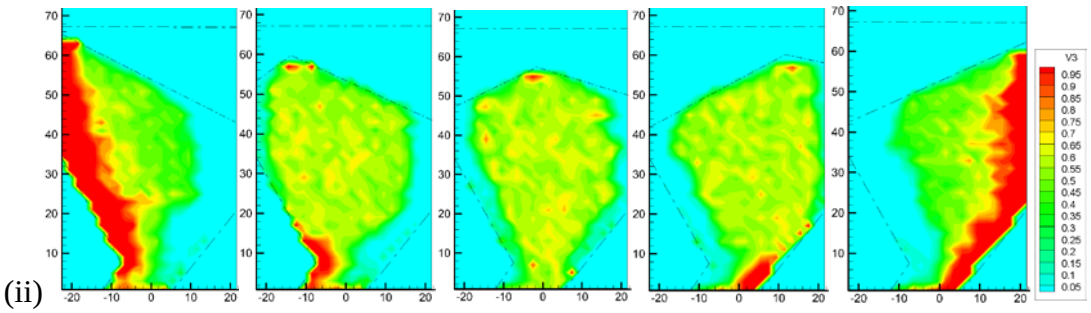

Figure 6-2 (i) Flow patterns of hopper filling at different positions (outlet size is 3 d_p); (ii) Spatial distribution of concentration of small particles in the hopper (the grid is 2.0 d_p, V3 is a concentration of small particles) (a): P1 – left side wall; (b) P2 – ¼ of hopper width from the left side wall; (c) P3 – the centre; (d)P4 – ¾ of hopper width from the left side wall and (e) P5 – the right side wall

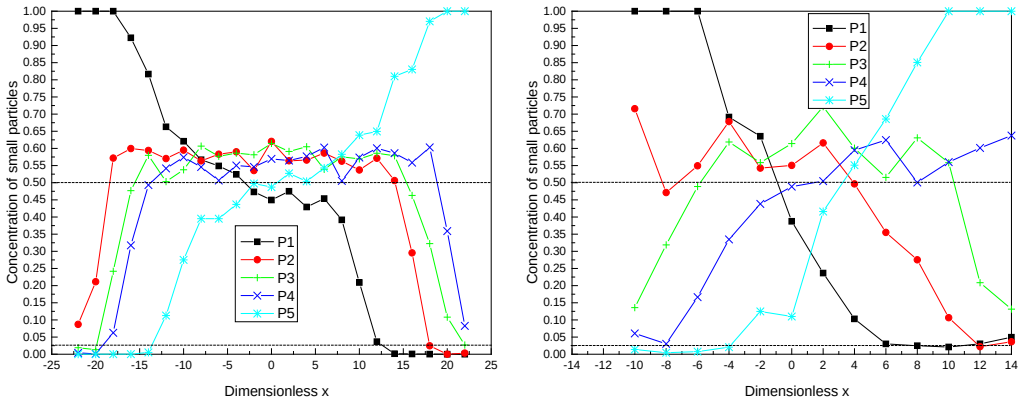

Figure 6-3 Concentration distribution of small particles in the hopper at dimensionless z (a) 35-45 d_p and (b) 15 d_p

There are many mixing indexes to characterise the mixing extent. For charging in a hopper, the degree of segregation (D_s) proposed by Shinohara et al. (1972) which is defined by the following equation is a good way to illustrate the segregation degree in a bounded heap flow.

$$D_s = 1 - \frac{L_s}{L_h} \tag{6-1}$$

where L_s is the farthest distance along the heap line from the heap top to the point that small particles can reach. L_h is the distance from the heap top of height to the hopper wall along the heap surface. This method considers the effect of the difference of heap length due to various filling positions. Here the horizontal cross-section is used to replace the heap line, and the filling point is used to replace the heap top. Hence, L_s is the farthest distance along the horizontal cross section from the filling point to the point where small particles concentration is less than 0.025. Therefore, from Figure 6-3, it is 33 d_p, 29.25 d_p, 22.5 d_p, 30.25 d_p, and 34.5 d_p for P1, P2, P3, P4 and P5 respectively. Then L_h is the distance from the filling point to the hopper wall along the horizontal cross-section, which is 43.5 d_p, 33.75 d_p and 22.5 d_p, for P1, P2, P3 respectively. The P1, P2, P3, P4 and P5 are the same with P1 and P2. Similarly, from the concentration distribution of small particle at height 15 d_p, L_s is 16 d_p, 22 d_p, 14 d_p, 22 d_p and 18 d_p. L_h is chosen as the distance from the wall due to the narrow cross-section, which is 24 d_p, 24 d_p, 14 d_p, 24 d_p and 24 d_p, respectively.

Compared with Figure 4-4(b), the concentration distribution of small particles of P3 and the simple geometry hopper is similar because the targeting height is in the upper part, ignoring the special shape of PW hopper in the lower part.

The segregation degree D_s as defined in Eq. (6-1) is calculated and shown in Figure 6-4. It can be found that segregation degree shows the same trend at both dimensionless z and decreases with the filling position moving right and reaches a minimum value at the central filling position. It can be found that Eq. (6-1) takes the effect of heap length, the left filling and right filling positions into account.

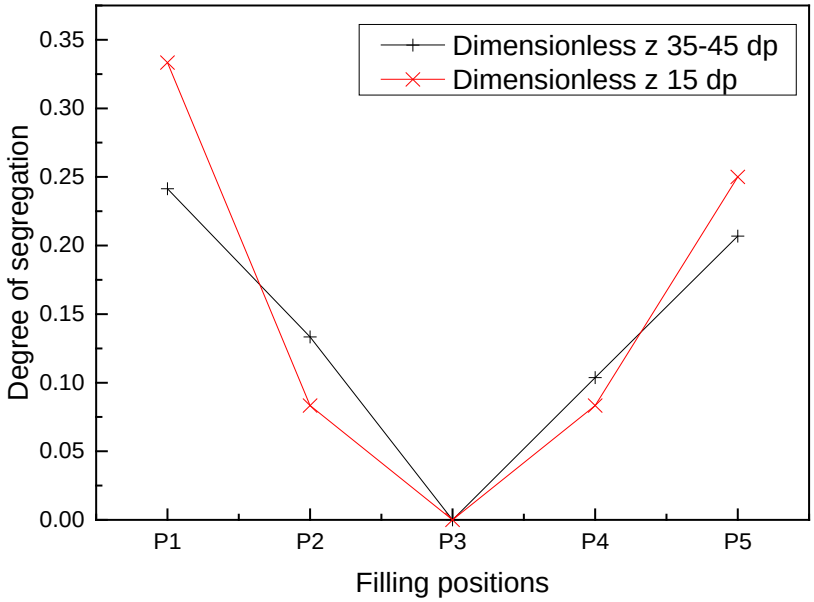

Figure 6-4 Degree of segregation at different filling positions at various z

Wear of the hopper wall can influence the operation of the hopper and is detrimental to the industry. Therefore, after particles are fully charged into the hopper, the wall stress on the unsymmetrical PW hopper is investigated and demonstrated in Figure 6-5. It can be found that the wall pressure focuses on the inclined slope which supports the particles. The pressure is large for P5 on the left wall and P1 for the right wall. This is understandable because the wall in the opposite direction of the filling position undertakes more pressure. Furthermore, the maximum wall stress for a certain filling position is the higher part of the slope for both left and right side walls. Interestingly, there is a turning point for P3 P4 and P5 at the lower left side wall. This is caused by the impact of high packing height at the right of the wall. To conclude, attention needs to be paid on the wear of the wall which is opposite to the filling point and the maximum part of the slope.

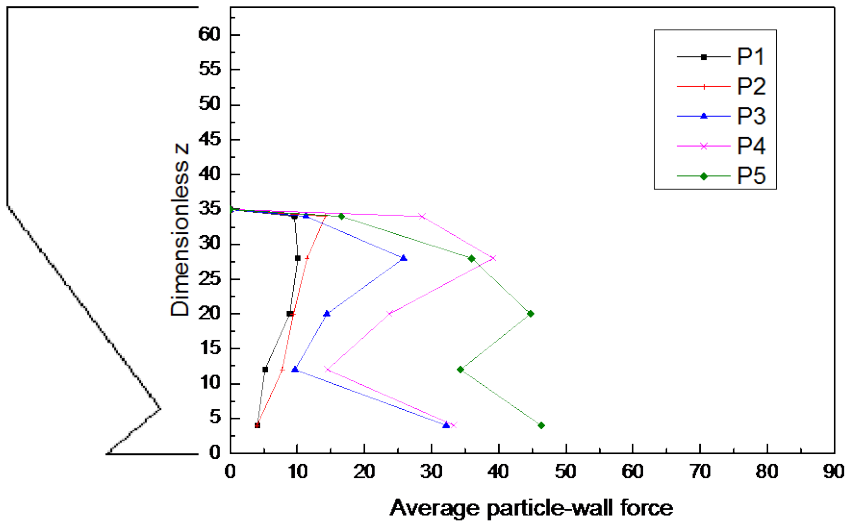

(a)

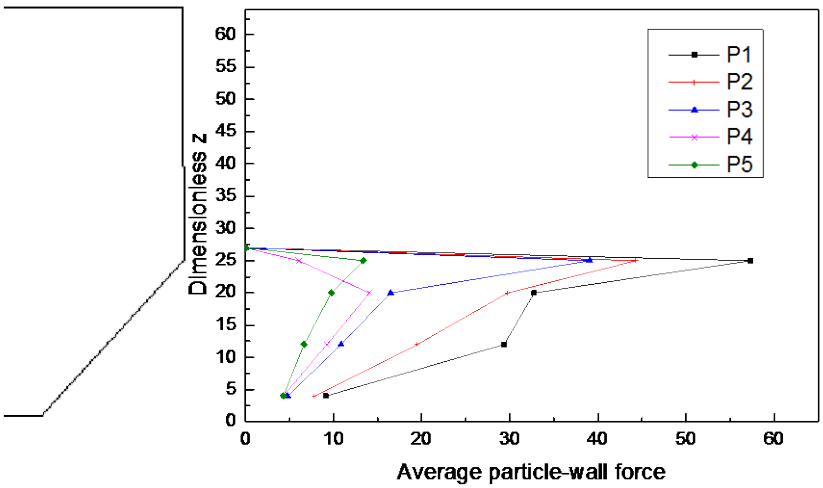

(b)

Figure 6-5 Wall stress on (a) the left side and (b) the right side wall in a PW hopper under various filling positions.

6.3.1.2 Effect of filling angle in a Paul-Wurth hopper

To examine the effect of filling angle on flow pattern in the hopper, seven different filling angles ranging from 0^o-150^o are studied here. The dropping points of the feeder hopper are guaranteed the same and in the centre by using various chute lengths.

Particles fall under gravity in the path of different chute angles, the same function of the tilting chute as shown in Figure 6-1 (b). The flow patterns are obtained in Figure 6-6. It can be observed that the patterns are similar for filling angles between 30^{o} and 60^{o}, with large particles gathering at the right-bottom and left-top parts. Likewise, when filling angles are 120^{o} to 150^{o}, the distribution of large particles is at right-top and left-bottom. The reason for this distribution can be further explored from an example of the chute angle of 30^{o}, as shown in Figure 6-7. It can be observed that particles which hit the side wall of feeder hopper first along the angled chute and then fall along the side wall (Figure 6-7 (a)). After the time of 1661 s, as shown in Figure 6-7 (b), particles fulfil the bottom area below the hitting point of the left side wall. Here for these particles under the hitting point, they are similar with the left filling case. Small particles gather at the opposite direction of hitting-place, which is the right lower hopper. Then the left edge of the surface slope exceeds the filling point, the situation changes (Figure 6-7 (c)). Large particles begin to gather at the left side wall. It is similar with P2 in Figure 6-3 (b). From Figure 6-7 (d), it can be found that there are less large particles on the right side wall compared with P2. This is because the trajectory has a significant effect on the inclined chute compared with straight line filling. The trajectory mechanism was reviewed by Williams (Williams, 1976), saying that large particles travel longer horizontal distance than small ones when they are jetting out along an inclined surface together.

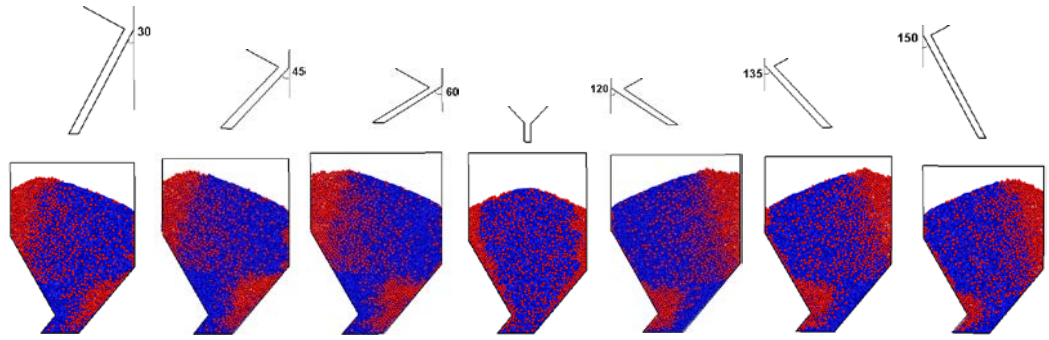

(a) 30º (b) 45º (c) 60º (d) 90º (e) 120º (f) 135º (g) 150º

Figure 6-6 Flow patterns of hopper filling at same dropping positions but different filling angles

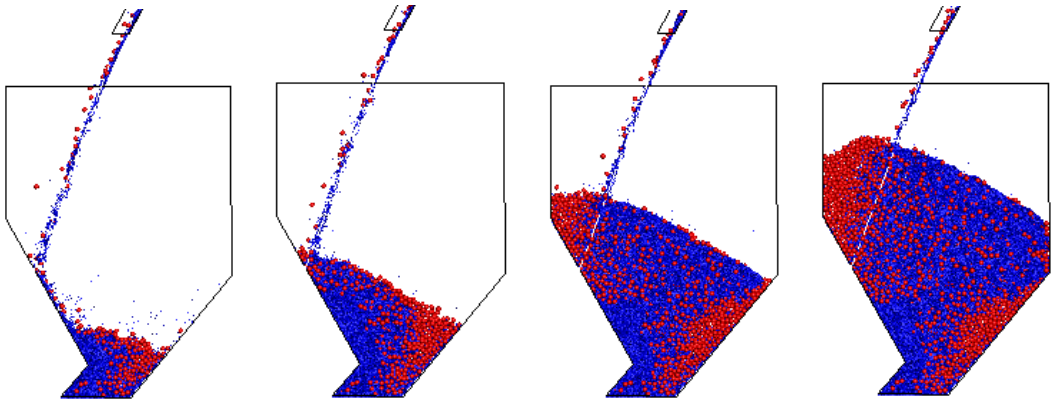

Angle 30 º: Real-time (a) 996s (b) 1661s (c) 2989s (d) 4318s

Figure 6-7 Flow patterns at a different time step of hopper filling at angle 30 º

This quantitative concentration distribution of small particles along the radial position at dimensionless *z* is shown in Figure 6-8 to determine the degree of segregation by Eq. (3). At the height of 15 d_p, the filling points do not have a huge difference between various angles due to the bounce on the wall, therefore, L_h is 24 d_p. L_s varies at 20 d_p, 17 d_p and 17 d_p for filling angle 30º, 45º and 60º, respectively. Thus, the segregation degree D_s is 0.17, 0.29 and 0.29 respectively. It is a little different at height 35-45 d_p. Due to the trajectory, the effect of filling angle on flow patterns is totally different from filling positions. Large particles gather at the left side of filling positions rather than segregating to the right side wall. Instead, small particles gather in the right side wall.

Consequently, D_s which use the farthest distance of small particles concentration cannot be used to show segregation degree here. However, from the concentration line, it can be found that the areas where concentration is below 0.025 and above 0.65 are different because of filling angles. But the difference is not significant. This is because trajectory mechanism plays a key role in terms of filling angles and makes segregation serious in all 30^o to 60^o cases.

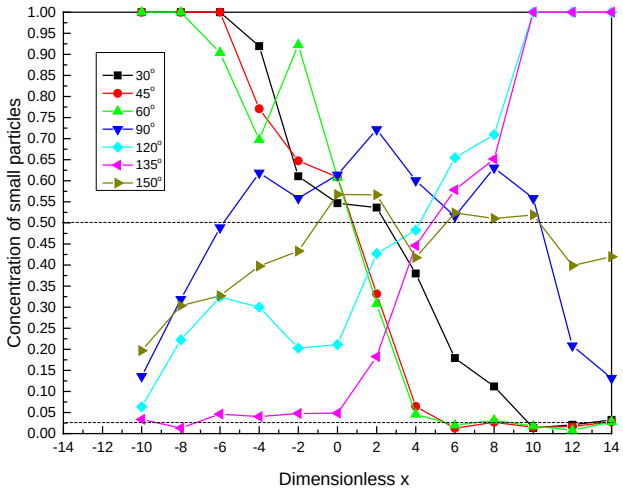

(a)

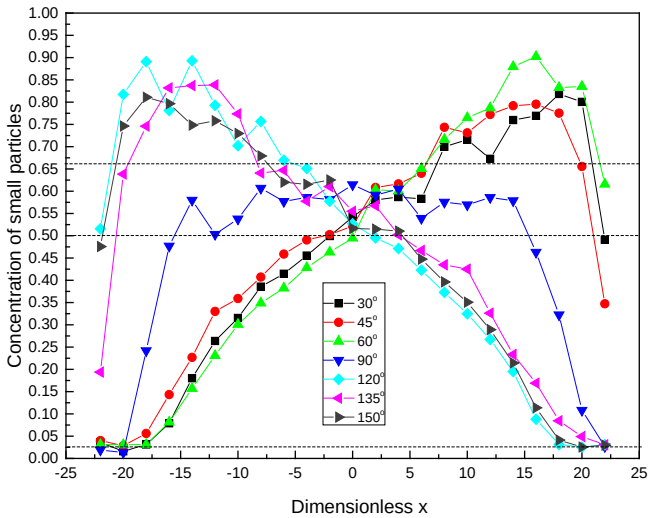

(b)

Figure 6-8 Concentration distribution of small particles in the hopper at dimensionless z: (a) 15 d_p, and (b) 35-45 d_p

Wall stress on the left side and right wall of PW hopper for different filling angles are shown in Figure 6-9. The same with the wall stress under different filling positions, the stress focus on the inclined wall which supports the particles' weight in the lower hopper. It can be observed that most of the maximum stress for a certain filling angle also appears at the higher part of the slope, except for 120°, 135° and 150°, which have a large pressure at the left lower slope due to the tall packing on the right, and 30°, 45° and 60°, which have a flat pressure distribution at the right middle slope.

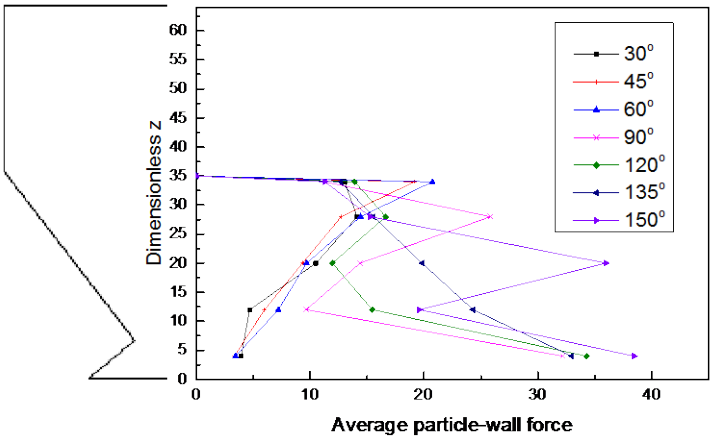

(a)

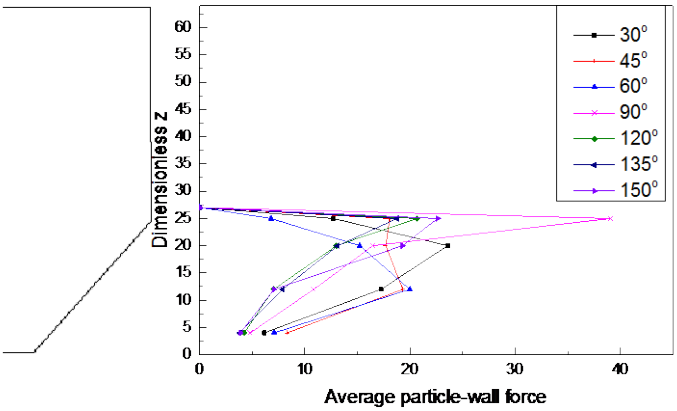

(b)

Figure 6-9 Wall stress on (a) the left side and (b) the right side wall in a Paul-Wurth hopper under various filling angles.

To conclude, different with the straight filling method, particles filling at various angles show different flow patterns. The large particles gathering area exists not only under the filling point but also appears in the left-lower side wall and right-upper side wall. From the analysis of travel distance at certain timestep, it can be found that in the lower hopper part, particles bouncing after hitting the wall leads to segregation. Differently, in the feeder bin, except for embedding and rolling down, the trajectory also influences particles distribution. For various filling angles, the area with a large concentration of small particles and the area with a large concentration of large particles are much larger with increasing filling angles, which shows that segregation is much serious in large filling angles. Furthermore, the flowing layer is smallest at large chute angle of 60^o. This is because, under a large filling angle, particles flow rate and momentum are smaller. Embedding is not as significant as other filling angles.

6.3.1.3 Effect of outlet size in a Paul-Wurth hopper

The case of P2 and angle 30^o is used to study the effect of flow rate, which is represented by various orifice sizes of 3 d_p, 6 d_p and 10 d_p, respectively. From the flow pattern shown in Figure 6-10, it can be found that segregation happens in all situations, and the extent decreases with the increasing of orifice size. At 10 d_p, large particle Gathering area is smallest at the right side wall for P2 (Figure 6-11 (a)) and the upper left side wall for 30o (Figure 6-11 (b)), and disappears in the lower hopper.

Eq. (6-1) is also utilised to present the degree of segregation for different outlets. The concentration distribution of small particles in the hopper at dimensionless z = 35-45 d_p and the height of 15 d_p for P2 filling can be obtained from Figure 6-11. The area where the concentration of small particles above 0.025 is treated as the farthest distance where

small particles can reach along the horizontal cross-section. The distance between it to the filling point is defined as L_s, which is 28.75 d_p, 31.25 d_p and 33.25 d_p for orifice size 3 d_p, 6 d_p and 10 d_p, respectively at dimensionless z 35-45 d_p. L_h is 33.75 d_p for the same filling position, which is the distance from the filling point to the side wall. Therefore, the segregation degree D_s is 0.148, 0.074 and 0.015 respectively. For height 15 d_p (Figure 6-11 (b)), L_s is 33 d_p, 37.5 d_p and 37.5 d_p for orifice size 3 d_p, 6 d_p and 10 d_p, respectively. L_h is 43.5 d_p, 42 d_p and 40 d_p. So the degree of segregation D_s is 0.241, 0.107 and 0.063 respectively, as shown in Figure 6-12, which can clearly show that the segregation degree decreases with the increase of the outlet size quantitatively.

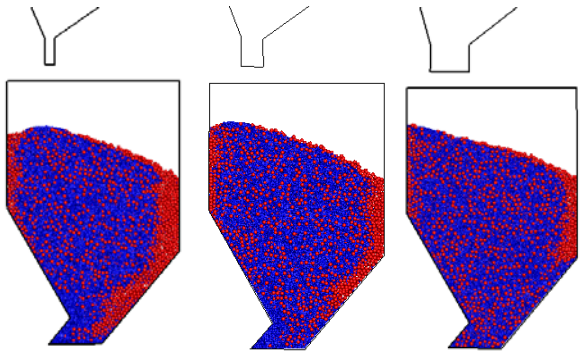

(a) P2, 3 d_p P2, 6 d_p P2, 10 d_p

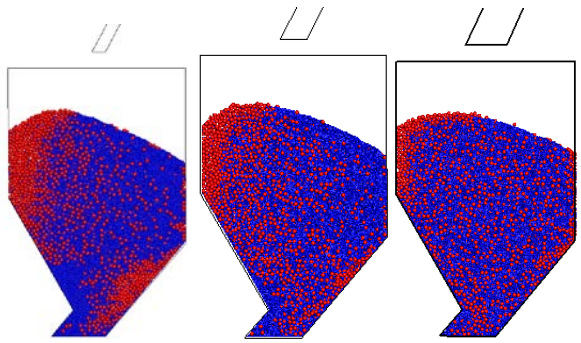

(b) 30°, 3 d_p 30°, 6 d_p 30°, 10 d_p

Figure 6-10 Flow patterns of P2 filling position and filling angle 30^o at various flow rates (orifice size)

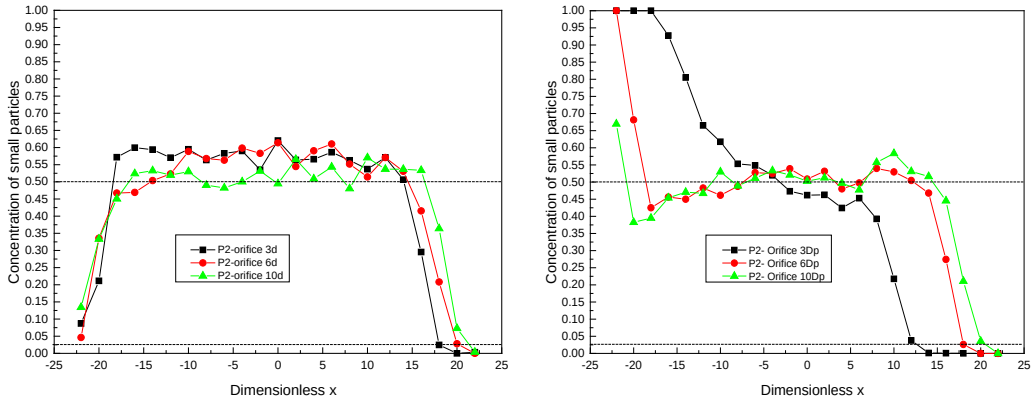

(a) (b)

Figure 6-11 Concentration distribution of small particles in the hopper at dimensionless *z* (a) 35-45 d_p and (b) 15 d_p for P2 at various outlet sizes.

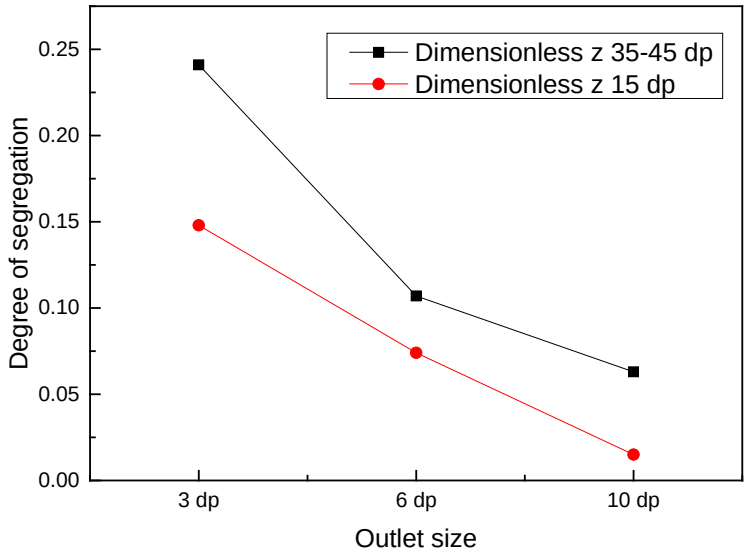

Figure 6-12 Degree of segregation for different outlet sizes at various height z.

6.3.2 Discharging from a Paul-Wurth hopper

Charging into a Paul Wurth hopper at the different positions leads to different packing states in the hopper as shown in Section 3.1. Then when the outlet of the Paul-Wurth hopper is opened, particles will discharge from the hopper. The distribution of the

discharged particles is a significant parameter because this affects the mixtures packing in the next process. Therefore, to study the concentration of particles discharging from the hoppers with different initial status is the aim of this section.

6.3.2.1 Effect of filling position on discharging from PW hopper

Due to various filling positions when charging into PW hopper, the initial status before discharging is different as shown in Figure 6-2. This leads to the different particle distributions during the discharging. Figure 6-13 illustrates the concentration of small particles changing with the fraction of particles which have been discharged from the hopper for case P1 to P5. It can be found that before 20% particles discharged (*t2* as marked in Figure 6-13), P1 and P2 are similar with a sharp concentration drop from 0.8 to around 0.4, then it turns to 0.5, the initial concentration of small particles. On the contrary, P4 and P5 show a consistent increase from 0.2 to 0.6 without a turning point in this stage. This can be explained by the discharged contour from Figure 6-14.

Figure 6-14 shows the different time needed for certain particles to discharge out the hopper. At time *t1*, the different contours from P1 to P5 are shown in Figure 6-14 (a). For the particles below the black line marked in the figure, the contours are almost the same. When connecting the maximum points, it points to the outlet. It means that this area is not affected by the above pattern and only relates to the outlet size and positions. Therefore, it is the initial concentration at that position which determines the discharged concentration of particles. It is full of small particles for P1 and P2 and full of large particles for P4 and P5. For the particles above the black line, when connecting the maximum points, their directions are different. Taking P1 for example, this means that particles in the left side discharge quicker than those in the right side. This altitude

difference decreases with time and becomes zero at around *t2* (Figure 6-14 (b)). From *t2*, a depression appears in the middle of the surface, and since then, large particles on the surface gather into this depression. Until *t3* (Figure 6-14 (c)), 50% of particles discharged, many large particles have gathered in the depression and are deep in depth. As can be seen from Figure 6-13, for P1 and P5, their concentrations decline earlier than P2, P3 and P4. This is because P1 and P5 have a deeper depression (orange colour) in the centre than others, as shown in Figure 6-14 (d) and (e). Therefore, the low concentration of small particles appears earlier. For P2, P3 and P4, more large particles distribute on the surface uniformly. They will be discharged at the last stage, a drop in the mass discharged 90%. At last, due to the small outlet, there is a corner in the right bottom of the hopper, where particles stay. Interestingly, at last, for P1 and P5, the particles distribute half large and half small particles.

The wall stress during the discharging process is captured and illustrated in Figure 6-15. Figure 6-15 (a) is the pressure at different times, which are 30% mass discharged, 50% mass discharged and 70% mass discharged. It can be found that with time elapses, the wall stress on the right side wall does not change much. Therefore, the following wall stress analysis focus on 50% mass discharged from the left side wall (Figure 6-15 (b)) and the right side wall (Figure 6-15 (c)). Because of the leftwards shape near the outlet, the trend of wall stress on the left side wall is gentle while that of the right side wall is sharp. Similarly, P5 has the highest left side wall stress due to the tall packing height and large flowing speed at the right side hopper. On the contrary, the pressure on the right side wall is largest for P1. The upper part of the hopper bears more pressure than other places, therefore, attention needs to be paid on the upper part of the slope.

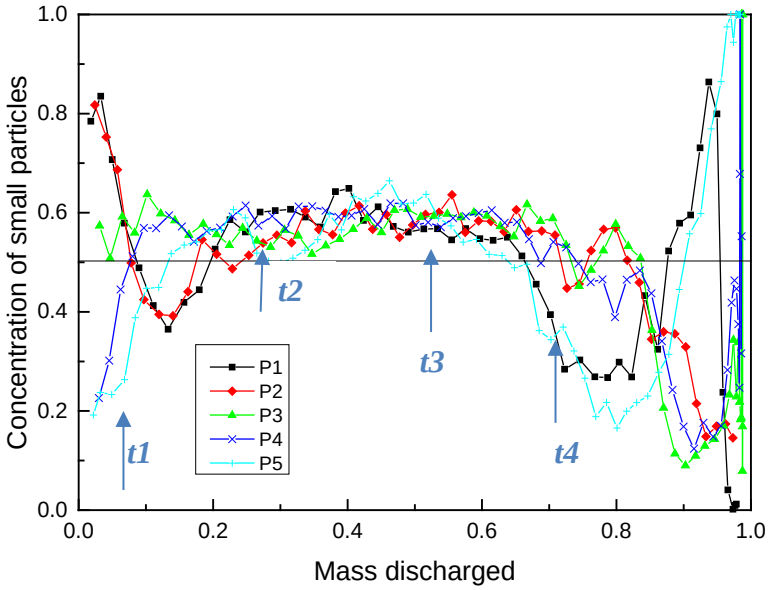

Figure 6-13 Concentration of small particles when discharging from the hopper with different positions initial statuses at the same outlet 6 d_p.

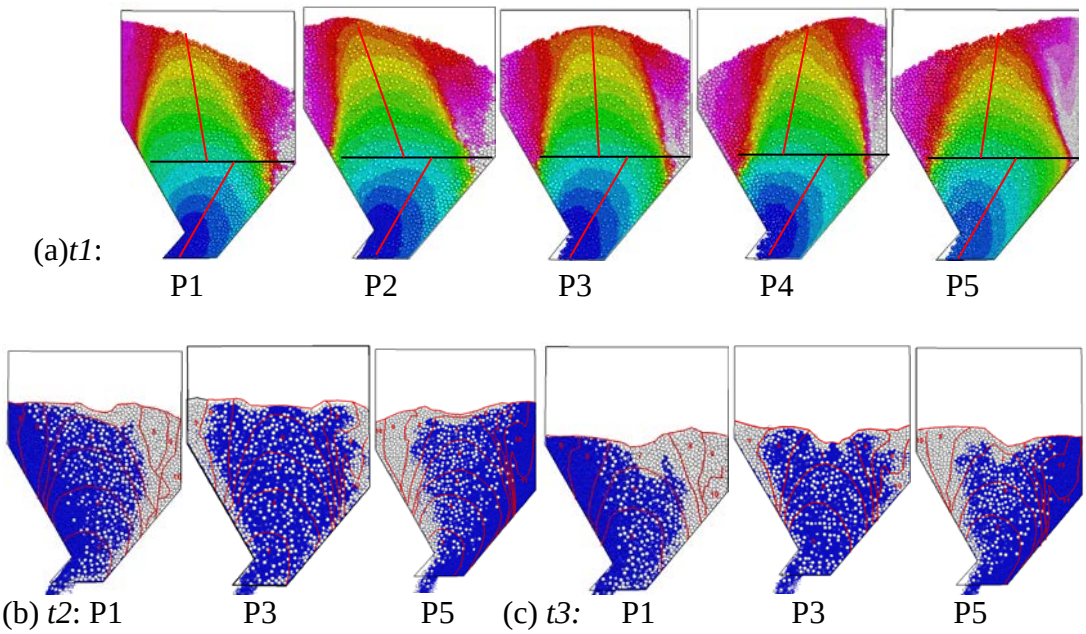

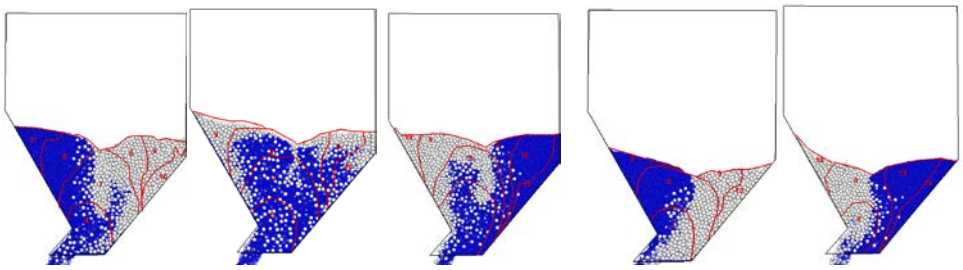

(d) *t4*: P1 P3 P5 (e) *t5:* P1 P5

Figure 6-14 Contours showing the discharged time for particles and flow patterns at a different discharging time.

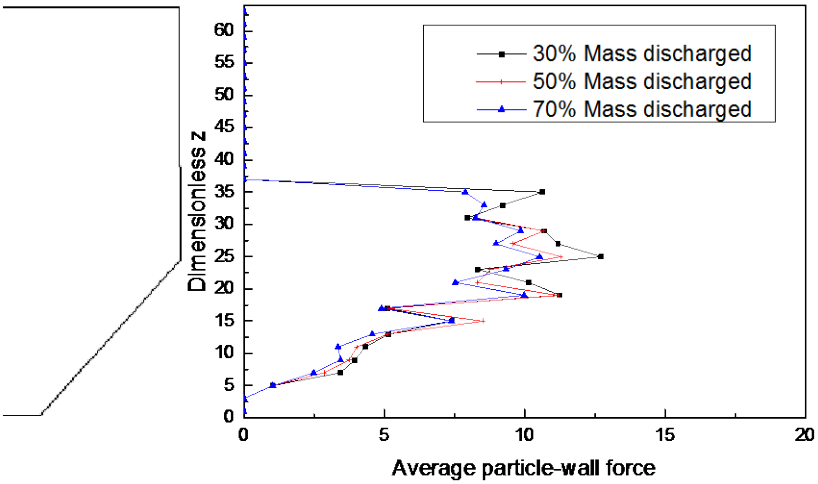

(a)

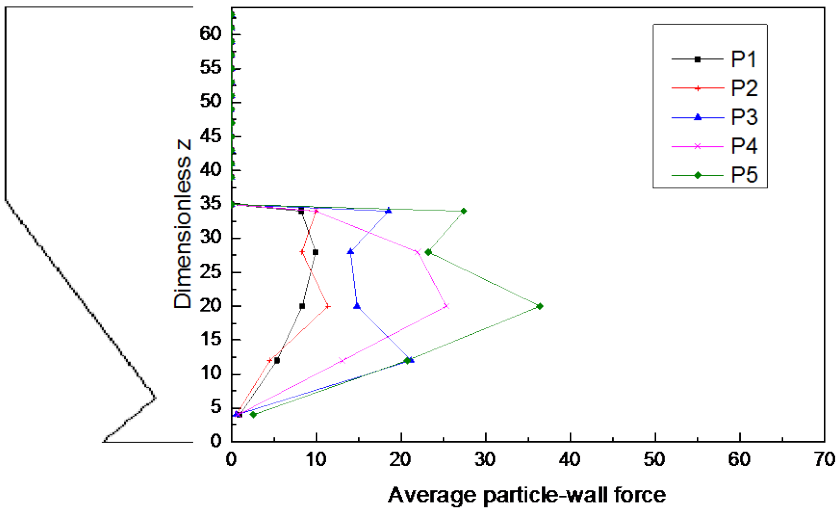

(b)

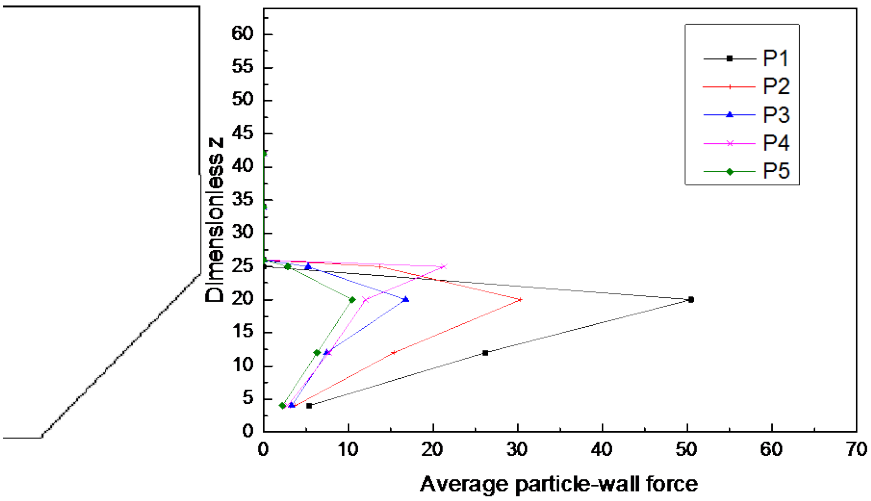

(c)

Figure 6-15 Wall stress distribution at (a) different discharging time and (b) the left side and (c) the right side wall when 50% mass discharged under various filling positions.

6.3.2.2 Effect of filling angle in a Paul-Wurth hopper

After charging into a hopper at various filling angles, the outlet of this hopper is turned on to discharge. The concentration of small particle during this discharging process change with discharged particles mass percentage is marked in Figure 6-16. It can be found that before 20% mass discharged, the concentration of small particles for 30°, 45° and 60° start from 0.8 and drops to 0.4. Then they go back to around 0.6, which is similar with that of P1 and P2. This is because the distribution of particles at the lower part hopper is the same. On the other hand, the concentration of small particles for 120°, 135° and 150° start from 0.2 and increase to maximum value 0.7, similar with P4 and P5. By connect the maximum points in the contour of discharged time for particles as shown in Figure 6-17 (a), the lines are same in the lower hopper and different in the feeder hopper. It bends significantly for the case of 60° in the feeder hopper, which

might be caused by percolation and different initial patterns. Percolation can be found from the left large particles gathering area, where small particles discharge faster than large ones (yellow small particles in Figure 6-17 (e)). Similarly, with P1 to P5, the surface of the patterns tends to be flat until *t2* (40% particles discharged) no matter what the altitude difference is at the beginning. At *t2*, the particles in contour 3, 4 and 5 (Figure 6-17 (b)) are well-mixed which leads to a steady discharge from *t2* to *t3* at 0.5 concentration of small particles. After that, a depression also appears on the surface. However, not many large particles roll into this area. This is because large particles are in the first discharging area. Taking 30° as an example, large particles at the left upper hopper discharge earlier than the small particles in the right upper hopper, which is different from P1. Therefore, a distinct drop of low small particles concentration before the end of discharging disappears compared with P1 to P5. After *t3*, the small particle concentration of 120° and 30° cases have a rise and a drop respectively. The reason can be found from the flow pattern in Figure 6-17 (c). The particles in areas marked 6 and 7 are with low or high small particle concentration, which is an accumulation of concentration differences between left and right part of the hopper. For the case of 60°, the concentration of discharged mixture does not fluctuate much with half large particles at the left and half small particles at the right until the last moment, when only small particles exist in area 10. The discharging process of 45°is similar with 60°. While the concentration of small particles of 135°and 150°also does not fluctuate much, as illustrated in Figure 6-16, but adversely with 45°and 60°, with large particles gathering in area 10 at the last moment, same with 120°. In all, the discharging process from a PW hopper with various filling angles have better mixture quality than that with various filling positions.

The wall stress on left side wall does not have a significant difference, as shown in Figure 6-18. Then the right-side wall bears the largest pressure at the upper slope, the same with the effect of filling position.

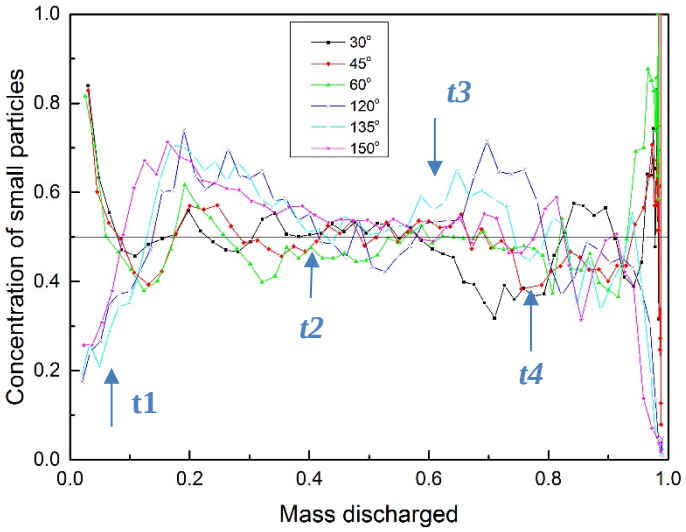

Figure 6-16 Concentration of small particles when discharging from the hopper with different angle initial statuses at same outlet 6 d_p.

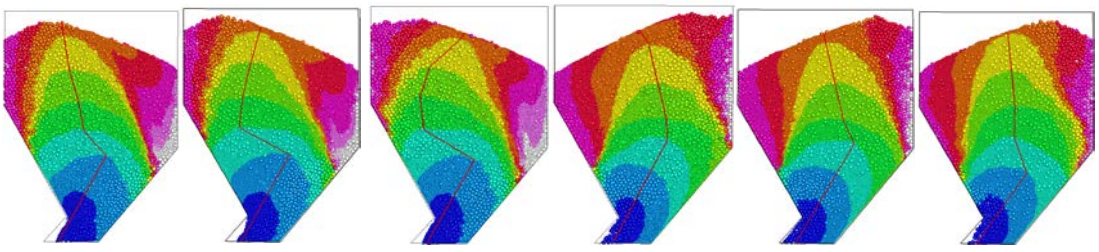

(a) *t1*: 30° 45° 60° 120° 135° 150°

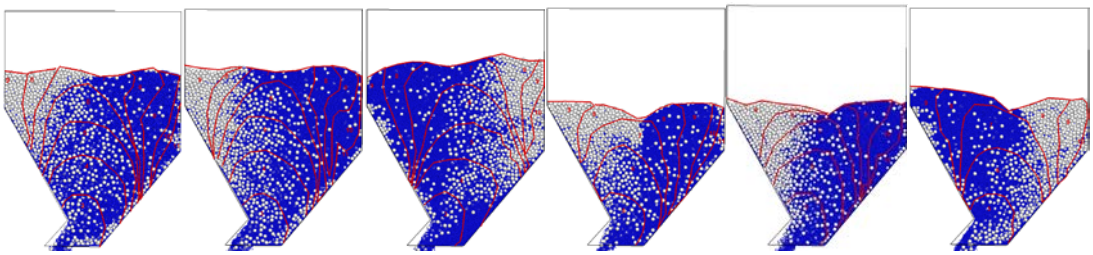

(b) *t2*: 30° 60° 120° (c) *t3*: 30° 60° 120°

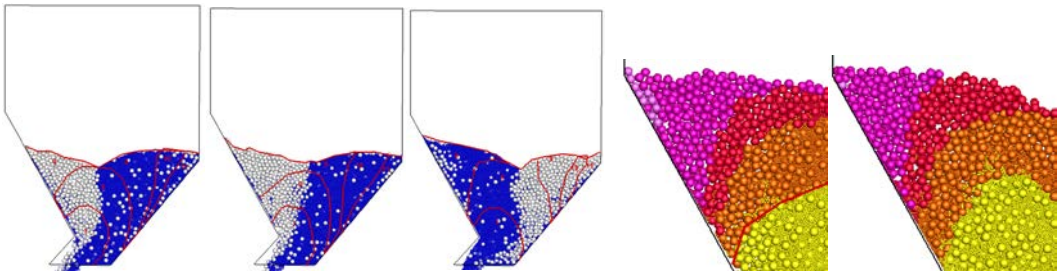

(d) *t4*: 30° 60° 120° (e) small particles' percolation

Figure 6-17 (a)-(d) Contour showing the discharged time for mixtures and the flow patterns at different discharging time; (e) percolation of small particles in orange area.

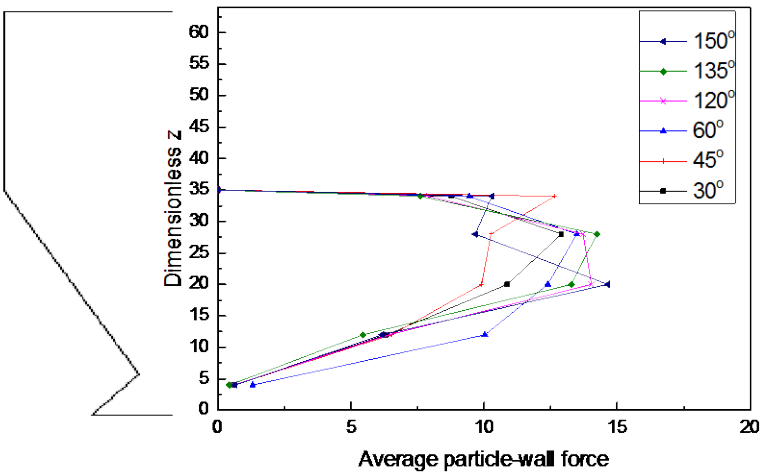

(a)

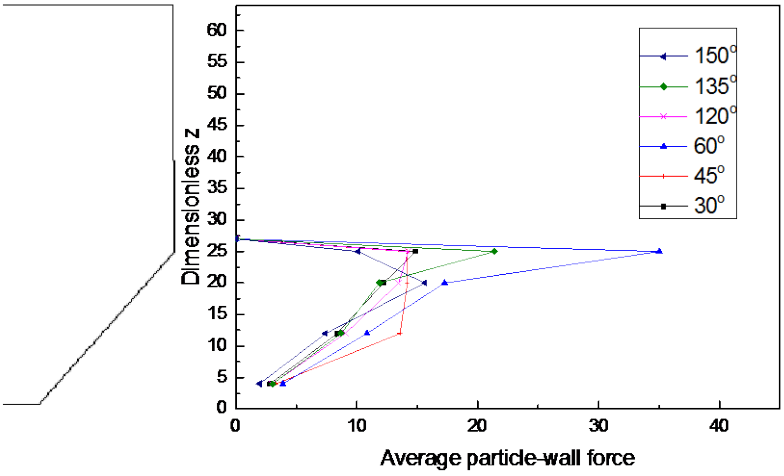

(b)

Figure 6-18 Wall stress distribution at (a) the left side and (b) the right side wall when 50% mass are discharged under various filling angles

6.3.2.3 Effect of outlet size when discharging from a Paul-Wurth hopper

When the outlet size of the hopper changes, the trends of concentration of small particles shown in Figure 6-19 are similar, which means that the outlet size does not have a significant effect on segregation when discharging. While the contour of different outlets depicts various flow pattern. From Figure 6-20 (a), it can be found that in the lower hopper, the contour at large outlet is more roundish, on the contrary, the contour at the small outlet is more parabolic, which makes the maximum point connection line along the discharging points. In the upper part, the maximum point connection line also shows different shapes, caused by different discharging time. The same with the contour shape, the depression on the surface exists in different places. For example, the depression is near the left side wall for 4 d_p. But the effect related to flow rate on the discharging particles concentration diminishes when the discharging time is normalized by total discharging time.

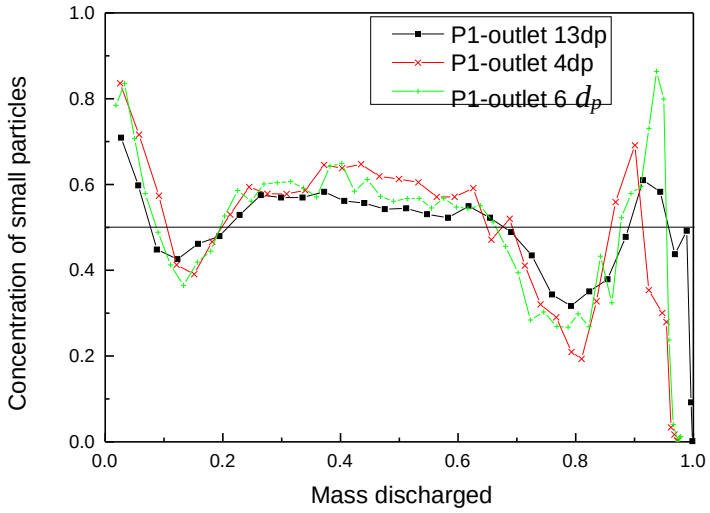

Figure 6-19 Concentration of small particles during discharging from the hopper at different outlets

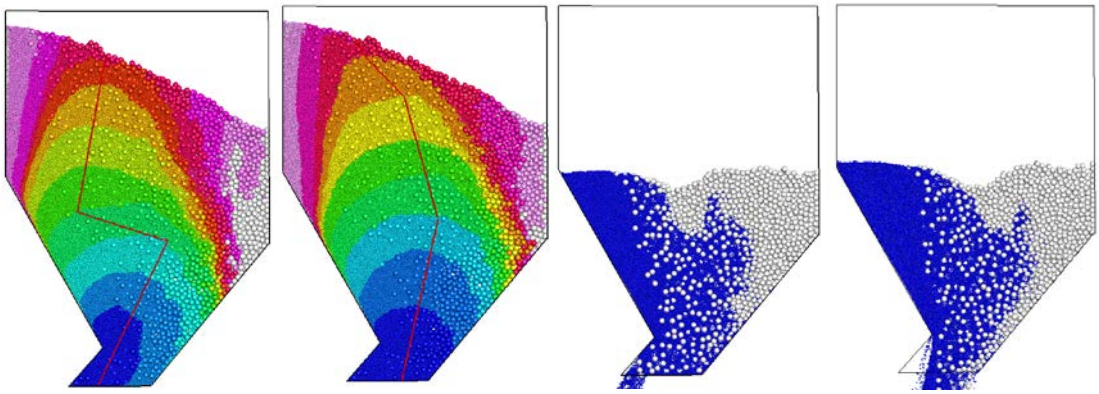

Figure 6-20 (a) Contour showing the discharged time for particles at different outlets and (b) flow patterns at a certain discharging time.

6.4 Conclusions

Based on the quasi-3D DEM slot model, variables related to operation conditions including filling positions, filling angles and the discharging outlet size relating to the industry are investigated here. The conclusions are given below.

- Different filling methods have a huge difference in heap contour, concentration distribution and force. Embedding is the main mechanism at various filling positions. For the left filling, due to the effect of the right side wall, the length of the heap slope is longer than other situations, which gives particles more time to segregation. Therefore, longer heap makes segregation more distinct, which should be avoided in the industry.
- The trajectory is another main mechanism related to different filling angles besides embedding. Small filling angle leads to the distinctive trajectory, where large particles are injected further due to large size in size and weight. This results in large particles gathering at the left side wall rather than the end of the

slope. Comparing the different filling angles, it can be found that if the filling angle is more vertical (30^o and 150^o), the segregation is not so serious. Therefore, in industry, particles can be mixed better when the discharged chute into a hopper is more vertical.

- The flow rate has a huge effect on segregation extent both at various filling positions and angles. Large flow rate leads to high velocity and makes the moving layer thicker. Embedding mechanism is not distinct here due to small velocity difference between the filling points and the area near it. In addition, large velocity causes less packing time. It also makes particles have less time to segregate before they reach the side wall. Therefore, the relatively large flow rate could reduce the segregation extent.
- For discharging process, the component of the discharged mixture at the initial discharging process is only related to the already accumulated particles near the outlet, which is hard to control. Then in the middle of discharging process, a depression appears and leads to large particles gather in the centre. This is the main cause for the large fluctuation at the last stage of discharging, which is more significant for various filling positions than the filling angles. Therefore, attention needs to be paid to the prevention of the depression formation.
- The wall in the opposite direction of the filling point bears large pressure, and the upper slope of the right side wall is an easy-worn point which requires a protection.

This page is intentionally blank

CHAPTER 7 CONCLUSIONS AND FURTHER WORKS

7.1 Conclusions

This thesis focuses on the microscopic and macroscopic analysis on the topics of sandpile, hopper filling and discharging and the application in a Paul-Wurth hopper. DEM simulation method provides the microscopic properties, such as velocity, porosity and forces. Based on these data, the effects of materials properties, including sliding and rolling friction coefficients are examined. Moreover, the segregation phenomenon of mixtures with different size ratios and volume fractions is further investigated. In addition, the effects of moisture content and hopper geometry are also considered. The detailed conclusions of each chapter are divided into four main parts and are listed below separately.

(1) Sliding and rolling friction coefficients and the moisture contents are essential to the segregation of sandpile process. To study their effect on the particles flow is of great importance. The flow pattern is qualitatively validated with experimental results. Then the flow process is demonstrated and the effects of particle surface properties and the water content are examined. It can be found that the angle difference between the upper and lower piles is the primary reason for particles stratification. It means that the following packing patterns are determined by the local structure, which is also the reason for the four repeated loop of piling process. Regarding a large particle, only when the shape of its force chain is a tetrahedron and its velocity is tiny enough at that time, it can reach a steady state. Furthermore, the angle of repose of the pile is decided by the particles surface properties. Small sliding coefficient and rolling friction coefficient decrease particles flowability and lead to a small angle of repose. Mixture with both different surface properties and sizes show various mixing patterns. When particles with a large size and smooth surface, segregation is most serious. A small

particle with a small sliding friction and rolling friction has least grid number full of large and small particles. At last, when particles are wet, the volumetric moisture content has a significant effect on the packing structure. The angle of repose and the segregation extent increase with the moisture content and then saturate. The average capillary force decreases for all three particle contacts. The relationships between porosity, force ratio and angle of repose have been fitted by several correlations. It reveals the structural and force characteristics of sandpile formation process.

(2) In terms of a hopper filling process, it is a heap formation process with boundaries. A systematic investigation on effect of sliding and rolling friction coefficients is first implemented and a contour plot is given and is helpful to practice use. In detail, the simulation results are confirmed by the physical experiments to verify the feasibility of DEM. Then the simulation results confirm that large particles tend to travel further along the slope surface and stop at the side walls, whereas small particles tend to remain in the central region during the hopper filling process. The analysis of particle velocity, travelling time, cluster size and force networks is conducted in detail to obtain an understanding of particle segregation mechanisms. Both large and small particles at the side walls (e.g., $D_c = 17.5\ d_p$) have short travelling time, high velocity and small cluster size, which verifies the bouncing mechanism for small particles and rolling mechanism for large particles. Some particles are embedded into the bed then stay in the central region, due to cluster interactions and smaller initial potential energy with low velocity and large cluster size. Some particles with relatively large velocity and small cluster size travel further to $D_c = 12.5\ d_p$. But they spend more time because the particles here are pushed in an embedded particle layer. In addition, a contour plot is drawn by particle scale mixing index to quantify the effects of particle sliding and rolling friction

coefficients. The PSMI contours are approximately parabolic with the minimum value at $\mu_{r,pp} = 0.025 d_p$. Larger sliding friction leads to serious segregation. The smallest PSMI appears when sliding friction coefficient is 1.0 and rolling friction coefficient is 0.025 d_p. At last, a correlation is proposed for the concentration of small particles at side wall, mid-radius and centre. Results show that the parameter A is positive and has large absolute value in the side wall region, meaning that segregation is positive and significant. The segregation in the mid-radius section and the centre are negative ($A < 0$) and weak.

(3) Multigrid contact detection and GPU-based DEM are innovated combined to calculate particles flow in huge size ratio, which is more than 10.0. Specifically, mixture with large size ratio is discharged out a hopper and the concentration of large particles of the discharged particles has been validated with a physical experiment. The results show quantitative agreements, which certify the validity of the present DEM model. Based on this validation, further results are obtained. The velocity difference, which is an indicator marking the percolation mechanisms, between large and small particles is significant in the centre at the upper hopper. In addition, particles in the centre travel faster than that in the side wall. This difference is related to the porosity of large particle and the fraction of small particles in contact with large ones (N_{cs}/N_s). Results show that mixture with large porosity and small N_{cs}/N_s segregates seriously and has a large fully discharged time of small particles (SFDT). In addition, with the decrease of the size ratio, SFDT drops. For mixture with small size ratio, the velocity difference between large and small particles is tiny and N_{cs}/N_s is large. In our study, when the velocity difference is below 0.07 mm/s, and the number ratio N_{cs}/N_s is above 0.10, percolation is not the dominant mechanism, and segregation is not obvious. Under different hopper

geometry, the SFDT is related to the cross-section of the hopper. When the cone angle is large, the wide cross-section leads to fast small particles percolation. But because of the wall and the relatively small outlet slit width, small particles are gathered at the side wall and are impacted by the movement of large particles.

(4) Finally, based on a quasi-3D slot model by DEM, the study extends to the application in a PW hopper. The influences of parameters related to operation conditions including filling positions, filling angles and the flow rate related to the industry are investigated here. It can be observed that different filling methods have a huge difference in heap contour, concentration distribution, porosity, velocity and force. Embedding is the main mechanism at various filling positions. For left filling, because of the right-side wall, the length of the heap slope is longer than other situations, which gives particles more time to segregation. Therefore, a longer heap makes segregation more distinct, which should be avoided in the industry. Meanwhile, the trajectory is another main mechanism related to different filling angles besides embedding mechanism. Small filling angle leads to the serious segregation, where large particles travel further due to large size in size and weight. This makes large particles gathering at the left side wall rather than stopping at the end of the slope. Comparing the different filling angles, it can be found that if the filling angle is more vertical (30^o and 150^o), the segregation is not so serious. Therefore, in the industry, the particles can be mixed better when the discharged chute into a hopper is more vertical. Finally, the effect of flow rate on segregation extent both at various filling positions and angles has been considered. Large flow rate leads to big velocity and makes the moving layer thicker. Embedding mechanism is not distinct here due to small velocity difference between the filling points and the area near it. In addition, large velocity means less packing time,

making particles have less time to segregate before they reach the wall boundary. Therefore, the relatively large flow rate could make segregation decreased. For discharging process, the component of the discharged mixture at the initial discharging process is only related to the already accumulated particles near the outlet, which is related to charging process. Then in the middle of discharging process, a depression appears and leads to large particles gather in the centre. This is the main cause for the huge fluctuation at the last stage of discharging. It is more significant at various filling positions than that at various filling angles. Therefore, attention needs to be paid on the prevention of the depression formation. In terms of wall wear, results show that the wall on the opposite direction of the filling point bears large pressure, and the upper slope of the right-side wall is an easy-worn point needing protection.

7.2 future work

Several knowledge gaps have been solved in this thesis, while there are also some problems remaining. The following work can be future research targets.

(1) Piling studies show that the angle of repose of particles has an influence on segregation. Moreover, the angle of repose is also affected by the shape of particles. Therefore, the combined effects of size and shape of binary or ternary mixture on the piling, hopper filling and discharging processes can be explained further. The relationship between the structural properties and the force could be explored then to find the potential mechanism.

(2) Most of current studies focus on dry particles. It is known that the water content in the system has a significant effect on the distribution of particles. Using the capillary force in the DEM for binary or ternary mixture is still not fully explained. More physical

experiments need to be implemented combined with more simulation work on the effects of moisture content, the surface tension and contact angles.

(3) The mixtures in the real industry are always with different size distributions, which might range from ternary to multiple sizes. This mixture also has various size ratios or volume fractions. The studies on the effect of size ratio and volume fraction of the multi-sized mixture on segregation of hopper filling and discharging processes can be further examined.

(4) Segregation occurs in many industrial fields, including pharmaceutical, chemical engineering and mining, etc. Systems with complex geometries and complicated material properties are common. Based on the understanding of the mechanisms obtained from the simple systems, the segregation in more complex systems needs to be studied further.

This page is intentionally blank

LIST OF REFERENCES

ALEXANDER, A. W., CHAUDHURI, B., FAQIH, A., MUZZIO, F. J., DAVIES, C. & TOMASSONE, M. S. 2006. Avalanching flow of cohesive powders. *Powder Technology,* 164**,** 13-21.

AMINAGA, Y., KAJIWARA, Y., INADA, T., TANAKA, T. & SATO, K. 1987. SIZE SEGREGATION OF SINTER IN TOP BUNKER OF A BELL-LESS TYPE BLAST-FURNACE. *Transactions of the Iron and Steel Institute of Japan,* 27**,** 851-857.

ANAND, A., CURTIS, J. S., WASSGREN, C. R., HANCOCK, B. C. & KETTERHAGEN, W. R. 2008. Predicting discharge dynamics from a rectangular hopper using the discrete element method (DEM). *Chemical Engineering Science,* 63**,** 5821-5830.

ANAND, A., CURTIS, J. S., WASSGREN, C. R., HANCOCK, B. C. & KETTERHAGEN, W. R. 2010. Segregation of cohesive granular materials during discharge from a rectangular hopper. *Granular Matter,* 12**,** 193-200.

ARTEAGA, P. & TUZUN, U. 1990. Flow of Binary-Mixtures of Equal-Density Granules in Hoppers Size Segregation, Flowing Density and Discharge Rates. *Chemical Engineering Science,* 45**,** 205-223.

BALEVIČIUS, R., KAČIANAUSKAS, R., MRÓZ, Z. & SIELAMOWICZ, I. 2008. Discrete-particle investigation of friction effect in filling and unsteady/steady discharge in three-dimensional wedge-shaped hopper. *Powder Technology,* 187**,** 159-174.

BATES, L., HAYES, G. D. & BOARD, B. M. H. 1997. *User Guide to Segregation,* British Materials Handling Board.

BENITO, J. G., IPPOLITO, I. & VIDALES, A. M. 2013. Novel aspects on the segregation in quasi 2D piles. *Powder Technology,* 234**,** 123-131.

BENITO, J. G., UNAC, R. O., VIDALES, A. M. & IPPOLITO, I. 2014. Influence of geometry on stratification and segregation phenomena in bidimensional piles. *Physica a-Statistical Mechanics and Its Applications,* 396**,** 19-28.

BEVERLOO, W. A., LENIGER, H. A. & VANDEVELDE, J. 1961. The Flow of Granular Solids through Orifices. *Chemical Engineering Science,* 15**,** 260-269.

BOUTREUX, T. & DEGENNES, P. G. 1996. Surface flows of granular mixtures .1. General principles and minimal model. *Journal De Physique I,* 6**,** 1295-1304.

BOUTREUX, T., RAPHAEL, E. & DE GENNES, P. G. 1998. Surface flows of granular materials: A modified picture for thick avalanches. *Physical Review E,* 58**,** 4692-4700.

BRIDGWATER, J. 1976. Fundamental Powder Mixing Mechanisms. *Powder Technology,* 15**,** 215-236.

BRIDGWATER, J. 1994. Mixing and Segregation Mechanisms in Particle Flow. *In:* MEHTA, A. (ed.) *Granular Matter*. Springer New York.

BRIDGWATER, J. 2012. Mixing of powders and granular materials by mechanical means-A perspective. *Particuology,* 10**,** 397-427.

CARSTENSEN, J. T. & CHAN, P. C. 1976. Relation between Particle-Size and Repose Angles of Powders. *Powder Technology,* 15**,** 129-131.

CHANDRATILLEKE, G. R., YU, A. B., BRIDGWATER, J. & SHINOHARA, K. 2012. A particle-scale index in the quantification of mixing of particles. *AIChE Journal,* 58**,** 1099-1118.

CHEN, Y., ZHAO, Y., GAO, H. & ZHENG, J. 2011. Liquid bridge force between two unequal-sized spheres or a sphere and a plane. *Particuology,* 9**,** 374-380.

CLAGUE, K. & WRIGHT, H. 1973. Minimizing Segregation in Bunkers. *Journal of Engineering for Industry-Transactions of the Asme,* 95**,** 81-85.

CLEARY, P. W. & SAWLEY, M. L. 2002. DEM modelling of industrial granular flows: 3D case studies and the effect of particle shape on hopper discharge. *Applied Mathematical Modelling,* 26**,** 89-111.

COOKE, M. H., BRIDGWATER, J. & SCOTT, A. M. 1978. Interparticle Percolation - Lateral and Axial Diffusion-Coefficients. *Powder Technology,* 21**,** 183-193.

CUNDALL, P. A. & STRACK, O. D. L. 1979. Discrete Numerical-Model for Granular Assemblies. *Geotechnique,* 29**,** 47-65.

DASGUPTA, P. & MANNA, P. 2011. Geometrical mechanism of inverse grading in grain-flow deposits: An experimental revelation. *Earth-Science Reviews,* 104**,** 186-198.

DONG, K. J., YANG, R. Y., ZOU, R. P. & YU, A. B. 2012. Settling of particles in liquids: Effects of material properties. *AIChE Journal,* 58**,** 1409-1421.

DONG, K. J., ZOU, R. P., CHU, K. W., YANG, R. Y., YU, A. B. & HU, D. S. 2013. Effect of Cohesive Force on the Formation of a Sandpile. *Powders and Grains 2013,* 1542**,** 646-649.

DRAHUN, J. A. & BRIDGWATER, J. 1983. The Mechanisms of Free-Surface Segregation. *Powder Technology,* 36**,** 39-53.

ENGBLOM, N., SAXEN, H., ZEVENHOVEN, R., NYLANDER, H. & ENSTAD, G. G. 2012a. Segregation of Construction Materials in Silos. Part 1: Experimental Findings on Different Scales. *Particulate Science and Technology,* 30**,** 145-160.

ENGBLOM, N., SAXÉN, H., ZEVENHOVEN, R., NYLANDER, H. & ENSTAD, G. G. 2012b. Segregation of powder mixtures at filling and complete discharge of silos. *Powder Technology,* 215-216**,** 104-116.

ENSTAD, G. G. 2001. Segregation of powders — mechanisms, processes and counteraction. *In:* LEVY, A. & KALMAN, H. (eds.) *Handbook of Powder Technology.* Elsevier Science B.V.

FAN, L., CHEN, S. & WATSON, C. 1970. ANNUAL REVIEW Solids Mixing. *Industrial & Engineering Chemistry,* 62**,** 53-69.

FAN, Y., BOUKERKOUR, Y., BLANC, T., UMBANHOWAR, P. B., OTTINO, J. M. & LUEPTOW, R. M. 2012. Stratification, segregation, and mixing of granular materials in quasi-two-dimensional bounded heaps. *Physical Review E,* 86**,** 051305.

FAN, Y., JACOB, K. V., FREIREICH, B. & LUEPTOW, R. M. 2017. Segregation of granular materials in bounded heap flow: A review. *Powder Technology,* 312**,** 67-88.

FAN, Y., SCHLICK, C. P., UMBANHOWAR, P. B., OTTINO, J. M. & LUEPTOW, R. M. 2014. Modelling size segregation of granular materials: the roles of segregation, advection and diffusion. *Journal of Fluid Mechanics,* 741**,** 252-279.

FRETTE, V., MALOY, K. J., BOGER, F., FEDER, J., JOSSANG, T. & MEAKIN, P. 1990. Diffusion-Limited-Aggregation-Like Displacement Structures in a 3-Dimensional Porous-Medium. *Physical Review A,* 42**,** 3432-3437.

GAN, J. Q., ZHOU, Z. Y. & YU, A. B. 2016. A GPU-based DEM approach for modelling of particulate systems. *Powder Technology,* 301**,** 1172-1182.

GARVE, T. W. 1925. SEGREGATION IN BINS1. *Journal of the American Ceramic Society,* 8**,** 666-670.

GRASSELLI, Y. & HERRMANN, H. J. 1997. On the angles of dry granular heaps. *Physica A,* 246**,** 301-312.

GRASSELLI, Y. & HERRMANN, H. J. 1998. Experimental study of granular stratification. *Granular Matter,* 1**,** 43-47.

GRASSELLI, Y. & HERRMANN, H. J. 1999. Shapes of heaps and in silos. *European Physical Journal B,* 10**,** 673-679.

GRASSELLI, Y. & HERRMANN, H. J. 2001. Crater formation on a three dimensional granular heap. *Granular Matter,* 3**,** 201-204.

GRAY, J. M. N. T. & KOKELAAR, B. P. 2010. Large particle segregation, transport and accumulation in granular free-surface flows (vol 652, pg 105, 2010). *Journal of Fluid Mechanics,* 657**,** 539-539.

HASTIE, D. B. & WYPYCH, P. W. 2000. Segregation During Gravity Filling of Storage Bins. *In:* ROSATO, A. & BLACKMORE, D. (eds.) *IUTAM Symposium on Segregation in Granular Flows.* Springer Netherlands.

HE, K. J., DONG, S. B. & ZHOU, Z. Y. 2007. Multigrid contact detection method. *Physical Review E,* 75.

JENIKE, A. W. 1964. *Storage and Flow of Solids,* University of Utah.

JHA, A. K. & PURI, V. M. 2009. Percolation segregation of binary mixtures under periodic movement. *Powder Technology,* 195**,** 73-82.

JHA, A. K. & PURI, V. M. 2010. Percolation segregation of multi-size and multi-component particulate materials. *Powder Technology,* 197**,** 274-282.

KAJIWARA, Y., AMINAGA, Y., INADA, T., TANAKA, T. & SATO, K. 1988. Size Segregation of Sinter in Top Bunker of a Bell-Less Type Blast-Furnace. *Tetsu to Hagane-Journal of the Iron and Steel Institute of Japan,* 74**,** 978-984.

KAJIWARA, Y., JIMBO, T., JOKO, T., AMINAGA, Y. & INADA, T. 1984. Investigation of Bell-Less Charging Based on Full Scale Model Experiments. *Transactions of the Iron and Steel Institute of Japan,* 24**,** 799-807.

KETTERHAGEN, W. R., CURTIS, J. S., WASSGREN, C. R. & HANCOCK, B. C. 2008. Modeling granular segregation in flow from quasi-three-dimensional, wedge-shaped hoppers. *Powder Technology,* 179**,** 126-143.

KETTERHAGEN, W. R., CURTIS, J. S., WASSGREN, C. R. & HANCOCK, B. C. 2009. Predicting the flow mode from hoppers using the discrete element method. *Powder Technology,* 195**,** 1-10.

KETTERHAGEN, W. R., CURTIS, J. S., WASSGREN, C. R., KONG, A., NARAYAN, P. J. & HANCOCK, B. C. 2007. Granular segregation in discharging cylindrical hoppers: A discrete element and experimental study. *Chemical Engineering Science,* 62**,** 6423-6439.

LACEY, P. M. C. 1954. Developments in the theory of particle mixing. *Journal of applied chemistry,* 4**,** 257-268.

LANGSTON, P. A., NIKITIDIS, M. S., TUZUN, U., HEYES, D. M. & SPYROU, N. M. 1997. Microstructural simulation and imaging of granular flows in two- and three-dimensional hoppers. *Powder Technology,* 94**,** 59-72.

LANGSTON, P. A., TUZUN, U. & HEYES, D. M. 1995. Discrete Element Simulation of Granular Flow in 2d and 3d Hoppers - Dependence of Discharge Rate and Wall Stress on Particle Interactions. *Chemical Engineering Science,* 50**,** 967-987.

LEE, J. & HERRMANN, H. J. 1993. Angle of Repose and Angle of Marginal Stability - Molecular-Dynamics of Granular Particles. *Journal of Physics a-Mathematical and General,* 26**,** 373-383.

LIAN, G. & SEVILLE, J. 2016. The capillary bridge between two spheres: New closed-form equations in a two century old problem. *Advances in Colloid and Interface Science,* 227**,** 53-62.

LIAN, G., THORNTON, C. & ADAMS, M. J. 1993. A Theoretical Study of the Liquid Bridge Forces between Two Rigid Spherical Bodies. *Journal of Colloid and Interface Science,* 161**,** 138-147.

LIU, P. Y., YANG, R. Y. & YU, A. B. 2013. The effect of liquids on radial segregation of granular mixtures in rotating drums. *Granular Matter,* 15**,** 427-436.

LIU, S., ZHOU, Z. Y., DONG, K. J., YU, A. B., PINSON, D. & TSALAPATIS, J. 2015. Numerical Investigation of Burden Distribution in a Blast Furnace. *Steel Research International,* 86**,** 651-661.

LIU, S. D., ZHOU, Z. Y., ZOU, R. P., PINSON, D. & YU, A. B. 2014. Flow characteristics and discharge rate of ellipsoidal particles in a flat bottom hopper. *Powder Technology,* 253**,** 70-79.

LUDING, S. 1997. Stress distribution in static two-dimensional granular model media in the absence of friction. *Physical Review E,* 55**,** 4720-4729.

MAKSE, H. A. 1997. Stratification instability in granular flows. *Physical Review E,* 56**,** 7008-7016.

MAKSE, H. A., BALL, R. C., STANLEY, H. E. & WARR, S. 1998a. Dynamics of granular stratification. *Physical Review E,* 58**,** 3357-3367.

MAKSE, H. A., CIZEAU, P., HAVLIN, S., KING, P. R. & STANLEY, H. E. 1998b. Spontaneous self-stratification without shaking - "Potatoes from mashed potatoes". *Physics of Dry Granular Media,* 350**,** 671-680.

MAKSE, H. A., CIZEAU, P. & STANLEY, H. E. 1997a. Possible stratification mechanism in granular mixtures. *Physical Review Letters,* 78**,** 3298-3301.

MAKSE, H. A., CIZEAU, P. & STANLEY, H. E. 1998c. Modeling stratification in two-dimensional sandpiles. *Physica A,* 249**,** 391-396.

MAKSE, H. A., HAVLIN, S., KING, P. R. & STANLEY, H. E. 1997b. Spontaneous stratification in granular mixtures. *Nature,* 386**,** 379-382.

MAKSE, H. A., HAVLIN, S., KING, P. R. & STANLEY, H. E. 1998d. Experimental studies of stratification in a granular Hele-Shaw cell. *Philosophical Magazine B-Physics of Condensed Matter Statistical Mechanics Electronic Optical and Magnetic Properties,* 77**,** 1341-1351.

MAKSE, H. A. & HERRMANN, H. J. 1998. Microscopic model for granular stratification and segregation. *Europhysics Letters,* 43**,** 1-6.

MATUTTIS, H. G., LUDING, S. & HERRMANN, H. J. 2000. Discrete element simulations of dense packings and heaps made of spherical and non-spherical particles. *Powder Technology,* 109**,** 278-292.

MEAKIN, P. & JULLIEN, R. 1992. Simple-Models for 2 and 3-Dimensional Particle-Size Segregation. *Physica A,* 180**,** 1-18.

MIO, H., KADOWAKI, M., MATSUZAKI, S. & KUNITOMO, K. 2012. Development of particle flow simulator in charging process of blast furnace by discrete element method. *Minerals Engineering,* 33**,** 27-33.

MIO, H., KOMATSUKI, S., AKASHI, M., SHIMOSAKA, A., SHIRAKAWA, Y., HIDAKA, J., KADOWAKI, M., YOKOYAMA, H., MATSUZAKI, S. & KUNITOMO, K. 2010. Analysis of Traveling Behavior of Nut Coke Particles in Bell-type Charging Process of Blast Furnace by Using Discrete Element Method. *ISIJ International,* 50**,** 1000-1009.

MIO, H., KOMATSUKI, S., JUSUKE, H., MASATOMO, K., SHINROKU, M. & KAZUYA, K. 2009. Analysis of Particle Size Segregation at Bell-less Top of Blast Furnace by Discrete Element Method. *Journal of Iron and Steel Research International,* 16**,** 1121-1125.

MIO, H., NAKAUCHI, T., KAWAGUCHI, Y., ENAKA, T., NARITA, Y., INAYOSHI, A., MATSUZAKI, S., ORIMOTO, T. & NOMURA, S. 2017. High-speed Video Recording of Particle Trajectory via Rotating Chute of Nagoya No.3 Blast Furnace and its Comparison with Simulated Behavior Using DEM. *ISIJ International,* 57**,** 272-278.

MOSBY, J. 1996. segregation of particlate materials - mechanisms and testers. *Kona,* 14**,** 13.

NASE, S. T., VARGAS, W. L., ABATAN, A. A. & MCCARTHY, J. J. 2001. Discrete characterization tools for cohesive granular material. *Powder Technology,* 116**,** 214-223.

NEDDERMAN, R. M., TUZUN, U., SAVAGE, S. B. & HOULSBY, G. T. 1982. The Flow of Granular-Materials .1. Discharge Rates from Hoppers. *Chemical Engineering Science,* 37**,** 1597-1609.

NOWAK, S., SAMADANI, A. & KUDROLLI, A. 2005. Maximum angle of stability of a wet granular pile. *Nature Physics,* 1**,** 50-52.

ORR, F. M., SCRIVEN, L. E. & RIVAS, A. P. 1975. Pendular rings between solids: meniscus properties and capillary force. *Journal of Fluid Mechanics,* 67**,** 723-742.

QIU, J. Y., JU, D. C., ZHANG, J. L. & XU, Y. S. 2017. DEM simulation of particle flow in a parallel-hopper bell-less charging apparatus for blast furnace. *Powder Technology,* 314**,** 218-231.

RAHMAN, M., SHINOHARA, K., ZHU, H. P., YU, A. B. & ZULLI, P. 2011. Size segregation mechanism of binary particle mixture in forming a conical pile. *Chemical Engineering Science,* 66**,** 6089-6098.

RAHMAN, M., ZHU, H. P., YU, A. B. & BRIDGWATER, J. 2008. DEM simulation of particle percolation in a packed bed. *Particuology,* 6**,** 475-482.

REISNER, W. 1968. The behaviour of granular materials in flow out of hoppers. *Powder Technology,* 1**,** 257-264.

ROSATO, A., STRANDBURG, K. J., PRINZ, F. & SWENDSEN, R. H. 1987. Why the Brazil Nuts Are on Top - Size Segregation of Particulate Matter by Shaking. *Physical Review Letters,* 58**,** 1038-1040.

SAMADANI, A. 2002. *Segregation, avalanching and metastability of dry and wet granular materials.* 3064037 Ph.D., Clark University.

SAMADANI, A. & KUDROLLI, A. 2001. Angle of repose and segregation in cohesive granular matter. *Physical Review E,* 64**,** 051301.

SAMADANI, A., PRADHAN, A. & KUDROLLI, A. 1999. Size segregation of granular matter in silo discharges. *Physical Review E,* 60**,** 7203-7209.

SAVAGE, S. B. & LUN, C. K. K. 1988. Particle-Size Segregation in Inclined Chute Flow of Dry Cohesionless Granular Solids. *Journal of Fluid Mechanics,* 189**,** 311-335.

SCOTT, A. M. & BRIDGWATER, J. 1975. Interparticle Percolation - Fundamental Solids Mixing Mechanism. *Industrial & Engineering Chemistry Fundamentals,* 14**,** 22-27.

SCOTT, A. M. & BRIDGWATER, J. 1976. Self-Diffusion of Spherical-Particles in a Simple Shear Apparatus. *Powder Technology,* 14**,** 177-183.

SHIMOKAWA, M., SUETSUGU, Y., HIROSHIGE, R., HIRANO, T. & SAKAGUCHI, H. 2015. Pattern formation in a sandpile of ternary granular mixtures. *Physical Review E,* 91**,** 062205.

SHINOHARA, K. 1979. Mechanism of Segregation of Differently Shaped Particles in Filling Containers. *Industrial & Engineering Chemistry Process Design and Development,* 18**,** 223-227.

SHINOHARA, K. & GOLMAN, B. 2002. Particle segregation of binary mixture in a moving bed by penetration model. *Chemical Engineering Science,* 57**,** 277-285.

SHINOHARA, K., GOLMAN, B. & NAKATA, T. 2001. Size segregation of multicomponent particles during the filling of a hopper. *Advanced Powder Technology,* 12**,** 33-43.

SHINOHARA, K. & MIYATA, S. 1984. Mechanism of Density Segregation of Particles in Filling Vessels. *Industrial & Engineering Chemistry Process Design and Development,* 23**,** 423-428.

SHINOHARA, K. & SAITOH, J. 1993. Mechanism of Solids Segregation over a 2-Dimensional Dead Man in a Blast-Furnace. *ISIJ International,* 33**,** 672-680.

SHINOHARA, K., SHOJI, K. & TANAKA, T. 1970. Mechanism of Segregation and Blending of Particles Flowing out of Mass-Flow Hoppers. *Industrial & Engineering Chemistry Process Design and Development,* 9**,** 174-180.

SHINOHARA, K., SHOJI, K. & TANAKA, T. 1972. Mechanism of Size Segregation of Particles in Filling a Hopper. *Industrial & Engineering Chemistry Process Design and Development,* 11**,** 369-376.

SILVA, S., DYRØY, A. & ENSTAD, G. 2000. Segregation Mechanisms and Their Quantification Using Segregation Testers. *In:* ROSATO, A. & BLACKMORE, D. (eds.) *IUTAM Symposium on Segregation in Granular Flows.* Springer Netherlands.

SMITH, L., BAXTER, J., TUZUN, U. & HEYES, D. M. 2001. Granular dynamics simulations of heap formation: Effects of feed rate on segregation patterns in binary granular heap. *Journal of Engineering Mechanics-Asce,* 127**,** 1000-1006.

STANDISH, N. 1985. Studies of Size Segregation in Filling and Emptying a Hopper. *Powder Technology,* 45**,** 43-56.

STANDISH, N., LIU, Y. N. & MCLEAN, A. G. 1988. Quantification of the Degree of Mixing in Bins. *Powder Technology,* 54**,** 197-208.

TANAKA, T., KAJIWARA, Y. & INADA, T. 1988. Flow Dynamics of Granular-Materials in a Hopper. *Transactions of the Iron and Steel Institute of Japan,* 28**,** 907-915.

TANG, P. & PURI, V. M. 2004. Methods for minimizing segregation: A review. *Particulate Science and Technology,* 22**,** 321-337.

TANG, P., PURI, V. M. & PATTERSON, P. H. 2003. Design, development, and performance of second generation primary segregation shear cell for size segregation. *Icemi'2003: Proceedings of the Sixth International Conference on Electronic Measurement & Instruments, Vols 1-3***,** 2203-2207.

TUZUN, U. & ARTEAGA, P. 1992. A Microstructural Model of Flowing Ternary Mixtures of Equal-Density Granules in Hoppers. *Chemical Engineering Science,* 47**,** 1619-1634.

UNAC, R. O., VIDALES, A. M., BENEGAS, O. A. & IPPOLITO, I. 2012. Experimental study of discharge rate fluctuations in a silo with different hopper geometries. *Powder Technology,* 225**,** 214-220.

WANG, Y., LU, Y. & OOI, J. Y. 2014. Finite element modelling of wall pressures in a cylindrical silo with conical hopper using an Arbitrary Lagrangian-Eulerian formulation. *Powder Technology,* 257**,** 181-190.

WILLETT, C. D., ADAMS, M. J., JOHNSON, S. A. & SEVILLE, J. P. K. 2000. Capillary Bridges between Two Spherical Bodies. *Langmuir,* 16**,** 9396-9405.

WILLIAMS, J. C. 1976. Segregation of Particulate Materials - Review. *Powder Technology,* 15**,** 245-251.

WU, S., KOU, M., XU, J., GUO, X., DU, K., SHEN, W. & SUN, J. 2013. DEM simulation of particle size segregation behavior during charging into and discharging from a Paul-Wurth type hopper. *Chemical Engineering Science,* 99**,** 314-323.

XU, J., WU, S., KOU, M., ZHANG, L. & YU, X. 2011. Circumferential burden distribution behaviors at bell-less top blast furnace with parallel type hoppers. *Applied Mathematical Modelling,* 35**,** 1439-1455.

XU, Y., XU, J., SUN, C., MA, K., SHAN, C., WEN, L., ZHANG, S. & BAI, C. 2018. Quantitative comparison of binary particle mass and size segregation between serial and parallel type hoppers of blast furnace bell-less top charging system. *Powder Technology,* 328**,** 245-255.

YANG, R. Y., ZOU, R. P., DONG, K. J., AN, X. Z. & YU, A. B. 2007. Simulation of the packing of cohesive particles. *Computer Physics Communications,* 177**,** 206-209.

YANG, R. Y., ZOU, R. P. & YU, A. B. 2003. Numerical study of the packing of wet coarse uniform spheres. *AIChE Journal,* 49**,** 1656-1666.

YANG, W. J., ZHOU, Z. Y., PINSON, D. & YU, A. B. 2014. Periodic Boundary Conditions for Discrete Element Method Simulation of Particle Flow in Cylindrical Vessels. *Industrial & Engineering Chemistry Research,* 53**,** 8245-8256.

YANG, W. J., ZHOU, Z. Y. & YU, A. B. 2015. Discrete particle simulation of solid flow in a three-dimensional blast furnace sector model. *Chemical Engineering Journal,* 278**,** 339-352.

YU, Y. & SAXÉN, H. 2010. Experimental and DEM study of segregation of ternary size particles in a blast furnace top bunker model. *Chemical Engineering Science,* 65**,** 5237-5250.

YU, Y. W. & SAXEN, H. 2014. Segregation behavior of particles in a top hopper of a blast furnace. *Powder Technology,* 262**,** 233-241.

ZHANG, J., QIU, J., GUO, H., REN, S., SUN, H., WANG, G. & GAO, Z. 2014. Simulation of particle flow in a bell-less type charging system of a blast furnace using the discrete element method. *Particuology,* 16**,** 167-177.

ZHENG, Q. J. & YU, A. B. 2015. Finite element investigation of the flow and stress patterns in conical hopper during discharge. *Chemical Engineering Science,* 129**,** 49-57.

ZHOU, Y. C., XU, B. H., YU, A. B. & ZULLI, P. 2001. Numerical investigation of the angle of repose of monosized spheres. *Physical Review E,* 64**,** 062205.

ZHOU, Y. C., XU, B. H., ZOU, R. P., YU, A. B. & ZULLI, P. 2003. Stress distribution in a sandpile formed on a deflected base. *Advanced Powder Technology,* 14**,** 401-410.

ZHOU, Y. C., YU, A. B., STEWART, R. L. & BRIDGWATER, J. 2004. Microdynamic analysis of the particle flow in a cylindrical bladed mixer. *Chemical Engineering Science,* 59**,** 1343-1364.

ZHOU, Z. Y., ZHU, H. P., YU, A. B., WRIGHT, B., PINSON, D. & ZULLI, P. 2005. Discrete particle simulation of solid flow in a model blast furnace. *ISIJ International,* 45**,** 1828-1837.

ZHOU, Z. Y., ZHU, H. P., YU, A. B., WRIGHT, B. & ZULLI, P. 2008. Discrete particle simulation of gas-solid flow in a blast furnace. *Computers & Chemical Engineering,* 32**,** 1760-1772.

ZHOU, Z. Y., ZOU, R. P., PINSON, D. & YU, A. B. 2014. Angle of repose and stress distribution of sandpiles formed with ellipsoidal particles. *Granular Matter,* 16**,** 695-709.

ZHU, H. P., RAHMAN, M., YU, A. B., BRIDGWATER, J. & ZULLI, P. 2009. Effect of particle properties on particle percolation behaviour in a packed bed. *Minerals Engineering,* 22**,** 961-969.

ZHU, H. P. & YU, A. B. 2004. Steady-state granular flow in a three-dimensional cylindrical hopper with flat bottom: microscopic analysis. *Journal of Physics D-Applied Physics,* 37**,** 1497-1508.

ZHU, H. P., ZHOU, Z. Y., YANG, R. Y. & YU, A. B. 2007. Discrete particle simulation of particulate systems: Theoretical developments. *Chemical Engineering Science,* 62**,** 3378-3396.